MULTISCALE CHARACTERIZATION OF SKELETAL PROPERTIES IN DIABETES AND CHRONIC KIDNEY DISEASE

by

John George Damrath IV

A Dissertation

Submitted to the Faculty of Purdue University

In Partial Fulfillment of the Requirements for the degree of

Doctor of Philosophy

Weldon School of Biomedical Engineering

West Lafayette, Indiana

May 2022

THE PURDUE UNIVERSITY GRADUATE SCHOOL
STATEMENT OF COMMITTEE APPROVAL

Dr. Joseph M. Wallace, Chair

Department of Biomedical Engineering, Indiana University-Purdue University at Indianapolis

Dr. Sharon M. Moe

Department of Medicine, Indiana University School of Medicine

Dr. Matthew R. Allen

Department of Anatomy and Cell Biology, Indiana University School of Medicine

Dr. Sherry Voytik-Harbin

Weldon School of Biomedical Engineering

Dr. Sungsoo Na

Department of Biomedical Engineering, Indiana University-Purdue University at Indianapolis

Approved by:

Dr. Tamara L. Kinzer-Ursem

Dedicated to all those who have inspired me to infuse my passions into everything I do, especially my parents John and Tammy and fiancé Arvin.

ACKNOWLEDGMENTS

The completion of this doctoral dissertation would not have been possible without the encouragement and support that I received from my mentors, colleagues, friends, and family. First and foremost, I would like to express my deepest appreciation to my advisor, Dr. Joseph (Joey) Wallace, for his immense knowledge, his passion and excitement for the science, and his constant support and dedication to his students. His guidance and willingness to dive into the unknown has taught me the invaluable lesson of embracing and championing change, and I know that whenever I approach new opportunities and experiences, I can rely on his example to make the most of them. I would also like to extend my gratitude to the dissertation committee members I worked with over the past four years: Drs. Sharon Moe, Matthew Allen, and Sherry Voytik-Harbin, as well as collaborators Drs. Tom Nickolas and Karl Lewis. These individuals motivated me to think across disciplines and combine the principles of science, engineering, and medicine into a patient-centered research goal. Finally, I would also like to extend my heartfelt thanks to Drs. Maureen Harrington, Raghu Mirmira, Rebecca Chan, Brittney-Shea Herbert, Benjamin Gaston, and especially Jan Receveur from the Medical Scientist Training Program (MSTP) at the Indiana University School of Medicine. These individuals have fostered a student-focused environment and are always available to offer support not only for program-related topics, but also for the multitude of life experiences that we go through simply for being in one place for eight years.

I am also very grateful for the past and present members of the Bone Biology and Mechanics Lab (BBML) for always providing constructive feedback, bouncing ideas back and forth while in the lab office, and for the simple comradery built from those long days at the VA. I would especially like to thank those who worked closely with me on the projects presented in this dissertation and for the numerous “harvest parties” we partook in to execute these projects as efficiently and accurately as possible. I would also like to extend thanks to my entire cohort of MSTP students. There is a special bond that can only be formed while being in medical school and graduate school together for nearly six years now, and I can’t imagine a better group to venture into clinical clerkships with for the next two years.

There are many other individuals who I would like to acknowledge for making my time at the IUSM and Purdue memorable, and in some cases, life-changing. I want to thank my close friends, Jared Smith and Hannah Kline, for their encouragement when challenges arose both in lab

and in life. I also want to extend a special thanks to alumnus of the Weldon School of Biomedical Engineering and my fiancé, Arvin Soepriatna, for his constant support, for introducing me to the close-knit network in Purdue BME, and for proofreading and editing just about everything I've ever written during graduate school. I would also like to express my deepest gratitude to my parents, John and Tammy, for embracing my passion for engineering and medicine since childhood and providing me with everything I needed – whether in the form of Legos, stuffed animal microbes, or yet another book on the human body – to get to where I am now.

Finally, I would like to acknowledge the Weldon School of Biomedical Engineering Bioengineering Interdisciplinary Training in Diabetes Research Program (BTDR) and the National Institutes of Health F30 predoctoral fellowship. It was through these funding sources that the work described herein was able to come to fruition.

TABLE OF CONTENTS

LIST OF TABLES

LIST OF FIGURES

LIST OF ABBREVIATIONS

AD	Adenine Diet
AGE	Advanced Glycation End Product
AUC	Area Under Curve
BFR	Bone Formation Rate
BMD	Bone Mineral Density
BUN	Blood Urea Nitrogen
CaHA	Calcium-Hydroxyapatite
CaSR	Calcium-Sensing Receptor
CKD	Chronic Kidney Disease
CKD-MBD	Chronic Kidney Disease-Mineral and Bone Disorder
DKD	Diabetic Kidney Disease
DXA	Dual-Energy X-Ray Absorptiometry
eGFR	Estimated Glomerular Filtration Rate
E_r	Reduced Modulus
ESKD	End-Stage Kidney Disease
FGF23	Fibroblast Growth Factor 23
FTIR	Fourier Transform Infrared Spectroscopy
H	Hardness
HbA1c	Hemoglobin A1c
HR-pQCT	High Resolution Peripheral Quantitative Computed Tomography
MAR	Mineral Apposition Rate
MMR	Mineral-to-Matrix Ratio
MS/BS	Mineralizing Surface/Bone Surface
PBS	Phosphate-Buffered Saline
PMMA	Poly(Methyl Methacrylate)
PTH	Parathyroid Hormone
QBEI	Quantitative Backscatter Electron Imaging
SHPT	Secondary Hyperparathyroidism

STZ	Streptozotocin
T1D	Type 1 Diabetes
T2D	Type 2 Diabetes
TMD	Tissue Mineral Density
ε	Strain
μCT	Microcomputed Tomography
σ	Stress

ABSTRACT

Chronic kidney disease (CKD) affects 15% of Americans and dramatically increases their risk of skeletal fractures and fracture-related mortality. The progression of CKD is marked by abnormal biochemistries including disrupted mineral homeostasis and elevated parathyroid hormone (PTH). High PTH is linked to the bone alterations seen in CKD including cortical porosity and altered turnover. To mitigate the effects of sustained elevations in PTH, dialysis patients are commonly given calcimimetics which act by sensitizing the calcium-sensing receptor on parathyroid chief cells, lowering PTH synthesis and secretion. While calcimimetics are suggested to reduce fracture risk in dialysis patients, little is known about how these drugs impact bone tissue properties or whether they can be implemented in early CKD to prevent CKD-induced bone deterioration. Therefore, understanding how calcimimetics alter bone quality may reveal new strategies to prevent fractures in patients with CKD. While CKD represents a major global health crisis, nearly half of all CKD patients also have diabetes. Diabetes disrupts numerous physiologic systems and independently increases fracture risk by lowering bone mass and quality. Therefore, we have two major objectives in this work. Firstly, we developed a method for analyzing bone composition and material properties in a spatially resolved manner and found that calcimimetics increase mineral crystallinity and stiffness in newly formed periosteal bone while increasing relative mineralization, stiffness, and hardness in perilacunar bone. Further, we found that these properties depended on distance from the osteocyte lacunar wall. Secondly, we developed a novel combined murine model of type 1 diabetes and CKD which revealed a unique combination of detriments in structural and tissue-level bone microarchitecture, mechanical properties, and fracture toughness. Taken together, this work represents a thorough investigation of how diabetes and CKD alter bone quality on multiple scales and how calcimimetics improve bone quality in localized regions in early CKD.

1. INTRODUCTION

Chronic kidney disease (CKD) affects 15% of Americans, disrupting the homeostatic mechanisms regulating blood pressure, blood cell production, and electrolyte/mineral balance among others.[1-4] As renal function worsens, the kidney loses its ability to filter waste products and reabsorb the electrolytes and minerals that pass the filtration barrier, making dialysis a necessity in end-stage kidney disease. While dialysis removes most uremic waste products from blood, it is unable to filter the increased phosphorus load these patients exhibit.[5] This is thought to be the driving force behind CKD-mineral and bone disorder (CKD-MBD), a condition characterized by abnormal biochemistries including elevated parathyroid hormone (PTH) and fibroblast growth factor 23 (FGF23), cardiovascular and soft tissue calcification, and cortical bone pore formation and thinning.[6] Specifically, CKD patients are at a 3- to 10-fold greater risk of fracture compared to the normal age- and sex-matched population, and this risk is increased across all stages of CKD and worsens with age (**Fig. 1.1**).[7] Strikingly, up to 60% of CKD patients die within one year following hip fracture, a three times greater one-year mortality rate than the normal population.[8] These statistics highlight the critical need to better understand the mechanism of CKD-induced bone fragility and develop effective treatments.

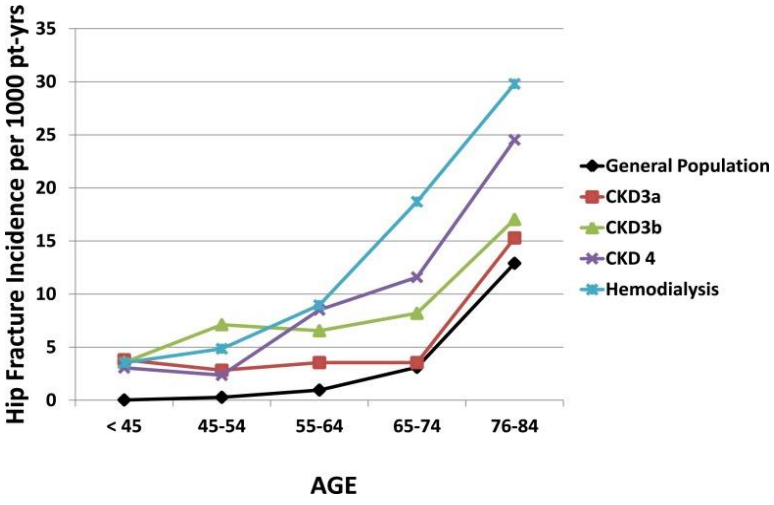

Fig. 1.1: Fracture risk increases as renal function declines and as patients age.

In CKD, several components of bone quality are altered that may contribute to increased bone fragility. These include decreased cortical bone thickness, increased cortical bone porosity,

and altered bone remodeling, which may lower bone mineral density (BMD).[9,10] These changes are thought to be caused by increased levels of circulating uremic toxins and parathyroid hormone (PTH).[9,11] While BMD and PTH levels are commonly used to assess fracture risk, CKD patients with normal BMD and controlled PTH levels surprisingly remain at an increased risk of fracture.[12,13] While serum PTH measurements do not correlate well with fracture risk, PTH-lowering therapy is common in dialysis patients. Commonly used PTH-lowering therapies include calcium-based phosphate binders, activated vitamin D, and calcimimetics. However, calcium-based phosphate binders have been shown to increase the risk of vascular calcification in CKD patients, and no studies have demonstrated improvements in fracture risk in CKD patients receiving vitamin D[14,15].

A secondary analysis of the Evaluation of Cinacalcet HCl Therapy to Lower Cardiovascular Events (EVOLVE) trial demonstrated that calcimimetics may reduce fractures in patients with CKD[16]. Calcimimetics, lower serum PTH by sensitizing the calcium-sensing receptor (CaSR) on parathyroid chief cells.[17] Experiments in rat models of CKD and secondary hyperparathyroidism (SHPT) have exhibited improvements in blood urea nitrogen [18], creatinine, PTH, and fibroblast growth factor 23 (FGF23), as well as improvements in cortical bone porosity and mechanical strength following calcimimetic treatment.[19-22] However, their effects on intrinsic material properties, including tissue-level measures of bone quality, remain unknown.[16] Taken together, these results suggest that an alternative, undiscovered mechanism involving PTH and/or calcium sensing contributes to the increased bone fragility in CKD patients.

While CKD is increasingly recognized as an important cause of fractures and fracture-related mortality, the effects of CKD etiology are rarely examined in preclinical and clinical studies. Diabetes, the single greatest risk factor for CKD, affects one in ten Americans, and the prevalence is predicted to increase to one in three Americans by 2050[23]. Diabetic kidney disease (DKD) affects one in three diabetics and is responsible for approximately 45% of end-stage kidney disease cases in both type 1 (T1D) and type 2 (T2D) diabetics[23]. Beyond the kidney, diabetes results in end organ damage to numerous tissues including the eye, heart, vasculature, skin, nerves, muscles, and skeleton[23-27]. CKD is also common among individuals with prediabetes and undiagnosed diabetes, highlighting the need for increased screening for both conditions[28]. Despite this clearly recognized link, few studies have examined the combined and potentially interactive effects of these frequently comorbid conditions.

As diabetes progresses, the disease impacts many of the same organ systems as CKD, especially when poorly controlled (**Table 1**). However, the mechanisms by which these effects occur may differ from tissue to tissue and may depend on the type of diabetes present. Strikingly, patients with diabetes have a greater risk of hip fracture with subsequently impaired fracture healing, increased hospital costs, and reduced mobility compared to healthy individuals[29,30]. While BMD is frequently used to estimate fracture risk, T1D only slightly reduces BMD while most T2D patients have increased BMD, indicating that diabetes alters the intrinsic material quality of the bone tissue[31-34]. These changes may include a combination of increased advanced glycation end products (AGEs) and non-enzymatic crosslinks in the collagen matrix due to oxidative stress and inflammation and potential alterations in microarchitecture[35]. Because CKD also alters bone quality on the tissue level and impacts many of the same organ systems as diabetes, there is a great clinical need for studies that examine the combination of diabetes and CKD on skeletal health. Furthermore, novel approaches to estimate fracture risk and prevent fractures in patients with diabetes and CKD are greatly needed for the aging population as traditional methods do not accurately capture the impact of these conditions independently.

Table 1.1: Clinical findings in diabetes and CKD.

Organ	**Diabetes**	**CKD**
Eye	Diabetic retinopathy [23]	Retinal microvascular damage [36]
Tendon	Tendinopathy [37]	Tendon rupture [38]
Muscle	Insulin resistance, reduced strength [25]	Sarcopenia [26]
Bone	BMD and microarchitecture alterations	Cortical porosity [27]
Nerve	Diabetic neuropathy [23]	Cognitive impairment, dementia [24]

Recent studies have incorporated measures of bone matrix composition and tissue-level mechanical properties utilizing vibrational spectroscopy and indentation, respectively, in rodent and human specimens.[11,39,40] While these techniques provide greater insight into bone quality, they require the user to select specific points to analyze on a bone specimen. Because the bone matrix is continuously remodeling, the selected points could represent several different tissue ages, which is an independent risk factor for fractures (**Fig. 1.2**).[12] Further, current spectroscopy and indentation devices lack the ability to spatially match the measures of tissue composition and mechanics, limiting the discovery of novel correlations between compositional parameters and

mechanical properties. Therefore, there is a need for a robust, high-level analysis of the CKD-induced changes in bone quality.

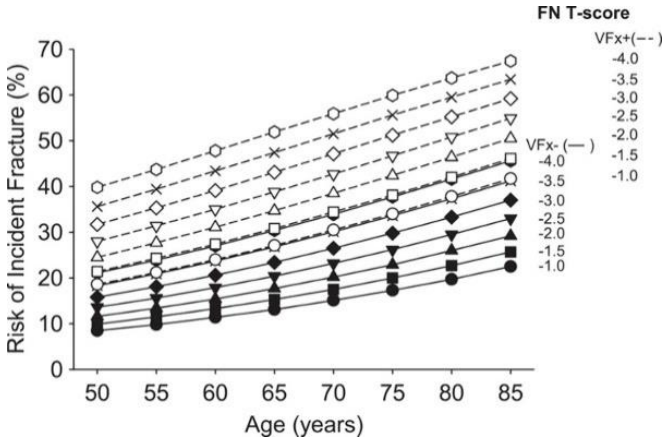

Fig. 1.2: Fracture risk increases with age**.** Predicting fracture risk from BMD alone is insufficient as patients with similar BMD have variable fracture risk with increasing age. FN: femoral neck, VFx-: no fracture, VFx+: fracture.[12]

2. BACKGROUND

Before discussing our investigation of multiscale bone tissue properties in chronic kidney disease (CKD) and type 1 diabetes (T1D), it is important to discuss the complex pathophysiology of these two disease states that precipitates the eventual skeletal alterations. This chapter provides an in-depth review of the current state of knowledge on CKD-mineral and bone disorder (CKD-MBD) and diabetes-induced bone alterations and discusses some of the most widely implemented tools to measure bone mass and quality in the clinic and laboratory. We will begin by describing the complex series of biochemical alterations that occur in these conditions and the preclinical models that have been used to better understand how these conditions affect the bone. We will then address the challenges and limitations of current methods to assess bone quality. Figures in this chapter have been adapted from our previous publication "The Impact of Advanced Glycation End Products on Bone Properties in Chronic Kidney Disease", published in *Current Opinion in Nephrology and Hypertension*.

2.1 Pathophysiology of Chronic Kidney Disease-Mineral and Bone Disorder

CKD is a disorder characterized by a progressive loss of kidney function. Throughout the disease course, the kidneys undergo fibrosis, atrophy of the renal tubules, and scarring of the glomeruli, the major filtration unit in the kidney.[41] Diagnosis is performed by measuring creatinine clearance, an estimate of the overall glomerular filtration rate (eGFR) normalized by body surface area. Elevations in BUN, termed azotemia, are also used as an indicator of kidney health, although this measure is less specific to renal function.[42] CKD is staged by measuring both eGFR and the amount of albumin in the urine (**Fig. 2.1**) regardless of the cause of CKD.[43] Once eGFR remains below 60 ml/min/1.73 m^2 for at least 3 months, the diagnosis of CKD is officially given, beginning at stage G3a. Albuminuria was recently added into the diagnostic scheme due to increased risk of complications if urine albumin levels remain high.[44] This is indicated by the heat map in Figure 3, where darker shades of red indicate greater risk of mortality, cardiovascular events, and CKD progression. When eGFR falls below 15 ml/min/1.73 m^2, the patient has reached stage G5, or end-stage kidney disease (ESKD), at which time either dialysis or kidney transplant is required.

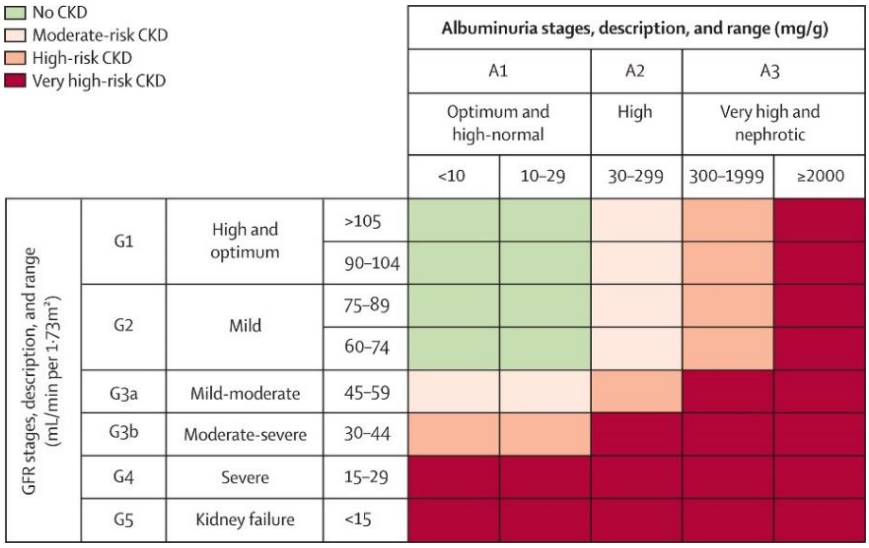

Fig. 2.1: CKD staging guidelines**.** Darker shade indicates greater risk of CKD progression, cardiovascular events, and all-cause mortality.[24]

Despite the assistance of dialysis, patients with CKD exhibit an increased phosphorus load, reflecting the kidney's inability to filter and eliminate phosphorus properly.[(5)] Excess phosphorus drives the production of FGF23, a phosphaturic hormone produced and secreted by osteocytes.[(45)] FGF23 decreases serum phosphorus by inhibiting the formation and promoting the degradation of 1,25-dihydroxyvitamin D ($1,25(OH)_2D$), the active form of vitamin D, and by increasing phosphorus excretion by the kidney.[(46)] The main function of $1,25(OH)_2D$ is to increase calcium and phosphorus absorption from the intestine.[(47)] With hyperphosphatemia and elevated FGF23 suppressing $1,25(OH)_2D$, the net loss of calcium is sensed by decreased CaSR activity. The CaSR is expressed ubiquitously, but notably by chief cells within the parathyroid gland.[(48)] Decreased CaSR activity in the parathyroid gland results in increased synthesis and secretion of parathyroid hormone (PTH), one of the most potent regulators of serum calcium levels.[(49)] While FGF23 normally suppresses extra PTH secretion via negative feedback, it is theorized that the kidney and parathyroid gland gradually become resistant to FGF23, resulting in SHPT.[(50-52)] Under normal conditions, PTH increases serum calcium by promoting $1,25(OH)_2D$ formation, increasing tubular reabsorption of calcium, and is involved in freeing calcium and phosphorus from the bone matrix by increasing bone resorption on bone surfaces and in the perilacunar matrix. However, the reduction in $1,25(OH)_2D$ levels due to continued suppression by FGF23 leads to sustained elevation of PTH. Therefore, bone resorption must continue to normalize serum calcium levels,

which further increases the phosphorus load. Together, these highly intertwined endocrine mechanisms maintain serum calcium levels in a disturbed yet effective manner (**Fig. 2.2**).

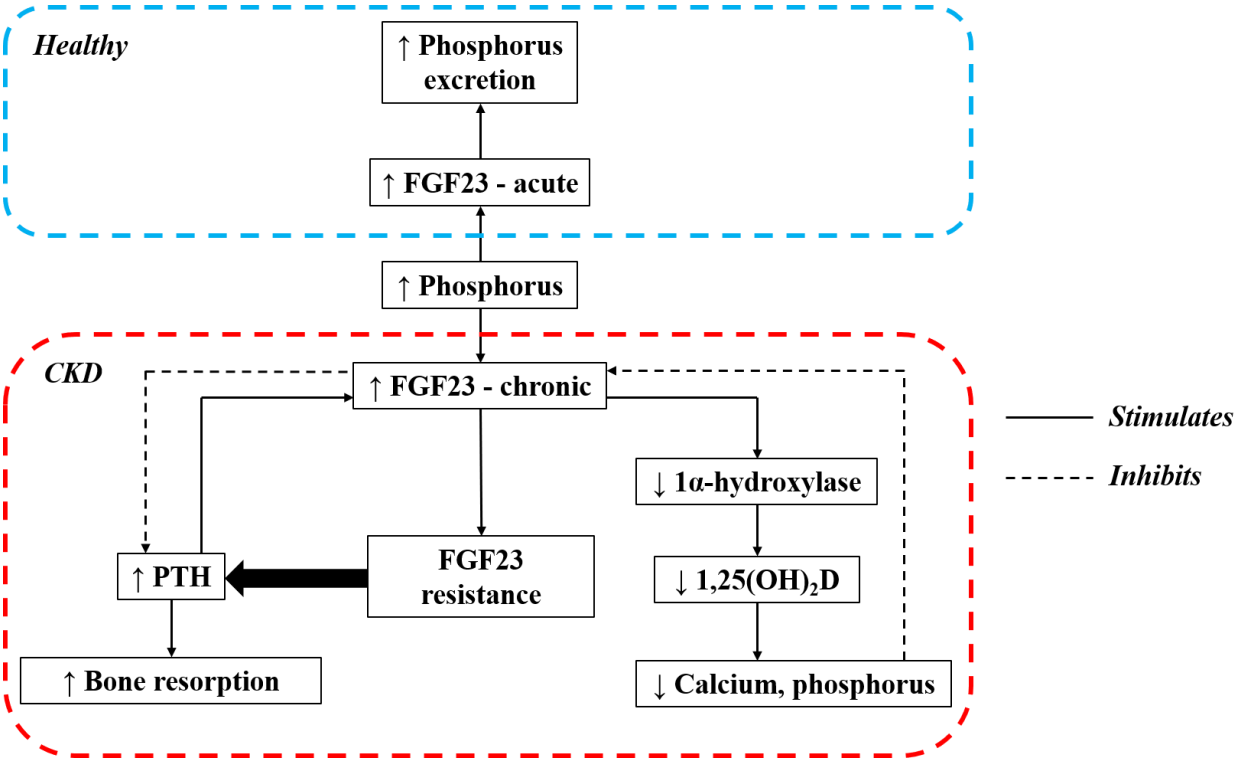

Fig. 2.2: Mineral homeostasis in CKD-MBD. FGF23: fibroblast growth factor 23; PTH: parathyroid hormone.

As renal function worsens, the above physiologic alterations result in several pathological sequelae including renal osteodystrophy, a CKD-induced bone disease. Renal osteodystrophy is diagnosed from transiliac crest bone biopsies that are analyzed for turnover rate, mineralization, and bone volume fraction.[3] In particular, bone turnover status plays an important role in making therapeutic decisions and is known to affect bone quality.[53] High turnover may result in increased bone resorption, suggesting the use of anti-resorptive drugs. Low turnover may indicate improper remodeling, suggesting the use of an anabolic drug.[54] Interestingly, while PTH is known to play a role in bone turnover, PTH levels correlate only modestly with turnover status in CKD patients.[55] Regardless, certain PTH-lowering interventions have been shown to reduce fracture risk in dialysis patients, indicating the need to better understand how PTH levels affect bone quality in CKD.

2.2 Animal Models of CKD

Due to the complex nature of CKD pathogenesis and the need to constantly monitor disease progression by measuring BUN and creatinine, animal models are frequently utilized to gain insight into the underlying mechanisms behind CKD-MBD. These models include one or more of surgical interventions, nephrotoxic agents, and genetic alterations. The most frequently used method for inducing kidney injury in rodents is performing a 5/6 nephrectomy (5/6 Nx). This technique involves removing one kidney and ligating the upper and lower poles of the remaining kidney, leaving a functional middle region in one kidney.[56,57] The remaining kidney segment undergoes glomerular hypertrophy, mesangial expansion, and increased collagen deposition.[56] Systemically, this model replicates elements of CKD including uremia, increased serum creatinine, and proteinuria.[58,59] Additionally, most studies report electrolyte and mineral disturbances including increased sodium, potassium, and calcium excretion. Interestingly, mice undergoing 5/6 Nx do not exhibit changes in serum phosphorus or phosphorus excretion.[58] Because disrupted phosphorus homeostasis is thought to be the driving force behind CKD-MBD in humans, this model may have limited use in studying bone changes in end stage renal disease. Indeed, mice given 5/6 Nx at 10 weeks of age only exhibited reductions in trabecular number following 11 weeks of kidney dysfunction with no alterations in whole bone mechanics.[60] These mice also failed to replicate the decreased cortical thickness and increased cortical porosity seen in CKD patients. This may be due to the rapid onset of CKD following an acute kidney injury, which follows a different time course compared to CKD in humans. Finally, while the concept of 5/6 Nx is relatively simple, animals often suffer from surgical complications including a 40% mortality rate.[61]

A less invasive method of inducing kidney injury is adding nephrotoxic agents to the rodent's diet. The most commonly used agent is adenine, which is added to a concentration of 0.2-0.75% within standard chow.[62,63] In the body, adenine is converted to 2,8-dioxyadenine which precipitates in the renal tubules, damaging the tubule and obstructing urine flow.[64,65] Depending on the concentration of adenine in the diet, kidney injury can occur within days or more gradually across several weeks. Rats fed a 0.75% adenine diet develop 5-fold increases in serum creatinine within just 16 days, an extremely rapid onset of CKD.[66] Interestingly, serum phosphorus levels decreased up until sacrifice, indicating that the kidney injury may be too rapid and severe to cause CKD-MBD. Mice and rats fed a 0.15-0.2% adenine diet reached 5-fold increases in serum

creatinine at 6 weeks, which remains a rapid decline in kidney function when compared to human disease. [67] These rats achieved a CKD-MBD-like phenotype when their phosphorus intake was increased from 0.8% to 1.8%, as indicated by increased serum phosphorus, PTH, and FGF23, decreased cortical bone mineral volume, and increased calcium deposits in the aorta and heart.[67] While these models may be useful for studying advanced CKD (stage 4/5), studying the effects of early stage CKD on the bone and vasculature may be difficult.

While diabetes and hypertension are the primary causes of CKD, 600,000 Americans suffer from polycystic kidney diseases (PKD), 50% of whom will reach kidney failure by age 60.[68] While PKD is caused by genetic mutations, the disease follows a gradual time course with symptoms typically appearing after age 30.[69] Therefore, animal models of PKD may be useful to study the systemic effects of slowly progressive kidney disease. The male Cy/+ rat is an autosomal dominant PKD (ADPKD) model that spontaneously forms cysts in the renal tubule over the course of several months.[70] These rats have a point mutation in the *Anks6* gene encoding SamCystin, a protein that is highly expressed in the proximal tubule of the nephron but has no known function.[71] Male rats heterozygous for the mutation (Cy/+) experience a gradual decline in renal function with azotemia beginning at 10 weeks of age.[72] In order to facilitate the development of CKD-MBD, rats are switched to a casein-based diet at 24 weeks, when their renal function is roughly 30% of their normal littermates, representing the transition of stage 3 to stage 4 CKD.[73] The casein-based protein source contains no dietary phytate, a phosphorus source that is not freely absorbed.[73] Therefore, the entire phosphate load in the casein diet is bioavailable, increasing serum phosphorus levels and promoting disease progression. Importantly, male Cy/+ rats exhibit elevated PTH with normal calcium and phosphate levels at this stage. By 35 weeks of age, male Cy/+ rats display all three components of CKD-MBD including biochemical abnormalities (elevated BUN, creatinine, PTH, FGF23, and phosphorus), cortical bone porosity, and vascular calcification (**Fig. 2.3**). Interestingly, female Cy/+ rats do not exhibit uremia until 80 weeks of age.[70,74] Even with ovariectomy, these rats do not exhibit overt signs of kidney disease or any of the components of CKD-MBD.[75] Regardless, the male Cy/+ rat replicates many aspects of human CKD-MBD.

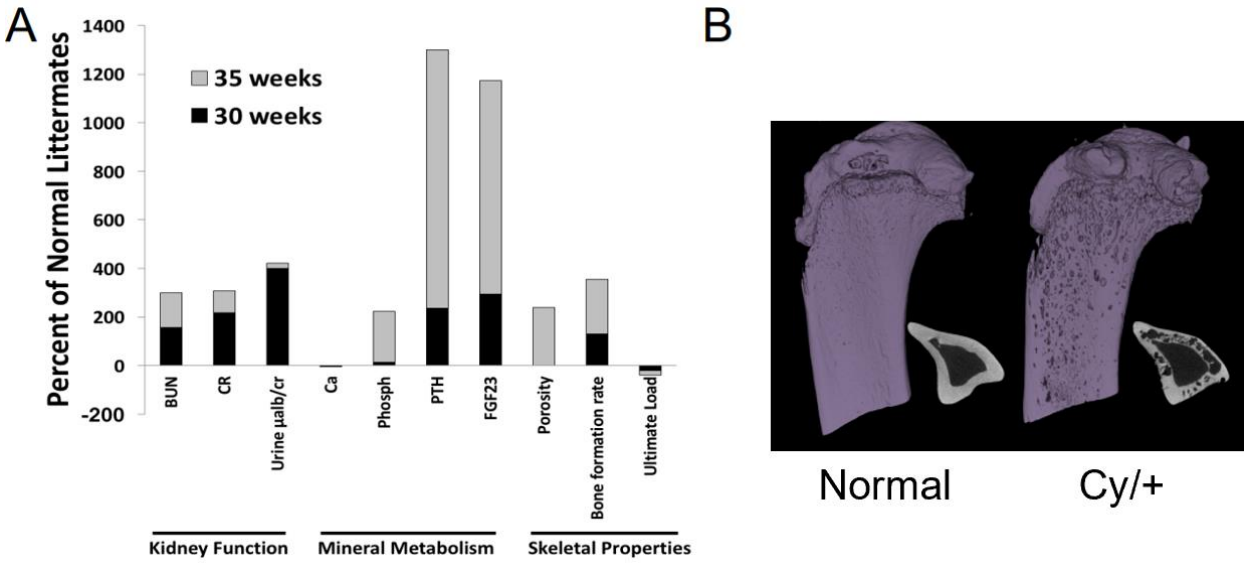

Fig. 2.3: The male Cy/+ rat develops hallmarks of CKD-MBD. (A) Changes in kidney function, mineral metabolism, and whole bone architectural and mechanical properties at 30 and 35 weeks. (B) The Cy/+ rat develops cortical porosity by 35 weeks of age.

2.3 Effects of CKD on Bone Quality

Bone quality is an umbrella term referring to any bone tissue properties that are independent of bone mass.[76] While the current gold standard assessment of fracture risk is dual-energy X-ray absorptiometry (DXA) to determine BMD, BMD alone underpredicts fracture risk. Even in the context of age-related osteoporosis, fracture risk increases with age beyond what BMD measurements predict.[77] Therefore, measures of bone quality, including architectural, mechanical, and compositional properties, must play a crucial role in determining bone strength.

2.3.1 Bone Microarchitecture

Bone tissue is comprised of two major compartments: cortical bone and trabecular bone. Cortical bone is a solid shell that forms the exterior bone surface and is responsible for supporting loads.[78] While cortical bone is present in all bones, it is most prevalent at the diaphysis, or middle region, of long bones and at the distal radius, making these locations common assessment sites for cortical porosity in CKD patients. Trabecular bone, found in great quantities in the vertebrae, is designed to distribute loads exerted from any direction.[79,80] Thus, it is comprised of interconnecting rods and plates that align with the principle directions of the bone tissue.[81,82]

Therefore, the geometry and architecture of cortical and trabecular bone likely play an important role in its overall mechanical properties.

The most common technique used to assess bone architecture *ex vivo* is microcomputed tomography (µCT) (**Fig. 2.4**).[83] This technique utilizes X-rays to nondestructively create a three-dimensional reconstruction of cortical and trabecular regions of interest, allowing for a volume of bone tissue to be imaged with minimal sample preparation. Importantly, bone can undergo µCT while frozen, preserving tissue hydration without changing its material properties.[84] Therefore, each sample can undergo mechanical testing following µCT. Due to the small thicknesses of cortical and trabeculae bone in rodents, most µCT devices have a minimum resolution of 6 µm, yielding trabecular and cortical dimensions that that correlate strongly with measurements taken from 2D histology.[85]

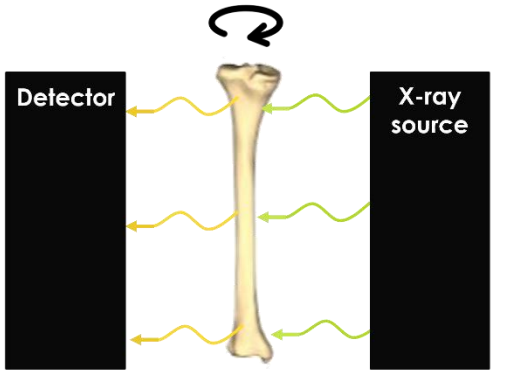

Parameter	Value
Resolution	9.8 µm voxels
Angle Step	0.9°

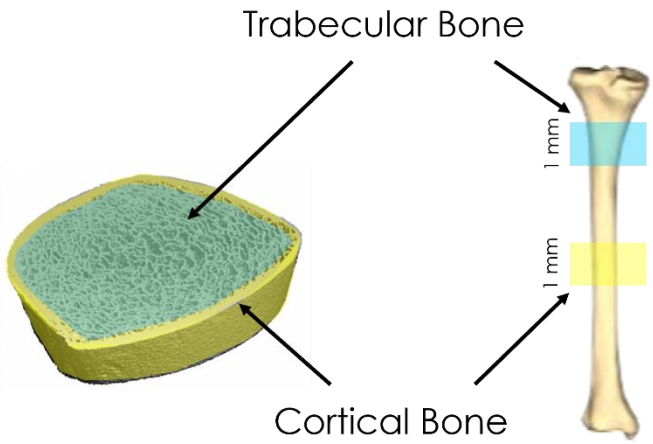

Fig. 2.4: Standard Setup for Microcomputed Tomography of the Mouse Tibia.

While changes in bone architecture in either compartment may impact the mechanical integrity of bone, CKD primarily affects cortical bone architecture and has little effect on the trabecular structure in ESKD.[9,86,87] Cortical bone analysis in rodents is typically performed on a 1 mm region of interest taken from the mid-diaphysis of long bones such as the femur or tibia.[88] The reconstructed image is then analyzed for cross sectional area and cortical bone area, both of

which are related to the bone's second moment of inertia and determine how the bone responds to mechanical stress. Importantly, cortical thickness decreases and cortical porosity increases in the 30-35 week range in the Cy/+ rat, indicating that cortical bone quality is reduced late in the course of CKD and may play an important role in determining late-stage fracture risk.[89] However, fracture risk is increased across all stages of CKD, indicating that changes in bone architecture are not the sole cause of decreased bone strength.[7]

While *ex vivo* measurement of bone architecture has superior resolution to *in vivo* measurements, the ability to track changes in bone architecture across all stages of CKD could allow physicians to better predict fracture risk. The most used clinical assessment of bone architecture is high resolution peripheral quantitative computed tomography (HR-pQCT). This technique also uses X-rays to create a three-dimensional volumetric image of the distal tibia and radius with an 80 μm resolution.[90] The distal radius is of particular interest in CKD because of the high proportion of cortical bone, making it a potentially valuable site to assess cortical porosity. In a retrospective study on predialysis patients, it was found that the total density of the ultradistal radius and cortical thickness of the distal tibia had the best potential to predict fracture.[87] However, the area under the receiver operator characteristic curve (AUC) was less than 0.7 for all parameters, where 1 indicates 100% sensitivity and specificity. This indicates that in humans, architectural changes are not solely predictive of the increased fracture risk in CKD. Interestingly, the AUC values for cortical parameters increased for patients with CKD for greater than 7 years, indicating that late-stage cortical thinning and porosity likely influence bone strength.

2.3.2 Structural and Tissue-level Mechanical Properties

Bone tissue is a composite material consisting of a type I collagen matrix impregnated with hydroxyapatite, a calcium and phosphate-based mineral.[91] On the molecular scale, water molecules bound to collagen and hydroxyapatite facilitate proper mineral alignment and the interaction between these two phases.[92] The mineral component of bone provides strength in compression while the collagen component provides 1) increased toughness, the area under the stress-strain curve, and 2) increased ductility, the amount of strain at fracture in tension (**Table 2.1**).[93,94] The most commonly used method for assessing bone mechanical properties is flexural testing. Flexural testing is performed by placing one of the long bones, such as the femur or tibia, on two support pins and slowly loading the bone with either one load point in the center of the

bone (three-point bending) or with two load points set a small distance apart (four-point bending).[11,95-97] The bone is loaded until failure, as indicated by a decrease in the measured force, and a force-displacement curve is generated (**Fig. 2.5A**). This curve is representative of the organ-level properties of the bone (**Table 2.1**). By utilizing the cross-sectional area of the bone determined from μCT to calculate the second moment of inertia (**Fig. 2.5B**), the curve can be transformed into a stress-strain curve (**Fig. 2.5C**) using (**Eq. 1**) and (**Eq. 2**) for four-point bending, where F is force, c is the distance from the centroid of the bone to its tensile surface, a is the distance from the support to the inner loading point, I is the second moment of inertia, d is displacement, and L is the length between the two lower supports.[84,98,99] This curve is analyzed to estimate the tissue-level properties of the bone (**Table 2.1**).

Table 2.1: Calculation of Select Mechanical Properties from Force-Displacement and Stress-Strain Curves

Organ-level Property	Tissue-level Property	Related Bone Property	Mechanical Definition	Clinical Interpretation
Stiffness	Modulus	Mineralization	Slope of elastic region	Ability to resist elastic deformation
Ultimate force	Ultimate stress	Mineralization	Highest point on the curve	Maximum load before loss of mechanical integrity
Work	Toughness	Collagen alignment and crosslinking, hydration	Area under the curve	Ability to dissipate energy that can cause damage
Post-yield displacement	Post-yield strain	Collagen alignment and crosslinking, hydration	Difference on X-axis between the yield and failure points	Ability to withstand fracture after damage and begin repair
Fracture Toughness		Collagen quality, microdamage	Resistance to crack propagation	Ability to resist fracture from existing flaws
Fatigue Life		Porosity, microdamage	Cycles to failure below yield force	Ability to resist fracture from small, repetitive loads

While flexural tests on bone benefit from an easy setup, three major assumptions made in using the above beam bending equations are that the material is linearly elastic, isotropic, and homogenous.[100] Of largest concern are the latter two assumptions because material properties differ between the cortex and trabeculae and between the surfaces and interior of bone.[101] Additionally, bone is a continuously remodeling tissue that may contain tissue of various qualities simultaneously.[102]

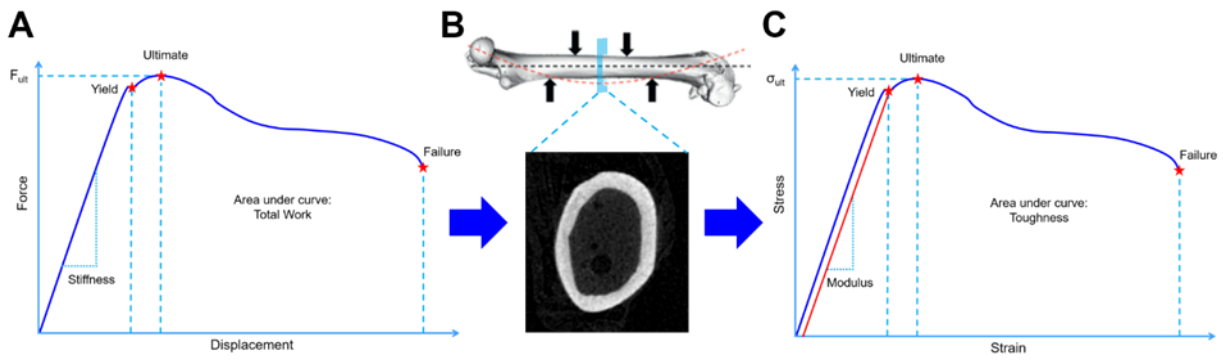

Fig. 2.5: Flexural test setup and curve analysis. A: three-point bending setup. B: force-displacement curve from healthy and diseased moues bone. C: force-displacement curve transformed into stress-strain curve.

$$Stress_{4pt} = \sigma = \frac{Fac}{2I}\ (MPa) \quad \textbf{(2.1)}$$

$$Strain_{4pt} = \varepsilon = \frac{6cd}{a(3L-4a)} \quad \textbf{(2.2)}$$

In the Cy/+ rat, mechanical properties are dramatically altered, indicating significant changes in bone mass and/or quality. Animals with CKD exhibit significant reductions in ultimate force, energy to failure, stiffness, and toughness.[103,104] Together, these findings indicate that less force is required to deform and break bone in CKD. While this data is valuable in understanding the overarching effects of CKD and potential treatments on bone mechanics, it gives little information on the microstructural alterations that may be responsible for these changes. Therefore, there is a great need to obtain true tissue-level measurements of bone microstructural material properties in CKD.

Tissue-level mechanical analysis of bone is a valuable counterpart to organ-level analyses and tissue-level estimations in that it can be performed on a point-by-point basis with submicron resolution. Techniques under this category include nanoindentation, reference point indentation, and atomic force microscopy indentation. While these techniques differ in their scale, they all utilize a probe that is pressed into the sample, held, and then retracted, generating a load-displacement curve.[105] For basic indentation, tissue hardness and reduced elastic modulus can be calculated with equations 3 and 4, where S is the stiffness estimated from the 40-95% region of the unloading slope, A is the probe contact area, h_c is the contact displacement, and P_{max} is the peak force.[106]

$$Reduced\ modulus = E_r = \frac{S\sqrt{\pi}}{2\sqrt{A(h_c)}} \quad \textbf{(2.3)}$$

$$Hardness = H = \frac{P_{max}}{A(h_c)} \quad \textbf{(2.4)}$$

The primary advantage of these techniques is the ability to navigate across a single sample and select any number of points to indent, allowing for mapping and correlating tissue-level and organ-level properties. However, for this technique to be used to study the effects of treatments on tissue-level mechanical properties, fluorescent labels such as calcein and alizarin that mark areas of new bone formation should be employed. If one such label is injected into a rodent during a treatment period, the new bone formed during that period will be marked by a fluorescent boundary.[107] Frequently, double labels are given to mark baseline and endpoint regions. Using these labels as guides, indentation can be aimed at the regions of bone formed under the presence of treatment. However no indentation studies on the Cy/+ rat have utilized fluorescent labels and no differences in tissue-level hardness or reduced modulus were found when averaging the data.[108] Taken together, spatial analysis and fluorescent labeling will allow us to more appropriately determine the effects of CKD and treatments on matrix mechanics by specifically identifying regions of bone formed during the disease and intervention periods. For the diabetic aims of the proposed experiments, determining the mechanical phenotype of the mice is at the forefront of our interest and will serve as an important way to establish disease severity and the effects of potential treatments.

2.3.3 Bone Matrix Composition

While proper bone architecture is an important factor in determining overall bone strength, the chemical composition of the bone tissue must also be of high quality in order to properly bear and distribute loads. Traditionally, bone mineral composition has been assessed via destructive methods such as gravimetric analysis to determine overall mineral content.[109] Additionally, the collagen matrix is usually analyzed for crosslinking and advanced glycation end-products (AGEs) utilizing fluorescent assays or high performance liquid chromatography (HPLC).[110] While well established, these techniques typically require sections of whole bone to be demineralized and digested, prohibiting the analysis of spatial differences in tissue composition. More recently, there has been an increased use of spectroscopic methods including Fourier transform infrared spectroscopy (FTIR) and Raman spectroscopy to examine tissue-level composition in bone. The main advantages of these techniques are that 1) they require only a thin section of bone, 2) they

are nondestructive, and 3) they have a roughly 1 μm resolution. Therefore, spectroscopy can be a valuable tool in forming correlations between composition and mechanics in bone tissue.

FTIR and Raman spectroscopy are similar in that they both nondestructively apply light (infrared light for FTIR and visible light for Raman) to change the vibrational energy state of the molecules within a sample. Because the different chemical motifs within the bone tissue have unique vibrational properties, the light that each motif emits following excitation has a unique wavenumber that can be collected and measured by a detector.[111] Typically, several measurements are taken from one point and then averaged, yielding a single spectrum (**Fig. 2.6**). This process can be repeated in multiple locations on a sample similar to nanoindentation, allowing for spatial differences in matrix composition to be determined. Importantly, these techniques can be used on either fresh bones or bones embedded in poly (methyl methacrylate) (PMMA), a polymer that can be used to stabilize thin samples. Because PMMA has its own chemical motif that overlaps with the bone spectrum, it may need to be subtracted from the final spectrum before analysis.[112] For FTIR, thin samples (2-5 μm) are necessary for proper light absorption, a range that is difficult to handle without embedding. On the other hand, samples for Raman spectroscopy can have any thickness because it relies only on surface light scattering. In either case, the part of the sample exposed to light must be flat and well-polished to prevent light scattering due to surface blemishes.

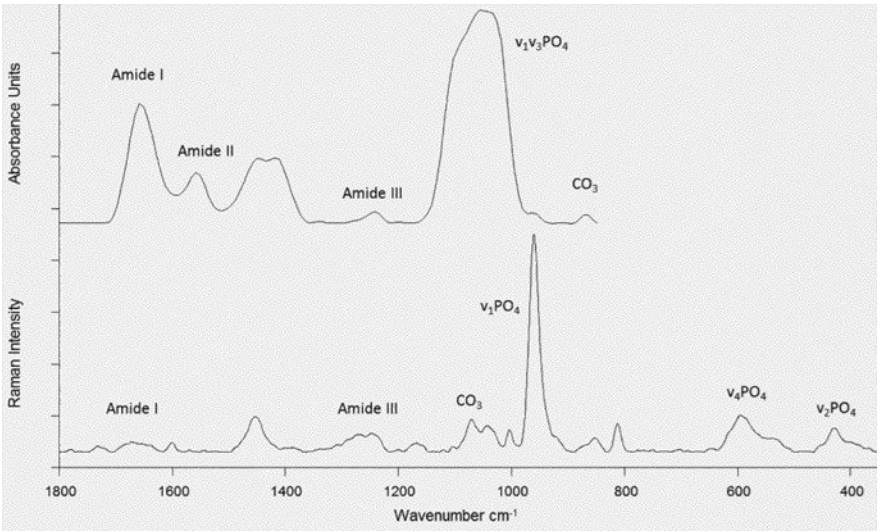

Fig. 2.6: Sample FTIR and Raman spectra. Spectral parameters are reported as either peak intensity or peak area ratios between the above marked peaks.

There are many chemical motifs that can be measured via spectroscopy that are related to mineral and matrix structure and relative quantity (**Table 2.2**). The most frequently reported is the mineral/matrix ratio, a measure of the extent of mineralization in the bone matrix. Additional measures include mineral crystallinity/maturity[113], carbonate substitution[114], proteoglycan content[115], lipid content[116], and collagen maturity[117] (**Table 2.2**).

Table 2.2: Parameters used to determine matrix composition using Raman spectroscopy.

Parameter	Peaks Used	Calculation
Relative Mineralization	Phosphate/Amide I Phosphate/CH_2 deformation Phosphate/Amide III	Area or intensity ratio
Crystallinity	Phosphate	1/full width half maximum
Carbonate Substitution	Carbonate/Phosphate	Area or intensity ratio
Proteoglycan Content	PG/Amide III	Area ratio
Lipid Content	Lipid/Amide III	Area ratio
Collagen Maturity	1660/1690 cm^{-1}	Area ratio

One limitation of spectroscopy is the general lack of parameters directly related to collagen quality. Upon investigation into the subpeaks with the amide peaks, which represent collagen, the area ratio between the 1660 cm^{-1} and 1690 cm^{-1} subpeaks was thought to be a measure of the relative quantity of enzymatic crosslinks between collagen fibrils.[118] However, in studies using a mouse model of osteolathyrism, a disease characterized by inhibition of crosslinking, no changes were found in the 1660/1690 ratio.[119,120] Additionally, the 1660/1690 ratio did not correlate with the quantity of enzymatic crosslinks determined by HPLC. However, the ratio correlated with crystallinity and relative mineralization, indicating that it may be reflective of changes in the secondary structure of collagen induced by mineralization. While the 1660 and 1690 peaks are more difficult to visualize in Raman spectroscopy than in FTIR, a positive correlation between the 1660/1690 and mineral/matrix ratios was also found, indicating that an increased ratio is likely associated with improved collagen quality/maturity.[117]

Both Raman spectroscopy and FTIR have been employed to understand the effects of slowly progressive CKD on bone matrix composition. Specifically, previous work has shown that administering PTH reduces crystallinity, increases the 1660/1690 ratio in mice, and reduces matrix mineralization as dosage increases.[121,122] Because hyperparathyroidism is common in dialysis

patients, it was hypothesized that altered matrix composition is partially responsible for lowering bone strength in ESRD patients. Several studies on the Cy/+ rat have indicated that there are no changes in mineral/matrix ratio, carbonate content, or crystallinity at 35 weeks of age.[11,104,108] Notably, the 1660/1690 ratio has not been reported in this model. Similar to the shortcomings of nanoindentation studies in the Cy/+ rat, spectroscopy has not been performed in regions with fluorescent labels indicating regions of bone formed with or without treatment, indicating the need for a more robust analysis.

2.4 Effects of PTH-lowering Therapies on CKD-MBD

SHPT is common in dialysis patients and has been linked to the development of increased bone fragility and mortality.[123,124] Therefore, strategies to lower PTH levels have been implemented to counteract these effects. One of the first methods employed was parathyroidectomy (PTX), or removal of the parathyroid glands. In a meta-analysis, PTX was shown to improve all-cause and cardiovascular mortality in CKD patients.[125] Additionally, PTX was associated with reduced fracture risk in CKD patients.[126] However, following PTX, lifelong calcium and vitamin D replacement therapy is required, and the anabolic effects of naturally produced PTH may be lost.[127] Current recommendations state that in CKD, PTH levels should be maintained within 2-9 times the upper limit and gradual changes in PTH levels should be monitored closely. Therefore, a non-surgical approach that can be titrated to maintain PTH levels in this range may be preferable.

One commonly used method of controlling PTH levels is calcitriol, the active form of vitamin D. While data examining the effects of calcitriol or other vitamin D analogues on bone is limited, meta-analyses have indicated that they are effective at lowering PTH levels.[128] In the Cy/+ rat, calcitriol also significantly lowered PTH. However, calcitriol treatment increased phosphorus levels and had no beneficial effects on bone architecture, organ-level mechanics, or tissue-level composition and mechanics.[108] A limitation here, however, was that fluorescent labels were not used, and thus, Raman spectroscopy and nanoindentation were performed on random points. Overall, while calcitriol may have the potential to suppress the effects of PTH on other components of CKD-MBD, it failed to improve skeletal properties.

PTH levels increase in response to low calcium in both healthy individuals and in those with CKD. However, the constant calcium deficit in CKD, as sensed by the decreased CaSR

activity in the parathyroid glands, results in SHPT. Therefore, the calcimimetic drugs cinacalcet and etelcalcetide were developed to agonize the CaSR, increasing both receptor activity and the affinity of calcium for the receptor.[129] Cinacalcet is an orally administered small molecule that reduced PTH to less than 250 pg/ml in 43% of patients after 26 weeks, a value well within the recommended range.[130] Similar findings were obtained in patients treated for two years.[131] Interestingly, upon reviewing data from cinacalcet trials, specifically for history of fracture, it was found that cinacalcet may reduce the rate of fracture from 16-29%.[16] It is important to note that the patient numbers in this analysis were statistically adjusted to account for study dropout, comorbidities, and concurrent medications that may influence bone health. Additionally, fracture risk was found to be more strongly improved in patients older than 65 (hazard ratio = 0.69) while there was no difference found in patients less than 65 (hazard ratio = 0.92).[16] As a whole, this study indicates that cinacalcet is the first drug that reduces fracture risk in CKD patients.

A newer peptide calcimimetic drug, etelcalcetide, has also been developed. This drug is administered intravenously three times per week following dialysis and was shown to have superior PTH control to cinacalcet, with nearly 70% of patients achieving greater than 30% reduction in PTH with lower incidence of side effects such as hypocalcemia.[21] Calcimimetics are a promising drug class for reducing fractures in CKD patients. Therefore, investigation into their effects on bone tissue-level properties may provide novel insight into the contribution of bone tissue-level properties to overall bone integrity. Furthermore, we are interested in determining whether calcimimetics can prevent the deleterious effects of chronically elevated PTH on the skeleton, which may prevent fractures. PTH also affects the process of perilacunar remodeling by osteocytes, so we also hypothesize that reducing PTH may improve bone properties adjacent to osteocyte lacunae.

3. CALCIMIMETICS ALTER PERIOSTEAL AND PERILACUNAR BONE MATRIX PROPERTIES IN EARLY CHRONIC KIDNEY DISEASE

As outlined in the preceding review of the literature, calcimimetics represent a promising drug class for lowering fracture incidence in patients with chronic kidney disease (CKD). However, it is not known whether calcimimetics can prevent CKD-induced bone deterioration early in CKD, which may occur in localized bone regions prior to the development of clinically visible bone disease. In this chapter, we describe a novel method for performing a colocalized assessment of bone matrix composition and material properties on hydrated bone specimens and apply it to a rat model of CKD treated with calcimimetics. Specifically, we will describe how CKD and calcimimetic treatment alter newly formed periosteal bone and perilacunar bone in a spatially dependent manner in early CKD, prior to the formation of cortical bone porosity. The content presented in this chapter is adapted from our previous works "Non-Additive Effects of Combined NOX1/4 Inhibition and Calcimimetic Treatment on a Rat Model of Chronic Kidney Disease-Mineral and Bone Disorder (CKD-MBD)" which was published in the *Journal of Bone Mineral Research Plus* and "Calcimimetics Alter Periosteal and Perilacunar Bone Matrix Properties in Early Chronic Kidney Disease", submitted to the *Journal of Bone and Mineral Research*. To produce a cohesive dissertation, we have focused on the skeletal data from the first study and made minor edits to the formatting and wording. The published version of the first referenced study chapter is made available under a Creative Commons Attribution License at the following link: https://doi.org/10.1002/jbm4.10600.

3.1 Abstract

Chronic kidney disease (CKD) affects 15% of Americans and greatly increases fracture risk due to elevated parathyroid hormone, cortical porosity, and reduced bone material quality. Calcimimetic drugs are used to lower PTH in dialysis patients, but their impact on bone matrix properties in early CKD remains unknown. We hypothesized that tissue-level bone quality is altered in early CKD and that calcimimetic treatment will prevent these alterations. To test this hypothesis, we treated Cy/+ rats, a model of spontaneous and progressive CKD-mineral and bone

disorder (CKD-MBD), with KP-2326, a preclinical analogue of etelcalcetide, early in the CKD disease course. To measure tissue-level bone matrix composition and material properties, we performed colocalized Raman spectroscopy and nanoindentation on new periosteal bone and perilacunar bone using hydrated femur sections. We found that CKD and KP treatment lowered mineral type B carbonate substitution while KP treatment increased mineral crystallinity in new periosteal bone. CKD lowered while KP treatment maintained reduced elastic modulus in this region. In perilacunar bone, KP treatment lowered type B carbonate substitution, increased crystallinity, and increased mieral-to-matrix ratio in a spatially dependent manner. KP treatment also increased reduced elastic modulus and hardness in a spatially dependent manner. Taken together, this data suggests that KP treatment improves material properties on the tissue level through a combination of lowering carbonate substitution, increasing mineral crystallinity, and increasing relative mineralization of the bone early in CKD. As a result, the mechanical properties on this scale were improved, and in some regions, were not different from control animals. Therefore, calcimimetics may help prevent CKD-induced bone deterioration by improving bone quality in new periosteal bone and in bone tissue near osteocyte lacunae.

3.2 Introduction

Chronic kidney disease (CKD) affects 15% of Americans and results in long-term mineral dysregulation, increasing the risk of skeletal fractures by 4-fold relative to the age- and sex-matched healthy population[7,132]. Skeletal fragility in CKD is precipitated by a combination of biochemical alterations including reduced 1,25-dihydroxyvitamin D and elevated parathyroid hormone (PTH)[3]. PTH, a potent regulator of serum calcium, has been positively correlated with the formation of pores in the cortical bone compartment, reducing its ability to bear loads on the structural level[133]. While cortical porosity is typically observed late in CKD, fracture risk is elevated across all stages of CKD[7]. Taken together, these findings indicate that CKD has detrimental impacts on bone matrix quality, increasing skeletal fragility on the intrinsic material level. Importantly, fracture-related mortality is up to three times higher in dialysis patients versus the age- and sex-matched population, indicating not only the need for therapies to reduce fractures, but to develop strategies to prevent fractures earlier in CKD[8].

Calcimimetics, a class of calcium-sensing receptor allosteric agonists, are frequently used to lower PTH levels in patients on dialysis. Previously, a secondary analysis of the Evaluation of

Cinacalcet Hydrochloride Therapy to Lower Cardiovascular Events (EVOLVE) trial demonstrated that calcimimetics may lower fracture incidence in patients with CKD, although the mechanism underlying this improvement has not been explored in clinical data[16]. Lowering PTH has been shown to cause cortical pore infilling in preclinical models of CKD and may therefore improve bone mineral density (BMD)[134]. While BMD is becoming more widely used to assess bone health in patients with CKD, high mineral content does not singularly improve bone toughness, the ability for the tissue to dissipate energy and prevent microdamage from rapidly progressing to mechanical failure[135]. Therefore, calcimimetics may partially increase fracture resistance by improving bone matrix quality. Matrix quality refers to the structural and compositional state of bone tissue on the nano- and micro-scales, understanding how these characteristics translate into material properties that impact whole bone mechanical integrity, and is critical to assessing fracture risk. Techniques such as Fourier-transform infrared spectroscopy (FTIR) and Raman spectroscopy have become widely utilized to measure compositional bone quality, including relative mineralization and crystallinity, and can be performed with a ~1 μm resolution[136,137]. Nanoindentation has become more common to measure intrinsic tissue stiffness and hardness on a similar length scale[138]. While these techniques provide a glimpse of the true tissue-level properties of bone, the heterogeneity of tissue properties at this scale can become problematic when averaging large datasets together without controlling for age of tissue in a specific region of bone and how recently it was formed[139]. Therefore, methods to control for tissue age are necessary, especially in the context of CKD where a progressive loss of kidney function is linked to worsened skeletal properties over time.

The mixed anabolic and catabolic effects of PTH on the skeleton are largely attributed to PTH signaling in osteocytes. Osteocytes respond to PTH by lowering sclerostin expression and secretion, increasing osteoblast bone formation activity[140]. When chronically elevated, as seen in CKD, PTH increases osteocyte-derived receptor activator of nuclear kappa-B ligand (RANKL), leading to increased osteoclast differentiation and bone resorption[141]. In rodents, these bone formation and resorption events primarily occur near bone surfaces, making the periosteal surface a promising location to detect matrix changes in CKD with high PTH and following calcimimetic treatment. Perilacunar remodeling, the process by which osteocytes alter their surrounding bone matrix, is also driven by PTH signaling[142,143]. This process involves a shift towards an osteoclastic gene expression profile within the osteocyte, including higher tartrate-resistant acid phosphatase, membrane-bound proton pumps, matrix metalloproteinases, and cathepsin K, indicating that

osteocytes are poised to remove both mineral and collagen[144,145]. While fewer studies have examined osteocytic matrix modeling, osteocytes upregulate mineral deposition genes in response to anabolic stimuli such as mechanical loading, and type I collagen expression has been detected using *in vitro* 2D osteocyte culture models[146]. Further, PTH signaling is essential for perilacunar remodeling and has been shown to mediate extracellular acidification, an essential step in the removal of bone mineral in the perilacunar region[147]. Therefore, it is plausible that the bone matrix near the osteocyte lacunae may present with differential compositional and mechanical properties in the settings of high PTH and calcimimetic-induced PTH suppression.

Previous studies from our group have demonstrated that the male Cy/+ rat, a model of progressive CKD-MBD, robustly develops hyperparathyroidism and cortical porosity by 35 weeks of age[73]. We recently noted that at 28 weeks of age, the CKD rats display hyperparathyroidism without altered cortical bone geometry or porosity[148], making this a potentially valuable timepoint to examine whether tissue-level composition and material properties are altered prior to cortical pore formation. Furthermore, this early timepoint provides the opportunity to determine whether calcimimetic treatment can prevent or limit CKD-induced alterations in bone quality. We hypothesized that bone matrix composition is disrupted and material-level mechanical properties are reduced in early CKD prior to the onset of structural deficits such as cortical porosity, and that calcimimetics will prevent these deleterious alterations. To test this hypothesis, we utilized male Cy/+ rats aged to 28 weeks, representing stage 4 CKD (~30% kidney function), and compared them to their healthy littermates and CKD rats treated with calcimimetics. We herein describe a novel method to evaluate colocalized compositional and material properties in the native hydrated state in newly formed periosteal bone guided by fluorochrome labeling, and in the osteocyte perilacunar region.

3.3 Materials and Methods

3.3.1 Animal Model

The Cy/+ rat model, containing a mutation in *Anks6* or SamCystin, was utilized as a gradually progressive model of CKD-MBD. Male, but not female, Cy/+ rats develop ESKD by 35 weeks of age. Previously, our group demonstrated that Cy/+ rats have elevated PTH without

cortical porosity at 28 weeks of age[148]. To determine whether matrix-level bone quality is altered early in CKD, we divided 28-week old male Cy/+ rats into three groups (*n*=12 per group):

1) Control Sprague Dawley littermates (CTRL)
2) Untreated Cy/+ rats (CKD)
3) Cy/+ rats treated with the calcimimetic drug KP-2326 (CKD/KP)

The study timeline is summarized in **Fig. 3.1**. All groups were placed on a standard rodent chow until 18 weeks of age, after which the animals were switched to a casein-based diet (0.7% Pi, 0.6% Ca, Envigo Teklad TD.04539). The casein diet increases dietary phosphorus content and creates a consistent CKD-MBD-like phenotype in CKD rats but does not alter biochemistries, vasculature, or bone in CTRL rats[73]. Treatment with KP-2326, a preclinical form of etelcalcetide, began at 18 weeks of age (0.6 mg/kg, thrice weekly, intraperitoneal injection (i.p.) in phosphate-buffered saline (PBS)). In our preliminary studies, this dose was shown to lower PTH without altering serum calcium levels. Calcein (30 mg/kg, i.p.) was administered 4 and 14 days prior to the end of the study to label actively forming bone surfaces. At 28 weeks of age, the animals were sacrificed by cardiac puncture and exsanguination followed by bilateral pneumothorax. The left femora were then harvested, wrapped in PBS-soaked gauze, and stored at -20°C until ready for sample preparation.

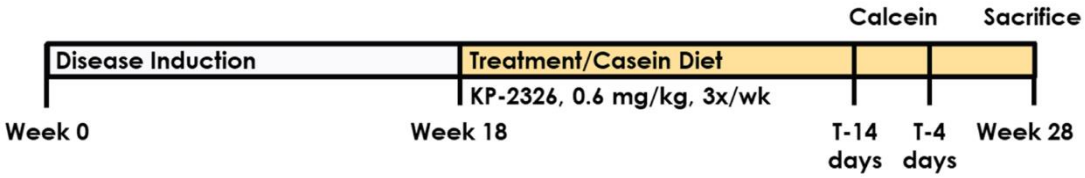

Fig. 3.1: Study Timeline. Animals were divided into three groups: healthy Sprague Dawley littermates (CTRL), Cy/+ (CKD), and KP-treated Cy/+ (CKD/KP). All animals were switched to a casein-based diet at 18 weeks of age. At this time, CKD/KP animals began treatment with 0.6 mg/kg KP-2326, thrice weekly. Calcein fluorochrome labels were administered 4 and 14 days prior to sacrifice at 28 weeks of age.

3.3.2 Blood Biochemistry

Blood plasma/serum was analyzed for blood urea nitrogen, creatinine, calcium, and phosphorus using colorimetric assays (Point Scientific, Canton, MI, or BioAssay Systems, Hayword, CA). Plasma intact PTH, serum C-terminal and intact FGF23 were determined by ELISA kits (Quidel, San Diego, CA).

3.3.3 Microcomputed Tomography of the Left Tibia and Femur

Micro-Computed Tomography (microCT) was performed using microCT (Skyscan 1172) at 12-micron resolution using methods previously published[149]. Briefly, a 1 mm region of interest of the proximal tibia starting approximately 0.5 mm from the distal end of the growth plate was used for analysis. Cortical bone parameters were assessed from 5 slices 4 mm distal to the end of the trabecular region. Trabecular bone volume fraction (BV/TV, %) and cortical porosity were quantified using CT analyzer (CTan). Whole left femora were scanned (Skyscan 1176) at 18-micron resolution to assess a subset of geometric properties at the mid-diaphysis for mechanical analysis using a custom MATLAB script. These properties include the distance from the centroid to the anterior bone surface (c) and the bending moment of inertia about the medial-lateral axis (I_{ML}). All CT analyses were done in accordance with standard guidelines[150].

3.3.4 Four-point Bending of the Left Femur

Femoral mechanical properties were assessed in 4-point bending on a mechanical testing system (TestResources). Bones were thawed to room temperature, hydrated in saline, and then placed anterior surface down on bottom supports (span = 18 mm). The upper supports (span = 7 mm) were brought down in contact with the specimen's posterior surface, and then testing was conducted at a displacement rate of 0.03 mm/s. Force versus displacement data were collected at 10 Hz and structural parameters were determined from curves using a custom MATLAB script. Material properties were estimated using the values of c and I_{ML} taken from the fracture site and standard beam-bending equations[151].

3.3.5 Sample Preparation for Tissue-level Analyses

The methods for sample preparation and subsequent analyses are summarized in **Fig. 3.2**. Left femora were placed into borosilicate glass culture tubes with the proximal end down. The proximal end was stabilized in modeling clay such that the sides of the bone were not touching the sides of the tube. Femora were embedded with a rapid-curing methylmethacrylate resin (Koldmount, Sigma), providing stability for subsequent polishing without infiltrating the bone matrix or dehydrating the specimen. After curing, two 1.5 mm thick sections were cut beginning at 37% along the length of the bone from the proximal end. Sections were sanded on both sides to

1 mm thickness. Specimens were polished on each side using a first a 3 µm and then a 0.05 µm water-based diamond suspension (Buehler, Lake Bluff, IL, United States). Finally, specimens were sonicated in PBS for 1 minute to remove residual polishing debris. Fluorescent imaging was performed to visualize calcein labels, marking regions of newly formed bone on the periosteal surface (**Fig. 3.2A**). These regions were mapped and utilized for selecting points in subsequent Raman spectroscopy and nanoindentation.

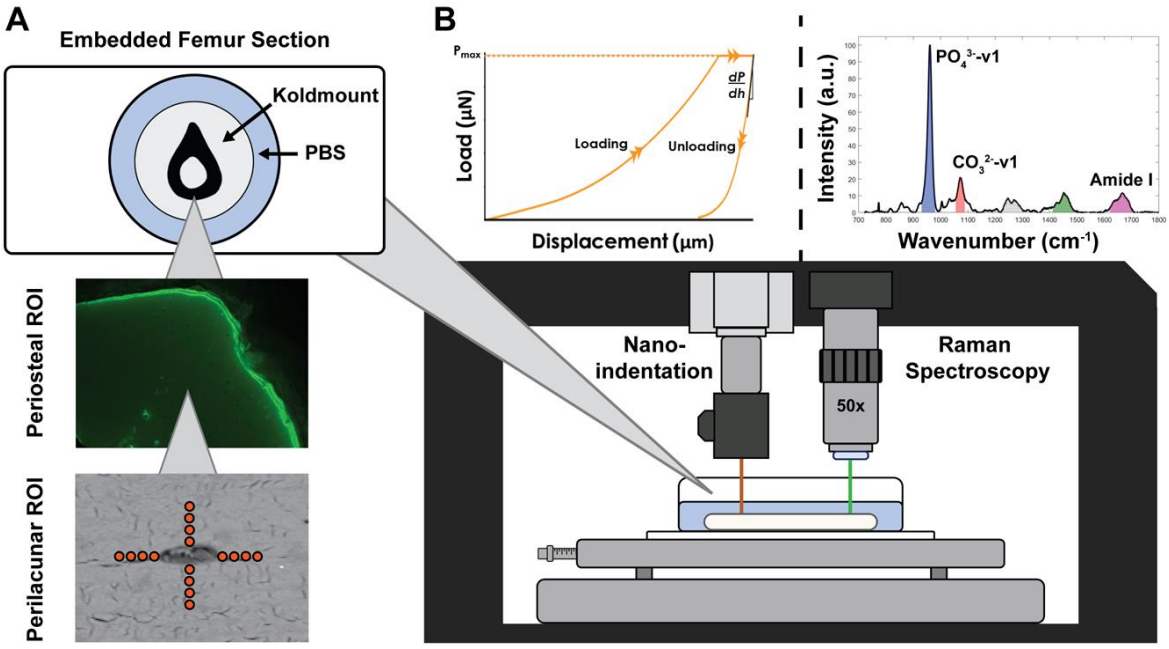

Fig. 3.2: Experimental Design. Left femora were embedded in Koldmount, sectioned, sanded, polished, and sonicated. To prepare for colocalized Raman spectroscopy and nanoindentation, a petri dish was superglued to a glass slide and the embedded sections were superglued into this dish (A, upper). Fluorochrome labels were used to select new periosteal regions (A, middle) while a second section was used to select perilacunar regions 1, 3, 5, and 7 µm from the lacunar wall of six lacunae per sample (A, lower). The hybrid system chamber (B, lower) was humidified prior to performing all Raman spectroscopy, which was analyzed for phosphate, carbonate, and amide I bands (B, upper right). PBS was added to the petri dish to submerge the samples prior to nanoindentation. P_{max} and the slope of the unloading curve (dP/dh) were used to calculate material properties at the same locations where Raman was performed (B, upper left).

3.3.6 Colocalized Raman Spectroscopy and Nanoindentation

Raman spectroscopy (inVia confocal Raman microscope, Renishaw, Wotton-under-Edge, United Kingdom) and nanoindentation (Hysitron TI 980 TriboIndenter, Bruker, Billerica, MA,

United States) were performed using a custom hybrid system equipped with a 50x objective, 785 nm laser and a 1.03 µm radius spherical diamond probe. Just prior to measurements, the samples were superglued to the bottom of a petri dish which was then superglued to a glass slide. The glass slide maintains rigid contact without slipping using a vacuum pump fed into the stage of the hybrid system. Prior to placing the samples, the interior chamber was humidified with damp paper towels to minimize sample dehydration and fluid evaporation. Submerging the samples in PBS was not possible at this step because it distorts the laser path, greatly lowering the amount of detectable Raman scattering from the bone. Raman spectroscopy was performed at 8 locations between calcein labels to analyze the matrix composition of newly formed bone and to control for tissue age across all specimens. Spectrographs were averaged across 8 accumulations with 8 seconds of exposure at 50% laser power, with a spatial resolution of ~1 µm. The averaged spectrograph underwent baseline correction using an 11^{th} order polynomial followed by cosmic ray removal. Smoothing was performed using a modified Savitzky-Golay function with maximum likelihood estimation to preserve features near bands of interest. Compositional parameters were calculated from smoothed spectrographs as described previously: mineral-to-matrix ratio (MMR, $\nu1\text{-}PO_4^{3-}$/Amide I band areas), type B carbonate substitution ($\nu1\text{-}CO_3^{2-}/\nu1\text{-}PO_4^{3-}$ band areas), and crystallinity (inverse of the full width at half maximum of a Gaussian curve fitted to $\nu1\text{-}PO_4^{3-}$) using a custom MATLAB script (**Fig. 3.2B**, upper right)[152]. The output parameters from each specimen were averaged, yielding one value per parameter per specimen.

Immediately following Raman spectroscopy, nanoindentation was performed at the same locations to determine material properties with a 1 µm resolution. The dish containing the sample was filled with PBS to maintain hydration throughout the course of indentation. Indents were performed in load control up to 1,000 µN, held for 45 seconds, and subsequently unloaded. The resulting load-displacement curves were analyzed for reduced elastic modulus (**Eq. 2.1**) and hardness (**Eq. 2.2**), where S is the slope of the 95%-40% region of the unloading curve, β is a geometric factor derived from the shape of the indenter probe, A is the contact area of the probe with the specimen surface, and P_{max} is the maximum load on the load-displacement curve.

A second section from each femur (adjacent to the previous) was used for colocalized Raman spectroscopy and nanoindentation in osteocyte perilacunar bone regions. Six osteocytes per sample within the posterolateral region were selected, and points were chosen at 1, 3, 5, and 7

μm from the lacunar wall in the four directions shown in the lower panel of Figure 2A. Colocalized Raman spectroscopy and nanoindentation were performed as described above.

3.3.7 Quantitative Backscatter Electron Imaging (QBEI)

Following nanoindentation, samples were removed from their slides and dehydrated using a vacuum pump for 48 hours. Specimens underwent carbon coating using carbon evaporation in preparation for backscatter electron imaging on a scanning electron microscope (JEOL 7800F, Akishima, Tokyo, Japan), a technique that has been validated for measuring mineral density distribution in bone[153]. Regions of newly formed bone were imaged and contrast-adjusted using backscatter images of standards with known atomic number: aluminum (Z=13) and carbon (Z=6). Brightness and contrast adjustments were performed by obtaining a gray level for aluminum of 225 ± 1 and carbon of 25 ± 1. Histograms of newly formed bone regions were created using ImageJ and were used to calculate bone mineral density distributions (BMDD). Distributions were analyzed for mean calcium content (Ca_{Mean}), peak calcium content (Ca_{Peak}), and calcium content heterogeneity (Ca_{Width}).

3.3.8 Statistical Analysis

For blood biochemistries, statistical analyses were conducted by first excluding outliers using ROUT (Q = 1%). For blood biochemistries, microcomputed tomography, and four-point bending, a normality test was performed ($p < 0.05$ with Anderson-Darling Test). If normality testing was fulfilled, we used a One-way ANOVA and, if overall ANOVA showed $p < 0.05$, we conducted within group comparisons by Dunnett's post hoc analyses, comparing untreated CKD rats versus each of the other groups. If normality was not fulfilled, then the data for each group was first log transformed, normality confirmed, and then the identical analyses as above performed. Periosteal data (Raman spectroscopy, nanoindentation, and QBEI) were analyzed by one-way ANOVA with posthoc Tukey's test to determine differences in composition and mechanical properties between the three animal groups. Perilacunar cumulative distribution data for Raman spectroscopy and nanoindentation were analyzed by Anderson-Darling and Kolmogorov-Smirnov tests with a Bonferroni correction (significance set at $p = 0.0167$) to determine differences in

property distributions in the perilacunar region. The results are expressed as means ± standard deviation [47] (GraphPad Prizm Software, La Jolla, CA).

3.4 Results

3.4.1 The Effects of KP Treatment on CKD-MBD Biochemistries

There were no differences in body weight between the animal groups. There was impaired kidney function at the endpoint, as indicated by a 2.4-fold higher plasma BUN (**Fig. 3.3A**) and serum creatinine (**Fig. 3.3B**) levels in CKD compared to normal rats with no effect of treatment. Plasma phosphorus levels were higher in CKD animals compared to normal animals (**Fig. 3.3C**), but plasma calcium levels were not different between animal groups (**Fig. 3.3D**). The plasma levels of PTH (**Fig. 3.4A**) were significantly higher than normal in all CKD groups. As expected, CKD rats treated with KP-2326 had lower PTH levels compared to non-treated CKD animals (1.9-fold decrease in CKD/KP compared to CKD). CKD animals also demonstrated higher serum C-terminal and intact FGF23 levels compared to normal animals (**Fig. 3.4B,C**).

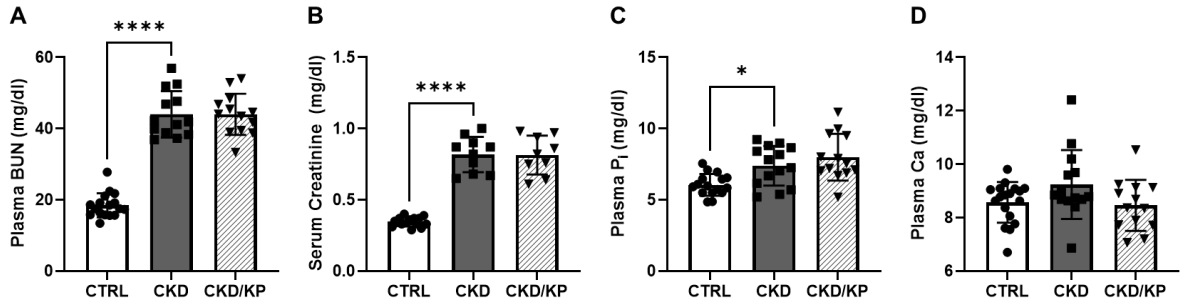

Fig. 3.3: Serum markers of CKD in 28-week old Cy/+ rats. BUN (A), creatinine (B), and phosphorus (C) were elevated in CKD animals compared to normal. Calcium levels were not altered in CKD animals (D). No biochemistries were altered by the treatments. Data are shown as mean ± SD and analyzed by One-way ANOVA. If $p < 0.05$, Dunnett's multiple comparison test was performed for each group versus CKD: *$p < 0.05$, ****$p < 0.0001$.

3.4.2 Effects of KP Treatment on Bone Structure and Mechanics

MicroCT assessment of the proximal tibia demonstrated lower trabecular bone volume fraction and trabecular number in CKD animals compared to normal animals (**Fig. 3.5A**, **Appendix A.1**). The average trabecular thickness was unchanged by CKD and treatment while the average separation between trabeculae was higher in CKD rats compared to normal rats (**Appendix A.1**). There was no effect of KP on trabecular bone geometry (**Fig. 3.54A**). Analysis of cortical bone at proximal 1/3 of the tibia showed no cortical porosity (**Fig. 3.5B**) in CKD rats, likely due to the earlier study endpoint and therefore less severe CKD compared to our previous studies[149]. Furthermore, there were no changes in cortical bone area, or cortical thickness in CKD animals compared to normal (**Appendix A.1**). Analysis of force-displacement and stress-strain mechanical data revealed a lower ultimate force, but no differences in the tissue-level properties in CKD animals compared to normal (**Table 3.1**). KP treatment did not alter any structural or tissue-level mechanical properties compared to CKD animals.

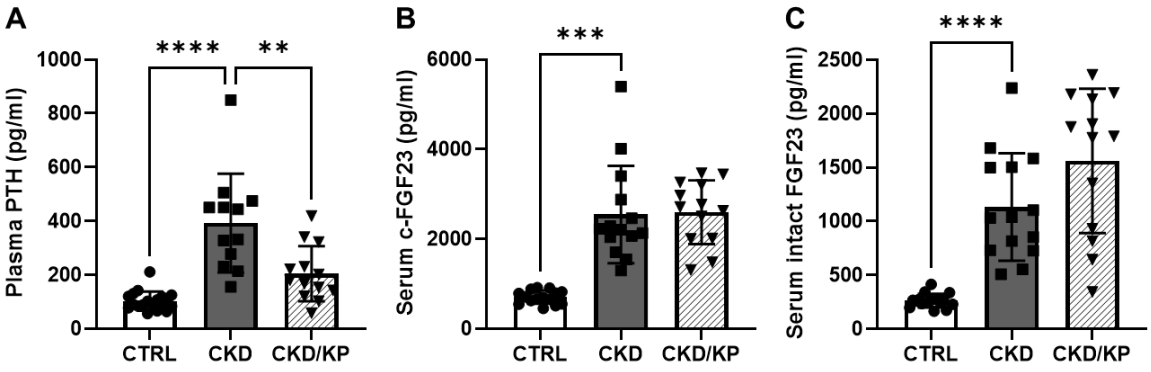

Fig. 3.4: Serum markers of mineral homeostasis and oxidative stress in 28-week old Cy/+ rats. PTH was significantly elevated in CKD animals and lowered by KP treatment (A). cFGF23 levels were elevated in CKD (B) while intact levels were increased in CKD but not altered by treatment (C). Data are shown as mean ± SD and analyzed by One-way ANOVA. If $p < 0.05$, Dunnett's multiple comparison test was performed for each group versus CKD: *$p < 0.05$, *$p < 0.01$, ***$p < 0.001$, ****$p < 0.0001$.

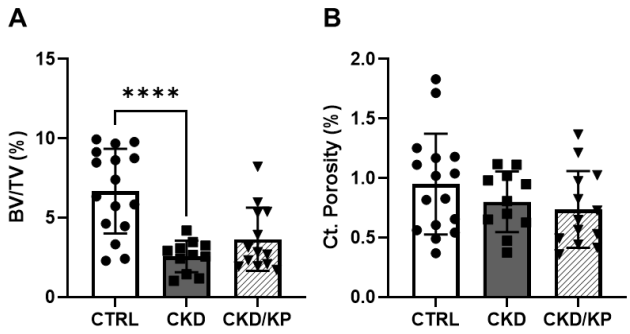

Fig. 3.5: The effects of KP treatment on trabecular and cortical bone. Bone volume fraction of trabecular bone was significantly decreased in CKD animals compared to normal animals and was not altered by treatment (A). Cortical porosity was not altered in CKD rats or by treatment (B). Data are shown as mean ± SD and analyzed by One-way ANOVA. If $p<0.05$, Dunnett's multiple comparison test was performed for each group versus CKD: *$p<0.05$, ****$p<0.0001$.

Table 3.1: Mechanical Properties of the Left Femur. Data are shown as mean ± SD and analyzed by One-way ANOVA. Dunnett's multiple comparison test was performed for each group versus CKD: **$p < 0.01$.

	Yield force (N)	Ultimate force (N)	Total displacement (mm)	Stiffness (N/mm)	Total work (mJ)	Yield Stress (MPa)	Ultimate Stress (MPa)	Total Strain (mε)	Modulus (GPa)	Toughness (MPa)
CTRL	220 ± 50	302 ± 35**	775 ± 95	529 ± 98	140 ± 30	121.± 23	167 ± 19	42.7 ± 5.98	5.41 ± 1.31	4.27 ± 0.86
CKD	199 ± 37	265 ± 23	772 ± 108	465 ± 66	125 ± 28	119 ± 22	160 ± 21	41.1 ± 4.80	5.24 ± 0.94	4.04 ± 1.08
CKD/KP	197 ± 32	273 ± 19	770 ± 82	502 ± 81	130 ± 17	122 ± 24	168 ± 12	40.5 ± 5.73	5.96 ± 1.38	4.19 ± 0.53

3.4.3 CKD and KP Treatment Alter Periosteal Bone Matrix Composition and Mechanics

Raman spectroscopy in new periosteal bone, taken as the region between calcein labels, revealed no differences in mineral-to-matrix ratio (MMR) between the three groups (**Fig. 3.6A**). Mineral crystallinity was significantly higher in CKD/KP animals vs CTRL (**Fig. 3.6B**). Type B carbonate substitution was significantly lower in CKD and CKD/KP animals vs CTRL (**Fig. 3.6C**). Nanoindentation in this periosteal region showed that reduced elastic modulus was significantly lower in CKD vs CTRL (**Fig. 3.7A**). Reduced modulus was higher in CKD/KP vs CKD, but failed to reach significance ($p = 0.059$, **Fig. 3.7A**). Tissue hardness was not different between the three groups (**Fig. 3.7B**).

3.4.4 KP Treatment does not alter Calcium Content in New Periosteal Bone

Bone mineral density distributions of newly formed bone regions were used to determine whether CKD or KP treatment alter calcium content in age-matched regions of bone. No differences were found in Ca_{Mean}, Ca_{Peak}, or Ca_{Width} between groups (**Fig. 3.8A-C**), indicating that changes in calcium, a metric that is not detected by Raman spectroscopy, was likely not responsible for the altered material properties seen using nanoindentation.

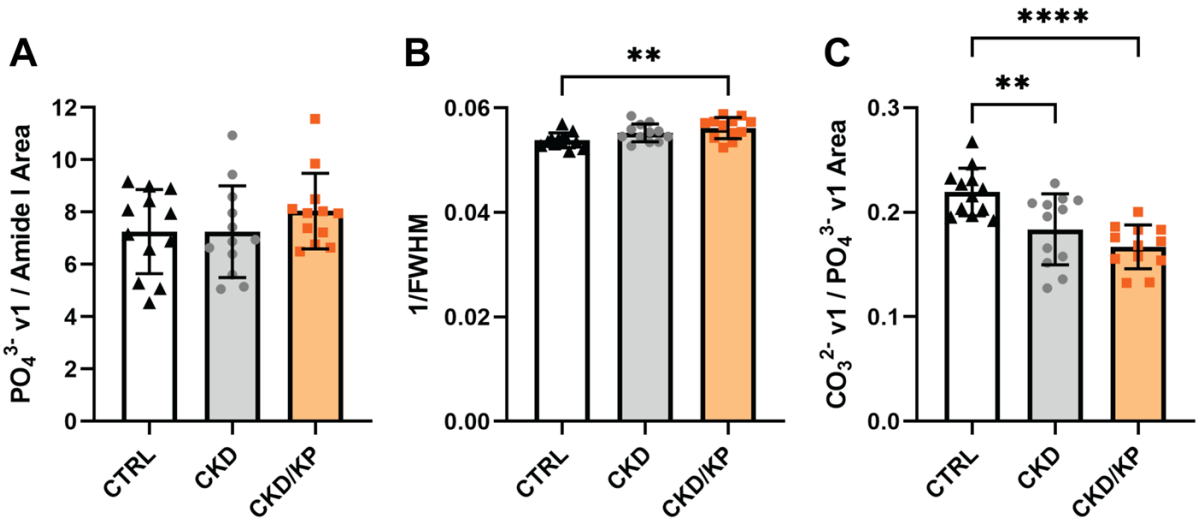

Fig. 3.6: KP Treatment Increases Mineral Crystallinity and Lowers Type B Carbonate Substitution. Mineral-to-matrix ratio was not different between groups (A). Mineral crystallinity was significantly higher in CKD/KP vs CTRL (B). Type B carbonate substitution was significantly lower in CKD and CKD/KP vs CTRL (C). $^{**}p<0.01$; $^{****}p<0.0001$.

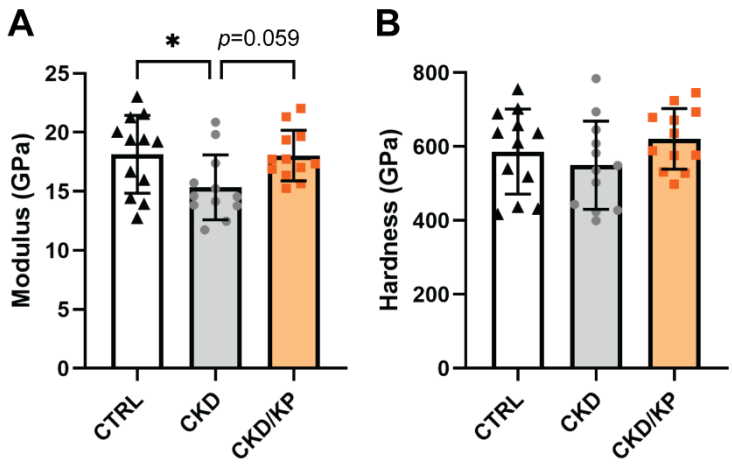

Fig. 3.7: KP Treatment Maintains Reduced Modulus at CTRL Levels. Reduced modulus was significantly lower in CKD vs CTRL (A). CKD/KP increased reduced modulus vs CKD but was not significantly different from CKD or CTRL (A). Tissue hardness was not different between groups (B). *p<0.05.

3.5 CKD and KP Treatment Alter Perilacunar Bone Matrix Composition and Mechanics in a Spatially Dependent Manner

To determine the large-scale distribution of compositional properties in the perilacunar region, we analyzed histograms incorporating all Raman signatures collected, separated by lacunar distance (144 measurements per lacunar distance per group). Type B carbonate substitution distribution was significantly right-shifted in CTRL and CKD vs CKD/KP at all distances (**Fig. 3.9A-D**). Mineral crystallinity was significantly right-shifted in CKD/KP vs CTRL at all distances and vs CKD at 3, 5, and 7 μm (**Fig. 3.9E-H**). Finally, we found that MMR distribution was significantly right-shifted in CKD/KP vs CTRL at all locations, and vs CKD at 1 and 5 μm from the lacunar wall (**Fig. 3.9I-L**). MMR in CKD/KP vs CKD at 3 μm had a right-shift trend but did not pass our modified p-value threshold from the Bonferroni correction.

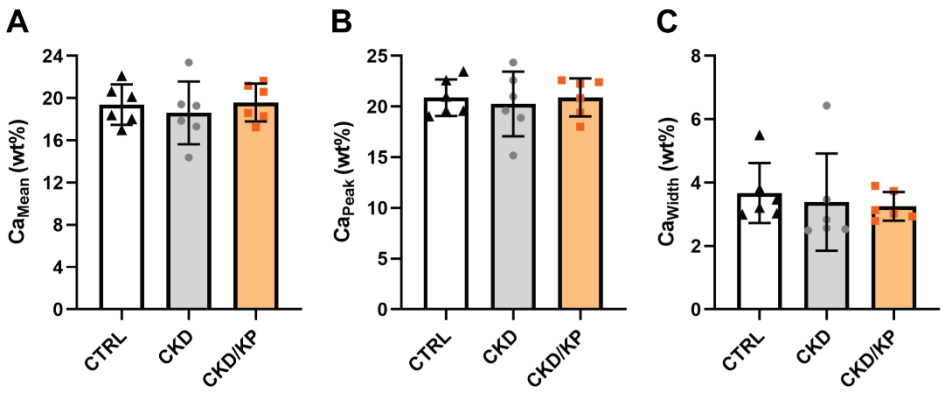

Fig. 3.8: CKD and KP Treatment do not alter Periosteal Calcium Content. No differences between groups were found in mean or peak calcium content or in calcium distribution width/heterogeneity (A-C).

Nanoindentation in the perilacunar region demonstrated a significantly right-shifted reduced modulus distribution in CKD/KP and CTRL vs CKD at all distances (**Fig. 3.10A-D**). Reduced modulus was also significantly right-shifted in CTRL vs CKD/KP at 1 μm but was not different at 3, 5, or 7 μm (**Fig. 3.10A-D**). For tissue hardness, distributions were significantly right-shifted in CKD/KP vs CKD at 3, and 5 μm (**Fig. 3.10E-G**) with a higher trend at 1 μm. CTRL distributions were significantly right-shifted vs CKD at 1, 3, and 5 μm and trended higher vs CKD/KP at 1 μm (**Fig. 3.10E-H**).

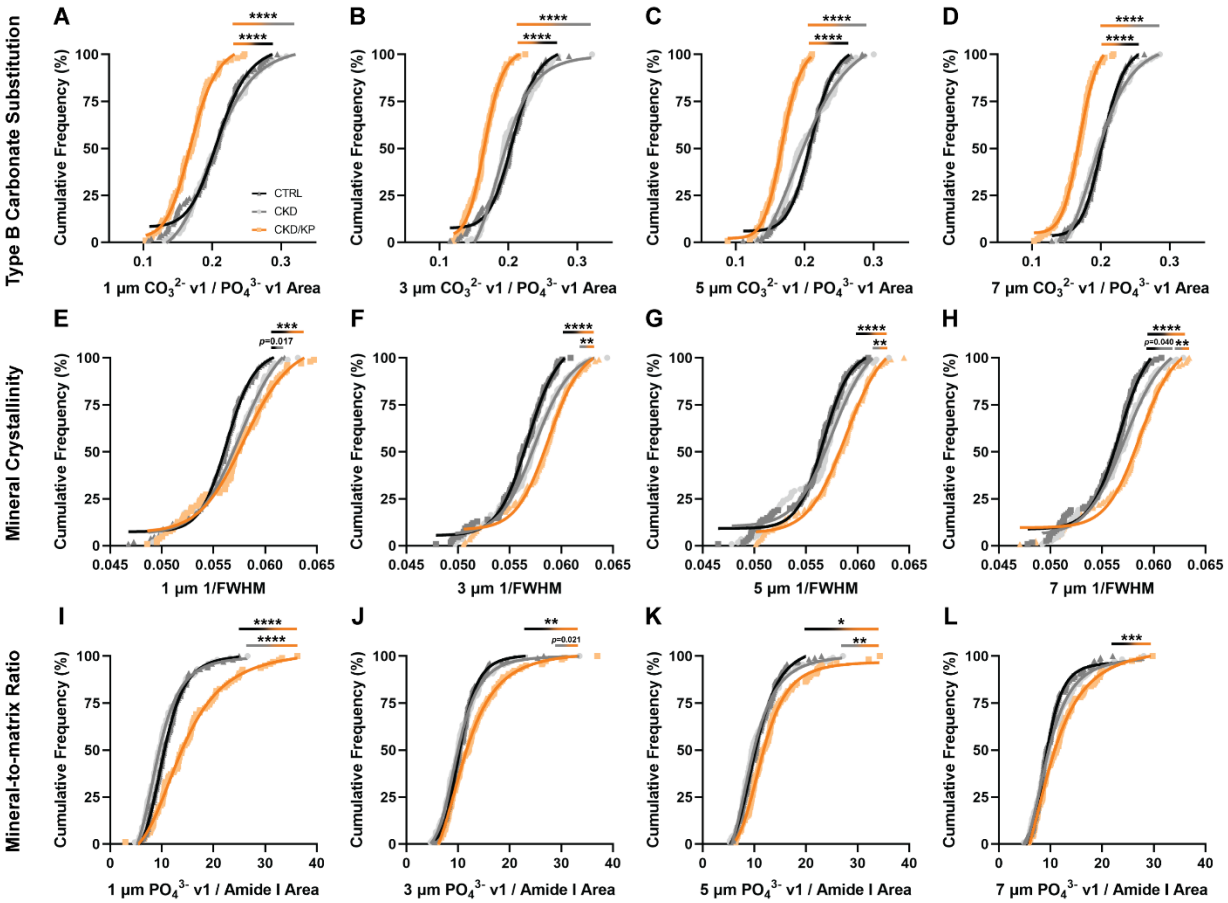

Fig. 3.9: KP Treatment Lowers Carbonate Substitution while Increasing Crystallinity and Mineral-to-matrix Ratio. Type B carbonate substitution was right-shifted in CTRL and CKD vs CKD/KP at all distances (A-D). Mineral crystallinity was right-shifted in CKD/KP vs CTRL at all distances and vs CKD at 3, 5, and 7 µm (E-H). Mineral-to-matrix ratio was right-shifted in CKD/KP vs CTRL at all distances and vs CKD at 1 and 5 µm. *p<0.0167; **p<0.01; ***p<.001; ****p<0.0001.

3.6 Discussion

In this study, we determined that early-stage CKD and calcimimetic intervention alter matrix-level bone composition and material properties in newly formed periosteal bone and in the osteocyte perilacunar region. CKD lowered type B carbonate substitution vs CTRL in new periosteal bone and lowered reduced modulus at all locations in perilacunar bone. CKD also lowered hardness up to 5 µm from the lacunar wall vs CTRL. KP treatment increased mineral crystallinity in new periosteal bone, lowered type B carbonate substitution in perilacunar bone, and generally increased reduced modulus and hardness in perilacunar bone vs CKD. These data support the idea that CKD has detrimental effects on the bone matrix that may occur prior to

clinically visible signs of bone disease (e.g. prior to the onset of increased cortical porosity) and that calcimimetics may help mitigate or prevent these alterations.

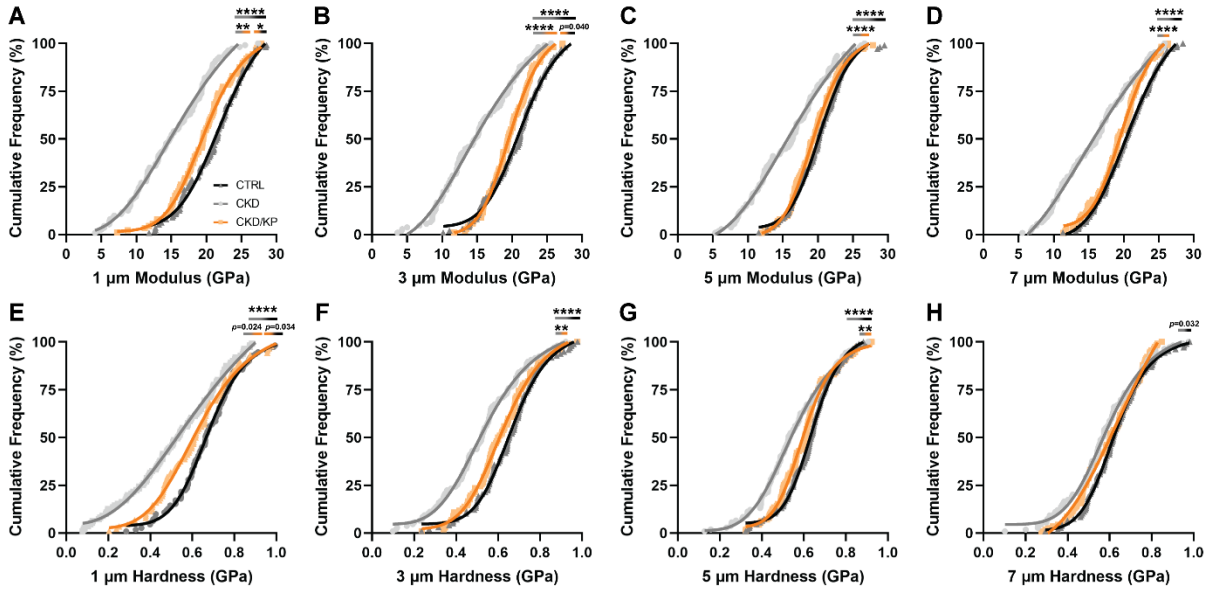

Fig. 3.10: KP Treatment Improves Material Property Distributions in Perilacunar Bone. Reduced modulus was significantly right-shifted CKD/KP and CTRL vs CKD at all distances. CTRL was significantly right-shifted vs CKD/KP at 1 µm. Hardness was significantly right-shifted in CKD/KP vs CKD at 3 and 5 µm and in CTRL vs CKD at 1, 3, and 5 µm. *p<0.0167; **p<0.01; ***p<.001; ****p<0.0001.

Male Cy/+ rats represent a robust and gradually progressive model of CKD-MBD, undergoing biochemical alterations related to mineral homeostasis, aortic calcification, culminating in structural bone alterations including cortical thinning and pore formation at 35 weeks of age. Recently, our group analyzed a cohort of 28-week old CKD rats and found that despite having low kidney function and high PTH vs control rats, microcomputed tomography detected no structural and limited mechanical changes in the long bones. Therefore, we hypothesized that performing Raman spectroscopy and nanoindentation on 28-week old specimens may reveal changes in the bone matrix that precede pore formation. While tissue-level analyses have been performed in rodent models of CKD, including the Cy/+ rat, controlling for tissue age by injecting calcein double labels is not common in published data. Indeed, Raman spectroscopy and nanoindentation of 35-week old Cy/+ rats without controlling for the tissue age of the selected regions has previously revealed no differences in tissue-level composition or mechanics vs CTRL rats[11]. Given the progressive nature of bone deterioration in CKD, we hypothesize that controlling

for tissue age was necessary to detect differences in compositional and material properties between groups in this study.

Numerous published studies perform Raman spectroscopy and nanoindentation on fixed and/or dehydrated specimens, often using matrix-infiltrating poly (methyl methacrylate) to embed the bones[154,155]. Recent research suggests that a loss of bone water during sample dehydration increases stiffness and lowers postyield properties such as toughness and can mask disease-induced alterations to bone matrix quality and material properties[156,157]. Postyield properties are critical to fracture resistance in bone, as material toughening mechanisms are necessary to prevent rapid crack propagation and mechanical failure, a feature that is partially portrayed in tissue hardness data[158]. Embedding media and sample fixation/dehydration have also have significant impacts on Raman spectral parameters, as the infiltrating media create overlapping bands in the Raman signature[159]. To the best of our knowledge, we are among the first to use fresh specimens while preserving hydration by humidifying the specimen chamber during Raman spectroscopy and submerging the samples in PBS during nanoindentation. We hypothesize that our method reduced the heterogeneity brought by averaging data points from all bone regions, allowing for a focused analysis on skeletal properties in regions formed under high PTH, with or without treatment. Taken together, our use of age-matched regions in fresh, hydrated samples preserved the native tissue state and the intrinsic compositional and mechanical features of the bone.

Bone mineral is a carbonated hydroxyapatite where substitution of phosphate for carbonate is driven by the similar size and charge between the two ionic compounds. We found significantly less type B carbonate substitution in new periosteal bone in CKD animals vs CTRL and a slight but non-significant increase in crystallinity in CKD vs CTRL (**Fig. 3.6B-C**). Previous studies suggest that carbonate substitution lowers mineral crystallinity as carbonate dilates the *c*-axis and shrinks the *a*-axis of the mineral crystal, indicating that the bond stretching induced by the presence of carbonate may not have been enough to measure a change in crystallinity using Raman[160]. However, we did observe a larger magnitude difference in carbonate substitution in KP-treated rats vs CTRL, which may have driven the significantly higher crystallinity observed in CKD/KP vs CTRL. This finding is also supported by the nanoindentation data, where we found no difference between reduced modulus in CKD/KP vs CTRL (**Fig. 3.7A**). Reduced elastic modulus is a tissue-level measure of material stiffness (resistance to elastic deformation) and is positively correlated

with higher crystallinity[161]. Therefore, these data support that higher mineral quality contributes to higher reduced modulus in KP-treated rats.

While MMR was not significantly different between groups in new periosteal bone, MMR trended higher in CKD/KP vs CKD (**Fig. 3.6A**). MMR is useful for approximating the relative mineralization of bone tissue, but it represents a ratio between mineral and collagen and does not distinguish which component underwent an absolute increase or decrease. Therefore, we performed QBEI in regions of new periosteal bone to determine whether mineral density was altered in CKD or by KP treatment. We found no differences in calcium content or heterogeneity between groups (**Fig. 3.8**). While surprising, this supports our hypothesis that the improvement in reduced modulus in CKD/KP vs CKD was caused by higher mineral crystallinity and lower type B carbonate substitution.

Intact PTH signaling is essential for triggering matrix remodeling by osteocytes, a process that is critical in mediating calcium release and restoration in lactation and weaning, respectively[147]. While this phenomena has not been explored in CKD where high PTH is common, we hypothesized that osteocyte interactions with the bone matrix could contribute to the skeletal detriments in CKD, and that altered matrix composition and material properties can be detected in the perilacunar region when PTH is high but porosity is not evident. Notably, we found a higher MMR at 1 and 5 μm from the lacunar wall in CKD/KP vs CKD, a higher trend at 3 μm, but no difference at 7 μm (**Fig. 3.9I-L**). MMR is reflective of the relative mineralization of the tissue, indicating that calcimimetics increase relative tissue mineralization in CKD up to 5 μm from the osteocyte lacuna. MMR was also higher in CKD/KP vs CTRL at all distances. Taken together, these data indicate that while CKD did not change relative mineralization of the perilacunar bone, calcimimetics are capable of increasing mineralization in the perilacunar region up to 5 μm from the lacunar wall.

Interestingly, the trends in matrix composition in CKD/KP vs CKD are paralleled by colocalized mechanical data obtained from perilacunar nanoindentation. Reduced modulus was higher in CKD/KP vs CKD at all perilacunar distances and modulus distributions in CKD/KP were not different from CTRL at 3, 5 and 7 μm (**Fig. 3.10A-D**). MMR was significantly higher or trended higher at all distances except 7 μm and crystallinity was higher at all but 1 μm in CKD/KP vs CKD. In particular, the MMR data points to a specific region around osteocytes that can undergo further mineralization by lowering PTH in CKD. While the changes in MMR and crystallinity do

not completely overlap, one or the other is increased at each perilacunar distance, which is likely responsible for the increased modulus seen at all locations.

While several compositional differences were found between CKD/KP and CKD in the perilacunar region, the only difference detected in CKD vs CTRL was a right-shift trend in mineral crystallinity at 1 and 7 μm from the lacunar wall while mechanical properties were lower at all perilacunar distances in CKD vs CTRL (**Fig. 3.9-3.10**). This likely indicates that CKD causes material alterations that were not detected by our methods, such as disrupted collagen quality through the formation of advanced glycation end products, which are formed in CKD due to increased oxidative stress and inflammation[162,163]. We hypothesize that the high crystallinity near the lacunae may be caused by high serum phosphorus in CKD, which may be incorporated by the osteocyte into newly formed, highly crystalline bone. However, additional detriments must exist that prevent this change from resulting in a higher reduced modulus in the region nearest the osteocyte lacuna.

Interestingly, tissue hardness was also higher in CKD/KP vs CKD perilacunar bone up to 5 μm from the lacunar wall (**Fig. 3.10E-H**). Hardness is reflective of the ability of a material to resist plastic/permanent deformation, a property that depends on the organic components of the bone matrix including collagen and water and has been correlated with higher mineralization[158]. While higher MMR and crystallinity typically increase reduced modulus and lower hardness, it is possible that collagen content/quality and/or bound water were also higher in these regions to compensate for the increased mineralization. Future studies specifically interrogating the role of collagen quality and hydration in bone material properties in CKD are warranted.

In conclusion, CKD and calcimimetic treatment altered bone matrix composition and mechanical properties in animals representing ~stage 4 CKD despite the lack of overt bone deterioration at this timepoint. These findings may contribute to the increased fracture resistance postulated by analysis of the EVOLVE trial, demonstrating a crucial parallel between microscale data and clinical findings. While the notion that microscale bone properties determine the macroscale material properties of the bone is not new, our study is among the first to analyze matrix composition and mechanics in colocalized, tissue age-matched regions of hydrated bone. This opens the possibility to use micromechanical testing to analyze viscoelastic properties, where maintaining native tissue hydration is critical. Future studies will also examine whether initiating treatment at this timepoint improves skeletal microarchitecture and mechanical properties at a later

timepoint representing ESKD, which may point to the efficacy of lowering PTH earlier in the disease course of CKD.

4. A NOVEL MURINE MODEL OF COMBINED TYPE 1 DIABETES AND CHRONIC KIDNEY DISEASE EXHIBITS UNIQUE SKELETAL ALTERATIONS VERSUS THE SINGLE DISEASE STATES

As described in the introduction and background, diabetes is the leading cause of chronic kidney disease (CKD) worldwide. While both conditions increase fracture risk independently, little is known about the skeletal phenotype of patients with both conditions. The cause of this is two-fold: firstly, patients with diabetes are frequently excluded from clinical trials patients with CKD. Secondly, there is a general lack of robust, combined preclinical models of diabetes and CKD. The creation of such a model coupled with a multiscale characterization of skeletal properties may be essential to drive a clinical interest in the combined disease state. This chapter highlights our recent efforts to develop a novel combined model of type 1 diabetes (T1D) and CKD. Specifically, we will describe the biochemical phenotype, bone turnover, microarchitecture, and mechanical properties of this model, which showcases a combined phenotype that does not fully match either disease individually. The content presented in this chapter is adapted from our work "A Novel Murine Model of Combined Type 1 Diabetes and Chronic Kidney Disease Exhibits Unique Skeletal Alterations versus the Single Disease States", submitted to the *Journal of Bone and Mineral Research*. Minor edits to the wording and formatting have been made to create a cohesive dissertation.

4.1 Abstract

Diabetes and chronic kidney disease (CKD) consistently rank among the top ten conditions in prevalence and mortality in the United States. Type 1 diabetes (T1D) and CKD each increase the risk of skeletal fractures and fracture-related mortality. While it is well established that T1D is a major cause of CKD, there exist no robust preclinical models of combined T1D and CKD to determine whether these diseases have interactive effects on the skeleton. We hypothesized that combining T1D and CKD in mice would cause structural and mechanical bone alterations that are more deleterious compared to the single disease states. Female C57BL6/J mice were divided into four groups: 1) Control (CTRL), 2) Streptozotocin-induced T1D (STZ), 3) Adenine diet-induced CKD (AD), and 4) Combination (STZ+AD). STZ and STZ+AD mice had significantly higher blood glucose, HbA1c, and glucose intolerance. AD and STZ+AD mice had higher blood urea

nitrogen while only AD mice had high serum parathyroid hormone and phosphorus vs CTRL. STZ+AD mice had a uniquely lower mineralizing surface while AD mice had high turnover vs all groups. Trabecular bone volume was not different in STZ+AD vs CTRL. Tissue mineral density was lower in all groups in trabecular bone but only in STZ and STZ+AD in cortical bone. Cortical porosity of the proximal tibia was higher while moment of inertia was lower in all disease groups, and most cortical properties were lower in STZ+AD vs AD. Ultimate force and toughness were lower in all groups vs CTRL while total displacement/strain were only lower in STZ+AD vs CTRL. Fracture toughness was lower in AD and STZ+AD vs CTRL. Taken together, structural and material-level bone properties are altered by STZ and AD while their combination resulted in several unique or worsened detriments, indicating that improving bone health in the combined disease state may require novel interventions.

4.2 Introduction

Type 1 diabetes (T1D), a disease caused by autoimmune destruction of pancreatic β cells, is characterized by elevated blood glucose, glucose intolerance, and high morbidity due to end organ damage to the heart, nerves, skin, brain, and kidneys [164,165]. 50-70% of patients with T1D will experience chronic kidney disease (CKD) in their lifetime as persistent hyperglycemia progressively damages the glomerulus, the major filtration unit of the kidney [132,166]. Consequently, CKD has broad systemic impacts due to chronic inflammation, oxidative stress, and unfiltered uremic byproducts [167,168]. While these sequelae of T1D and CKD are widely recognized, clinical studies have demonstrated that patients with either T1D or CKD alone experience more skeletal fractures than their age- and sex-matched healthy counterparts [7,169]. Strikingly, fracture-related mortality is increased 1.5-fold in T1D and 3-fold in CKD, demonstrating the importance of preserving fracture resistance in these patients [7,8,170].

While T1D and CKD increase fracture risk independently, clinical data suggests that they have both distinct and overlapping impacts on the skeleton. For example, skeletal fragility in T1D is linked to lower bone mineral density (BMD) and trabecular bone mass [171,172], and in CKD, lower BMD and higher cortical porosity have been positively correlated with increased fracture incidence [87,133]. Additionally, both diseases are known to affect bone quality by altering turnover and increasing the formation of advanced glycation end products (AGEs) that non-enzymatically crosslink bone collagen, increasing tissue stiffness while decreasing toughness and ductility [173,174].

Based on this, we hypothesized that T1D and CKD have additive detriments on bone structural properties while the unique matrix-level effects of each disease may magnify changes in tissue quality that are not typically present in the single disease states.

Despite the well-established link between T1D and CKD, their combined impact on systemic and skeletal health has not been explored due to the lack of robust preclinical combined disease models. Numerous models of T1D have been presented in the literature, including streptozotocin (STZ)-induced β cell ablation and the *Akita* and NOD transgenic mouse models [175]. While these models robustly develop and maintain hyperglycemia, kidney function typically remains intact without overt azotemia, uremia, or dysregulated mineral homeostasis [176,177]. Models of kidney disease typically involve adding nephrotoxic agents to the rodent diet or performing surgeries such as 5/6 nephrectomy or ureteral obstruction [178] However, the surgical models have high rates of mortality and rapidly lose kidney function, failing to model the progressive nature of CKD [61]. To develop a model with fine-tuned control over the onset of insulin loss and hyperglycemia with subsequently reduced kidney function, our group combined STZ-induced β cell ablation with a nephrotoxic adenine-containing diet to model the combined disease state of T1D+CKD. The overall goal of this study was to provide an entry point for investigating the complex interactive effects of co-morbid conditions that are exceedingly common and deadly in the population with diabetes.

4.3 Materials and Methods

4.3.1 Animal Model

Female C57BL6/J mice (N=49) were divided into four groups to determine whether a unique phenotype exists in combined T1D and CKD vs either disease alone:

1) Control (CTRL), N=12
2) Streptozotocin-induced type 1 diabetes (STZ), N=12
3) Adenine diet-induced chronic kidney disease (AD), N=12
4) Combined model (STZ+AD), N=13

The study timeline is summarized in **Fig. 4.1**. At 8 weeks of age, T1D was induced in STZ and STZ+AD mice by injecting streptozotocin (90 mg/kg, intraperitoneally (i.p.) in citrate buffer, daily for 5 days), a cytotoxic agent that selectively ablates β cells by entering the GLUT2 transporter

[179]. Citrate buffer was prepared with 65 mM citric acid monohydrate and 35 mM citric acid disodium trihydrate (Sigma Aldrich, St. Louis, MO, United States), diluted two-fold with sterile water, and adjusted to pH 4.5. At 14 weeks of age, CKD was induced in AD and STZ+AD mice by administering a 0.2% adenine-containing casein-based diet for 6 weeks. The casein diet has an altered mineral ratio (0.9% phosphorus, 0.6% calcium) and drives the robust mineral disturbances seen in CKD. During this timeframe, CTRL and STZ animals received a casein control diet without adenine to control for mineral levels. At 20 weeks of age, AD and STZ+AD animals were switched to the casein control diet to further their mineral disturbances for an additional 4 weeks. Calcein fluorochrome labels (30 mg/kg, i.p.) were administered 2 and 7 days prior to sacrifice to label actively forming bone surfaces. All animals were sacrificed at 24 weeks of age via cardiac exsanguination followed by cervical dislocation. The collected blood was stored for further analysis. Pancreata were harvested, fixed in neutral buffered formalin (NBF) for 48 hours, and transferred to 70% ethanol. The right femur was harvested, fixed in NBF, and serially dehydrated with an ethanol gradient. Bilateral tibiae, the right femur, and the L4 vertebrae were harvested, wrapped in PBS-soaked gauze, and stored frozen at -20°C. N=2 AD mice died unexpectedly at 16 weeks of age and were excluded from analysis.

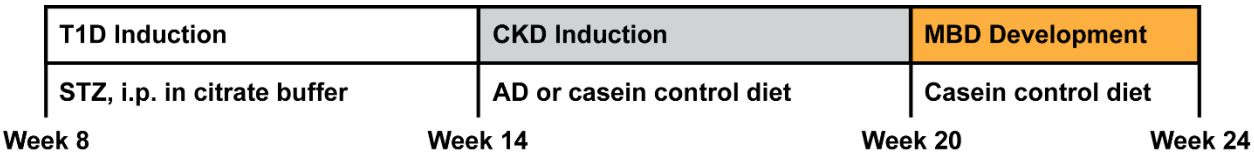

Fig. 4.1: Study Design. Streptozotocin was administered to STZ and STZ+AD animals at 8 weeks of age. At 14 weeks of age, AD and STZ+AD animals were switched to a 0.2% adenine-containing diet while CTRL and STZ animals were switched to a casein control diet. At 20 weeks of age, AD and STZ+AD animals were switched to the casein control diet.

4.3.2 Weight and Glucose Monitoring

Animal weights and blood glucose levels were monitored biweekly to track glycemic status using tail bleeds and an Alphatrak 2 glucometer (Parsipanny-Troy Hills, NJ, United States). Diabetes was defined as blood glucose >250 mg/dl on at least two subsequent readings and maintained for the study duration. Animals that failed to surpass the 250 mg/dl threshold were excluded from the final analysis (N=2 STZ and N=4 STZ+AD).

4.3.3 Glucose Tolerance Testing

Glucose tolerance tests (GTTs) were performed one week prior to sacrifice in all animals. Following an overnight fast, a baseline blood glucose was measured prior to glucose administration (1 g/kg, i.p.). Blood glucose was measured 10, 20, 30, 60, 90, and 120 minutes post-injection. To calculate glucose intolerance, the area under the baseline glucose measure was subtracted from the area under the glucose-time curve using the trapezoid rule [180].

4.3.4 Blood Biochemistries

Blood collected from cardiac exsanguination was used to measure serum blood urea nitrogen [18] via a colorimetric assay (BioAssay Systems, Hayward, CA, USA) to assess kidney function. Serum calcium and phosphorus were measured using colorimetric assays (Pointe Scientific, Canton, MI, USA), and serum 1-84 PTH was measured by ELISA (Immunotopics Quidel, San Diego, CA, USA).

4.3.5 β Cell Mass

Fixed pancreata were paraffin-embedded, and 6 μm thick sections were cut at 12 equidistant intervals across the length of pancreas. Sections 2, 5, 7, and 11 were stained for insulin using a rabbit anti-insulin antibody (Cell Signaling Technology, Danver, MA) to label β cells. β cell area fraction was calculated using ZEN (ZEISS, Oberkochen, Germany), by dividing the total insulin-positive pancreas area by the overall tissue area across the four sections per animal. β cell mass was determined by multiplying the area fraction by the mass of each pancreas.

4.3.6 Dynamic Histomorphometry

Fixed and dehydrated right femora were embedded in poly(methyl methacrylate) (Sigma Aldrich, St. Louis, MO, United States), and 4 μm thick frontal sections were cut for analysis of fluorescent calcein labels. Trabecular dynamic histomorphometry was performed using BIOQUANT (BIOQUANT Image Analysis, Nashville, TN, United States). All histomorphometric nomenclature follows standard guidelines [181]. Trabecular regions of interest were selected 0.02 mm from the primary spongiosa and excluded cortical bone surfaces. Total bone surface (BS), single-labeled surface (sLS), double-labeled surface (dLS), and interlabel distances were measured

at 20x magnification. Mineralized surface to bone surface (MS/BS; [dLS+(sLS/2)]/BS*100), mineral apposition rate (MAR; average interlabel distance/5 days), and bone formation rate (BFR/BS; MS/BS*MAR]*3.65) were calculated.

4.3.7 Fluorescent AGE Quantification

Following mechanical testing, left tibia had their marrow flushed with saline and were incubated in Immunocal (Decal Chemical Corporation, Congers, NY, USA) to demineralize the bone for 16 hours. The demineralized tibiae were then hydrolyzed in 6M HCL at 110°C for 16 hours. AGE content was determined using fluorescence readings at wavelengths of 370 nm/440 nm excitation/emission against a quinine sulfate standard on a plate reader (Spectramax M5, Molecular Devices, San Jose, CA, United States). The AGE content for each sample was normalized by the amount of collagen present, determined using a hydroxyproline assay kit (Sigma-Aldrich USA, St. Louis, MO, USA).

4.3.8 *Ex vivo* Microcomputed Tomography of the Tibia, Femur, and L4 Vertebrae

Frozen left tibiae, left femora, and L4 vertebrae underwent microcomputed tomography using a Skyscan 1172 (Bruker, Billerica, MA). Scans were performed at 60 kV in 0.5° steps with a 0.5 aluminum filter and 9.8 μm isometric voxels. Prior to scanning, a phantom calibration was performed using a hydroxyapatite standard (0.25 and 0.75 g/cm^3 CaHA). Trabecular bone microarchitecture was analyzed in a 1 mm region of interest immediately distal to the end of the growth plate in the proximal tibia. Bone volume fraction and trabecular geometry were analyzed using CT Analyzer (CTAn) (Bruker, Billerica, MA). Cortical bone properties were analyzed from a 1 mm region of interest taken in the mid-diaphysis, centered 50% along the length of the tibia. Cortical bone geometries and cortical thickness were calculated using a custom MATLAB script. Cortical porosity was further analyzed in 1 mm intervals spaced 10% of the tibia length apart ranging from 20% to 80% along the length of the tibia using CTAn.

Left femora and L4 vertebrae were scanned using the settings described above. Cortical geometry at the mid-diaphysis of the femur was calculated using a custom MATLAB script for fracture toughness testing and cortical porosity. A region of interest containing the entirety of the

vertebral body but excluding cortical bone was selected for the L4 vertebrae and analyzed for trabecular bone volume fraction and microarchitecture using CTAn.

4.3.9 Four-point Bending

Left tibiae were thawed to room temperature and mechanically tested to failure on an ElectroForce 5500(TA Instruments, New Castle, DE, United States) while hydrated in phosphate-buffered saline (PBS). The four-point bending setup consisted of a lower support span of 9 mm and an upper span of 3 mm. Bones were tested in load-control at a displacement rate of 0.025 mm/s until failure. The resulting load-displacement data were analyzed for structural mechanical properties using a custom MATLAB script as described previously [98]. The fracture site on each specimen was measured using calipers, and this site was analyzed for the moment of inertia about the bending axis (I_{AP}) and the furthest distance from the centroid of the bone to the tensile (medial) surface (c). These values were fed into standard beam bending equation to covert the load-displacement values into stress-strain values. From the resulting stress-strain curves, material-level properties were calculated using a custom MATLAB script. The yield point was defined using the 0.2% offset method on the stress-strain curve and elastic modulus was calculated as the slope of the linear (elastic) portion of the stress-strain curve.

4.3.10 Fracture Toughness Testing

Bone resistance to crack propagation was assessed using a linearly elastic fracture toughness testing approach. Right femora were notched at the anterior mid-diaphysis using a low-speed sectioning saw (Buehler, Lake Bluff, IL, United States) not more than halfway through the medullary cavity. The notch was sharpened using a scalpel coated with a 1 μm diamond suspension. Femora were loaded in three-point bending with the notched surface in tension, and the crack was advanced until failure. Marrow was removed and femora were dehydrated using a vacuum pump. After gold sputtering, the crack surface was imaged using a scanning electron microscope (JEOR, Akishima, Tokyo, Japan). Stable and unstable crack lines were identified using a custom MATLAB script, and the cortical bone geometry was used to calculate the stress intensity factors for crack initiation, maximum load, and fracture instability.

4.3.11 Statistical Analysis

Serial measurements (animal weights and weekly glucose testing) were analyzed by repeated measures ANOVA with posthoc Tukey's test to analyze properties between groups across time. Cortical porosity was analyzed by two-way ANOVA with posthoc Tukey's test for main effects of animal group and length along the tibia. Endpoint data were analyzed by one-way ANOVA with posthoc Tukey's test.

4.4 Results

4.4.1 Disease Induction

Body weights were lower in STZ and STZ+AD following STZ administration vs CTRL at all timepoints (**Fig. 4.2A**). AD animals had lower body weight vs CTRL after switching to the adenine diet but recovered once switched to the casein control diet, although this trend was not seen in STZ+AD animals (**Fig. 4.2A**). Next, type 1 diabetes induction was assessed using biochemistries and pancreas immunohistochemistry. Non-fasting blood glucose was significantly elevated in STZ and STZ+AD mice vs CTRL and AD within two weeks of STZ administration (**Fig. 4.2B**). Glucose tolerance tests revealed significant glucose intolerance (greater area under the curve) and elevated hemoglobin A1c (HbA1c) in STZ and STZ+AD animals vs CTRL and AD (**Fig. 4.2C-E**). Importantly, three animals in the STZ and four animals in the STZ+AD group never crossed the 250 mg/dl glucose threshold for diabetes, did not have elevated HbA1c, and were excluded from analysis. Insulin staining of the pancreas revealed intact islets in CTRL and AD mice, while insulin positive regions were sparse in STZ and STZ+AD mice (**Fig. 4.3A-D**). Pancreatic β cell area and mass were significantly lower in all groups vs CTRL and in STZ and STZ+AD vs AD (**Fig. 4.3E,F**).

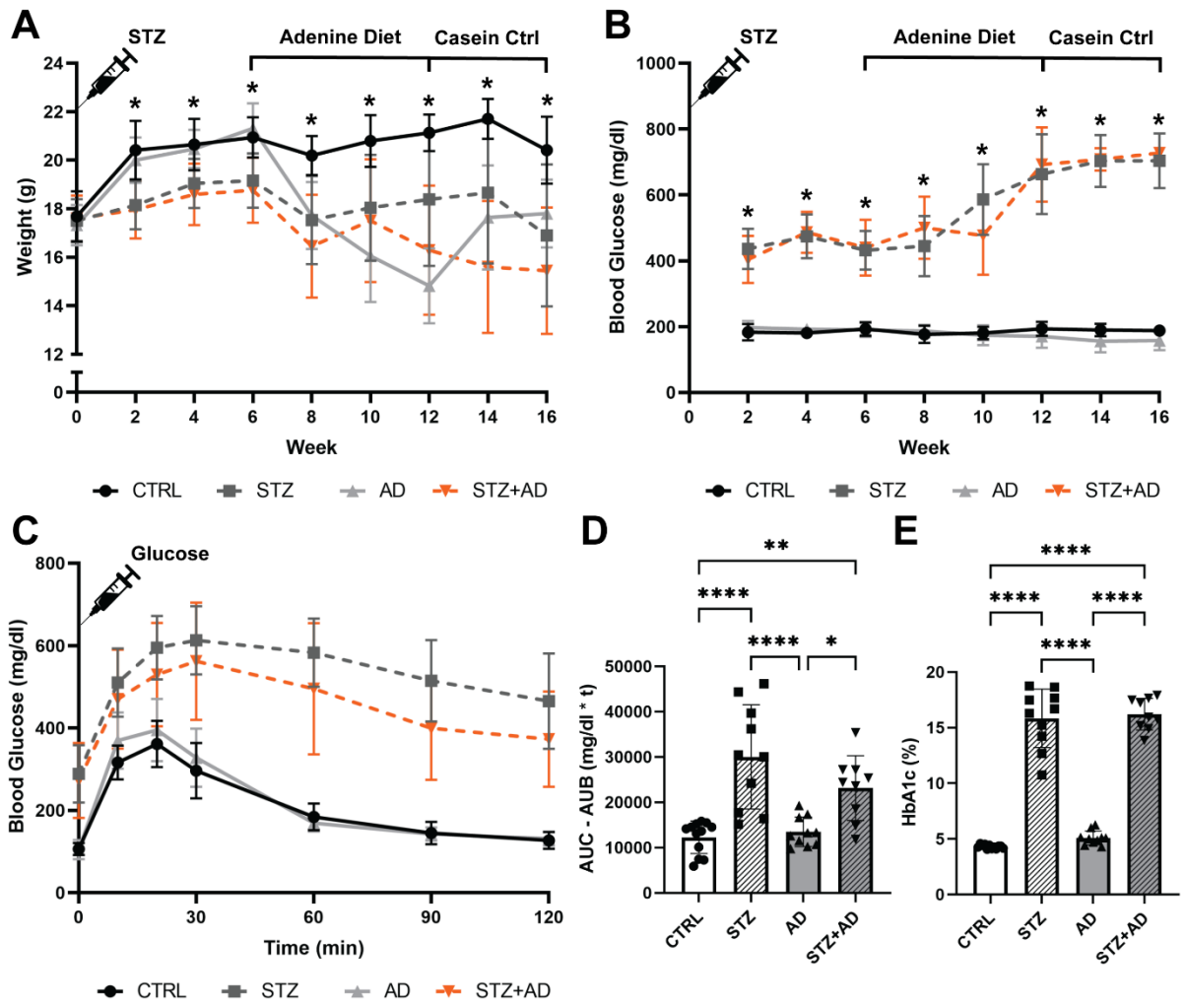

Fig. 4.2: Streptozotocin Induces a Type 1 Diabetes-like Phenotype in STZ and Combination Mice. Biweekly body weights indicated significant differences between at least two groups at all timepoints after baseline. In general, STZ and AD lowered body weight, but AD mice regained body weight when switched to the casein control diet (A). STZ led to higher blood glucose in STZ and STZ+AD at all timepoints post-injection (B). Glucose tolerance tests were performed by tracking blood glucose for two hours post-glucose injection (C), revealing glucose intolerance in STZ and STZ+AD (D). HbA1c was higher in STZ and STZ+AD mice (E). *AUC = area under curve; AUB = area under baseline; HbA1c = Hemoglobin A1c.* Serial measures: *p<0.05 between at least two groups. Endpoint measures: *p<0.05; **p<0.01; ***p<0.001; ****p<0.0001.

The induction of CKD and mineral disturbances were assessed using serum biochemistries. AD and STZ+AD animals displayed higher BUN vs CTRL, indicating reduced kidney function (**Fig. 4.4A**). Serum calcium was higher in AD vs STZ animals and phosphorus was higher in AD animals vs all groups (**Fig. 4.4B,C**). Interestingly, mineral levels were not altered in STZ+AD

animals vs CTRL (**Fig. 4.4B,C**). Finally, PTH was higher in AD vs all groups, and was not higher in STZ+AD vs CTRL (**Fig. 4.4D**).

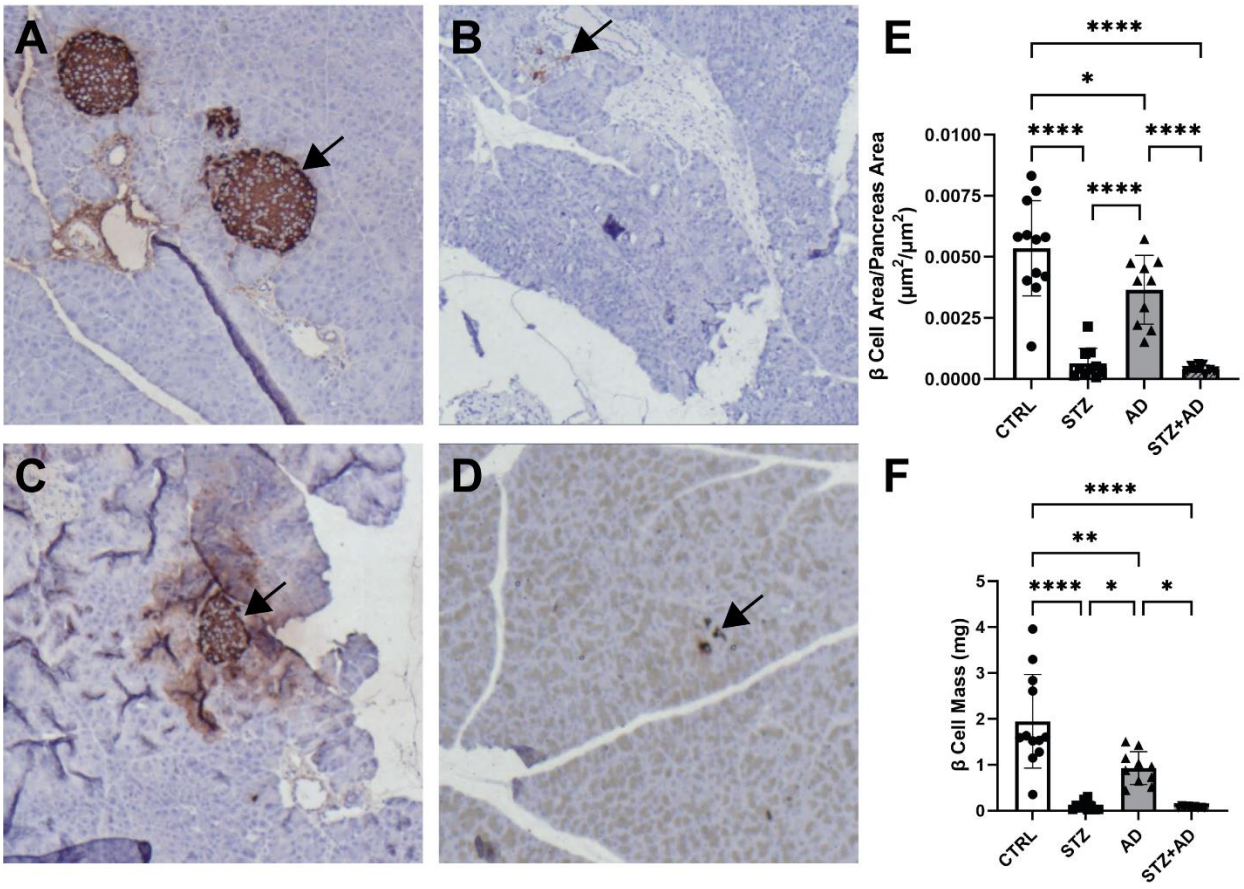

Fig. 4.3: Streptozotocin Ablates β Cells in STZ and Combination Mice. Pancreatic islets (arrows) in CTRL (A), STZ (B), AD (C), and STZ+AD (D) mice were stained with an anti-insulin antibody. Islets were abundant in CTRL and AD mice while insulin staining was only positive in small patches in STZ and STZ+AD mice. β cell area was quantified and divided by total pancreas area (E), demonstrating lower area fraction all groups vs CTRL. Area fractions were multiplied by raw pancreas mass to calculate β cell mass (F). β cell mass was significantly lower in all groups vs CTRL, especially in STZ and STZ+AD mice.

4.4.2 Dynamic Histomorphometry

Bone turnover was assessed by analyzing fluorescent calcein labels in the trabecular bone of the femur. MS/BS, the relative amount of mineralizing surface of the trabecular bone, was lower in STZ+AD vs CTRL and AD (**Fig. 4.5A**). MAR, the rate of mineral addition to the bone, was higher in AD vs STZ and STZ+AD (**Fig. 4.5B**). BFR/BS, a measure of bone turnover, was higher

in AD vs CTRL and STZ+AD (**Fig. 4.5C**). Importantly, several samples in the STZ, AD, and STZ+AD groups did not exhibit a clear second label and were not included in analysis for MAR or BFR/BS.

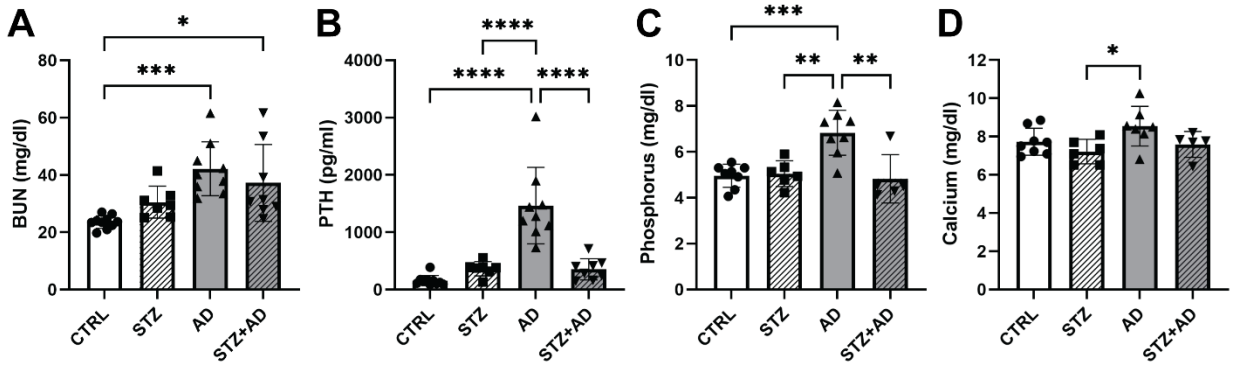

Fig. 4.4: Mineral Homeostasis is not Dysregulated in Combination Mice. AD and STZ+AD mice had higher BUN vs CTRL (A). AD mice had higher serum PTH (B) and phosphorus (C) vs all other groups. Calcium was higher in AD mice vs STZ (D). *BUN = blood urea nitrogen; PTH = parathyroid hormone.* **p*<0.05; ***p*<0.01; ****p*<0.001; *****p*<0.0001.

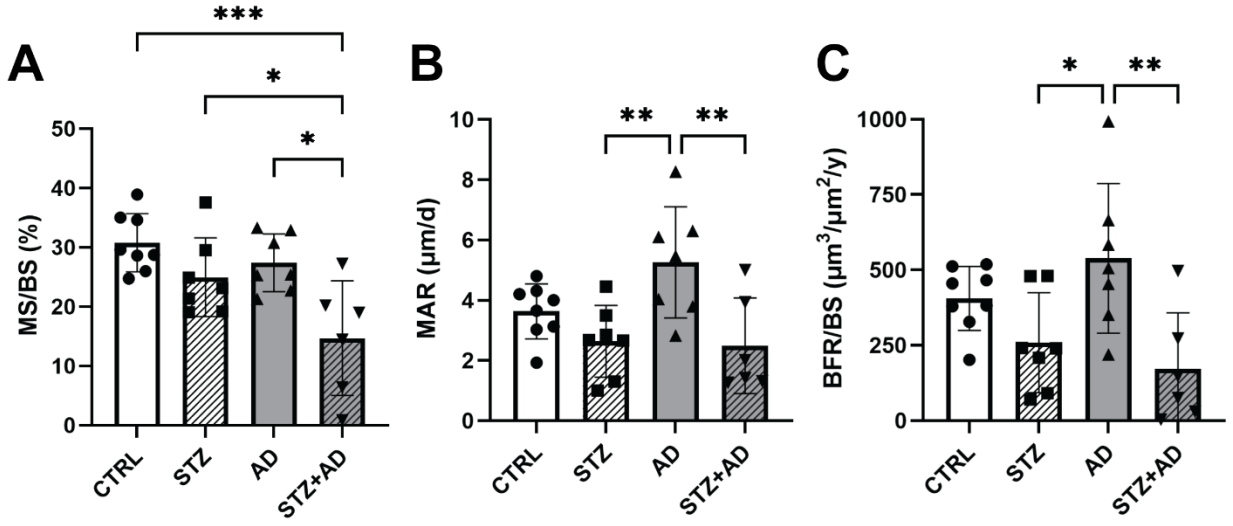

Fig. 4.5: Combination Mice Exhibit Lower Trabecular Mineralizing Surface without High Turnover. STZ+AD lowered MS/BS vs CTRL, STZ, and AD (A). AD mice had higher MAR and BFR/BS vs STZ and STZ+AD. *MS/BS = mineralizing surface/bone surface; MAR = mineral apposition rate; BFR/BS = bone formation rate/bone surface.* **p*<0.05; ***p*<0.01; ****p*<0.001.

4.4.3 Trabecular and Cortical Microarchitecture

Skeletal microarchitecture was assessed by MicroCT of the tibia and vertebrae. In the tibia, bone volume fraction (BV/TV) was lower in STZ vs CTRL and higher in AD vs CTRL and STZ (**Fig. 4.6A**). BV/TV was lower in STZ+AD vs AD but was not different from CTRL or STZ (**Fig. 4.6A**). Trabecular thickness was lower in all groups vs CTRL but was higher in AD vs STZ and STZ+AD (**Fig. 4.6B**). Trabecular number was higher in AD vs CTRL and STZ and was higher in STZ+AD vs CTRL (**Fig. 4.6C**). Trabecular separation was not different between any groups (**Fig. 4.6D**). Finally, tissue mineral density (TMD) was lower in all groups vs CTRL and in STZ+AD vs AD (**Fig. 4.6E**).

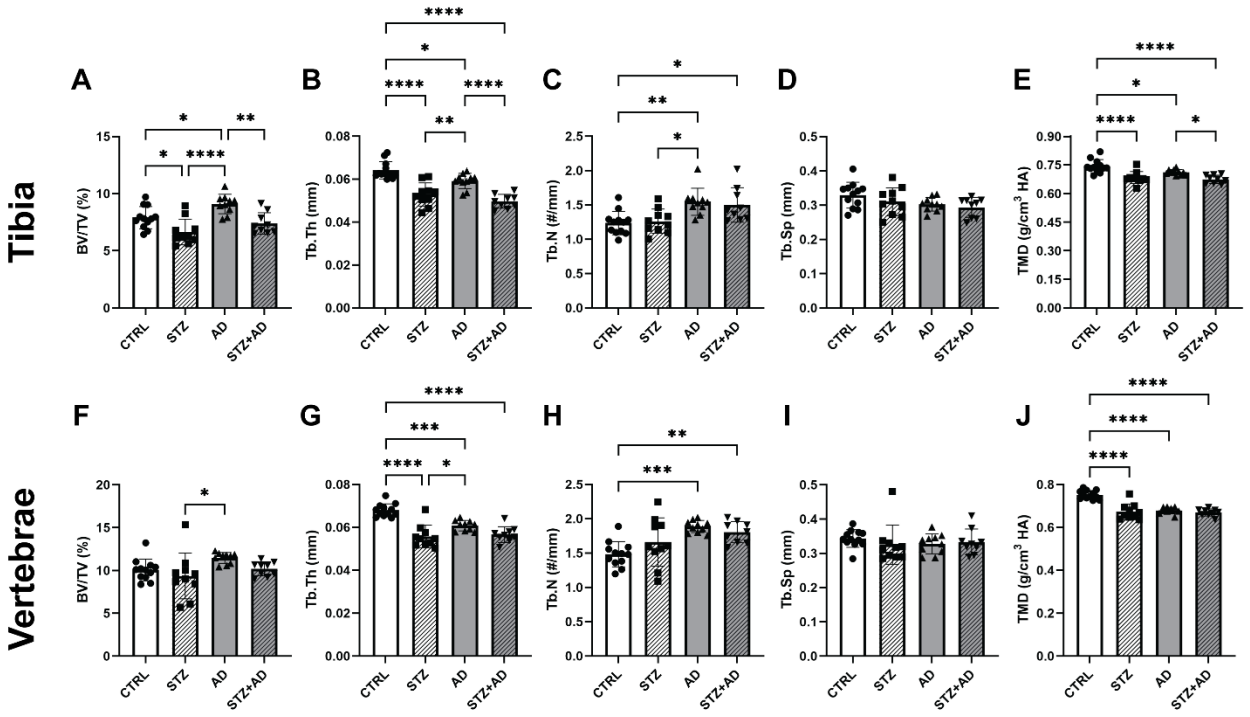

Fig. 4.6: Combination Mice Exhibit a Mixed STZ and AD Trabecular Phenotype. Tibia: BV/TV was lower in STZ vs CTRL and higher in AD vs all groups (A). Tb.Th was lower in all groups vs CTRL and higher in AD vs STZ and STZ+AD (B). Tb.N was higher in AD and STZ+AD vs CTRL and in AD vs STZ (C). Tb.Sp was not different between groups (D). TMD was lower in all groups vs CTRL and in STZ+AD vs AD (E). Vertebrae: BV/TV was higher in AD vs STZ (F). Tb.Th was lower in all groups vs CTRL and higher in AD vs STZ (G). Tb.N was higher in AD and STZ+AD vs CTRL (H). Tb.Sp was not different between groups (I). TMD was lower in all groups vs CTRL (J) *p<0.05; **p<0.01; ***p<0.001; ****p<0.0001. *BV/TV = bone volume/total volume; Tb.Th = trabecular thickness; Tb.N = trabecular number; Tb.Sp = trabecular separation; TMD = tissue mineral density.*

In the L4 vertebrae, BV/TV was increased in AD vs STZ, but no groups were significantly different from CTRL (**Fig. 4.6F**). Trabecular thickness was significantly lower in all groups vs CTRL but was higher in AD vs STZ (**Fig. 4.6G**). Trabecular number was significantly higher in AD and STZ+AD vs CTRL while trabecular separation was not different between groups (**Fig. 4.6H-I**). TMD was significantly lower in all groups vs CTRL (**Fig. 4.6J**).

Cortical bone of the tibia was analyzed for porosity and geometric properties. Cross sections centered at 20% (**Fig. 4.7A**) and 50% (**Fig. 4.7B**) along the length of the tibia demonstrate visible cortical bone thinning and porosity in STZ, AD, and STZ+AD mice. Cortical porosity at the mid-diaphysis and distal end of the tibia (40% to 80% of the bone length from the proximal end) was not different between any groups (**Fig. 4.7C**). However, porosity at the proximal end of the tibia (20% and 30% from the proximal end) was significantly higher in AD and STZ+AD vs CTRL (**Fig. 4.7C**). Cortical porosity was also significantly higher in AD vs all other groups in the femur mid-diaphysis (**Appendix B.1**). Cortical bone area was significantly lower in all groups vs CTRL and was lower in STZ+AD vs AD (**Fig. 4.7D**). Marrow area was higher in all groups vs CTRL (**Fig. 4.7E**). Total area was lower in STZ and STZ+AD vs CTRL and was higher in AD vs STZ and STZ+AD (**Fig. 4.7F**). Bone area/total area was lower in all groups vs CTRL (**Fig. 4.7G**). Moment of inertia was lower in all groups vs CTRL and in STZ+AD vs AD (**Fig. 4.7H,I**). Imin was also higher in AD vs STZ (**Fig. 4.7I**). Cortical thickness was significantly lower in all groups vs CTRL (**Fig. 4.7J**). TMD of the cortical bone was significantly lower in STZ and STZ+AD vs CTRL (**Fig. 4.7K**).

4.4.4 Bone Mechanics

Four-point bending was used to calculate extrinsic and intrinsic mechanical properties of the left tibia. On the structural level (**Table 4.1**), yield force and ultimate force were significantly lower in all disease groups vs CTRL. Ultimate force was also significantly lower in STZ+AD vs AD. Stiffness was significantly lower in AD and STZ+AD vs CTRL, and total work was significantly lower in all groups vs CTRL. Total displacement was significantly lower in STZ+AD vs CTRL but not vs the single disease groups. On the tissue level (**Table 4.2**), yield stress and ultimate stress were significantly lower in STZ and STZ+AD vs CTRL. Ultimate stress was also significantly lower in STZ+AD vs AD. Total strain was significantly lower in STZ+AD vs CTRL while strain to yield was lower in STZ and STZ+AD vs CTRL.

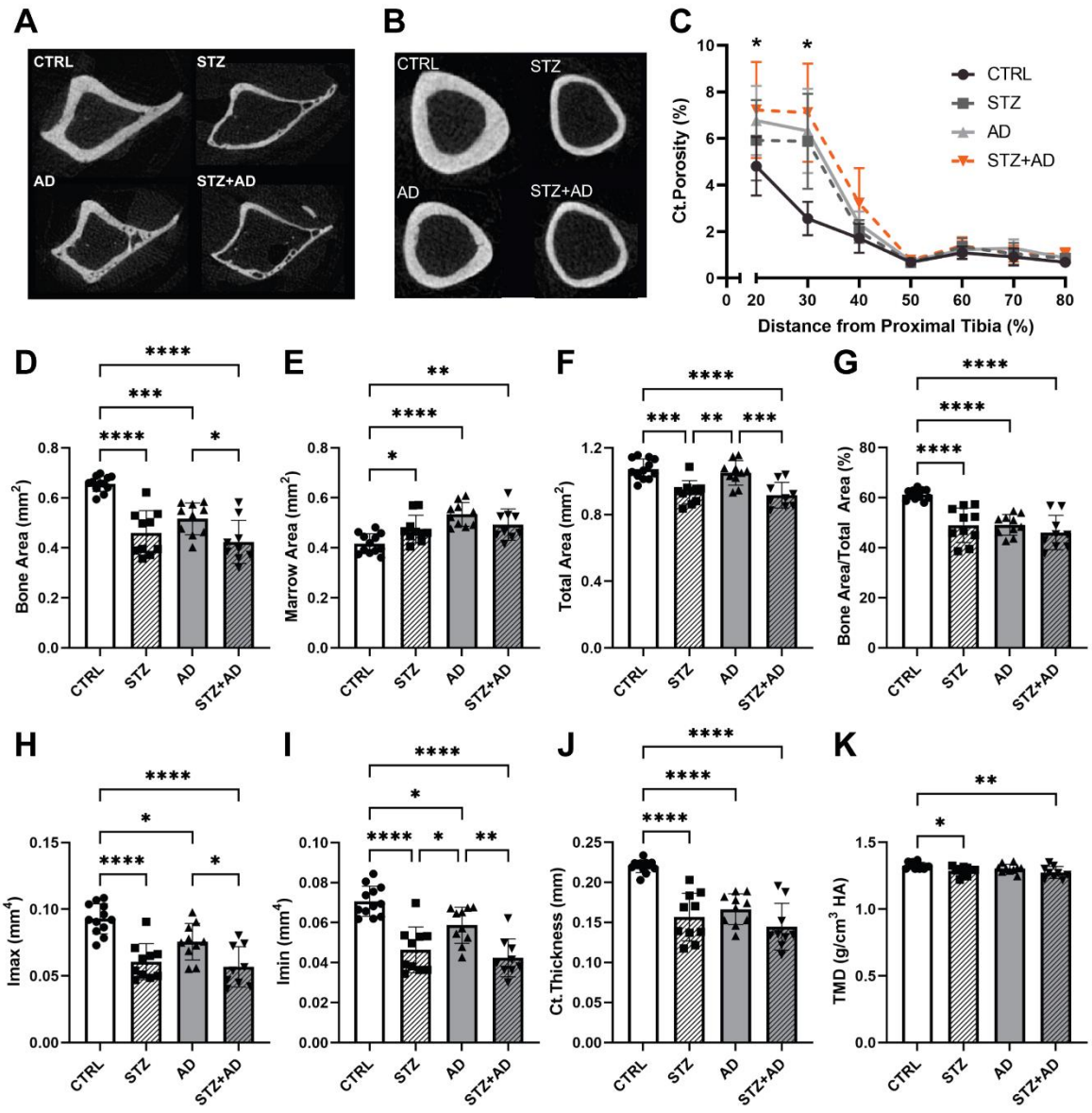

Fig. 4.7: STZ and AD Alter Cortical Geometry. MicroCT of the tibia revealed significant detriments in cortical properties at the 20% (A) and 50% (B) regions. Cortical porosity was significantly higher in all groups vs CTRL at the 20% region and was higher in AD and STZ+AD at the 30% region (C). Bone area was significantly lower in all groups vs CTRL and in STZ+AD vs AD (D). Marrow area was significantly higher in all groups vs CTRL (E). Total area was lower in STZ and STZ+AD vs CTRL and was higher in AD vs STZ and STZ+AD (F). Bone area fraction was lower in all groups vs CTRL (G). Imax and Imin were lower in all groups vs CTRL and in STZ+AD vs AD while Imin was higher in AD vs STZ and STZ+AD (H,I). Cortical thickness was lower in all groups vs CTRL (J). TMD was lower in STZ and STZ+AD vs CTRL (K). Cortical porosity: *p<0.05 between at least two groups. Endpoint measures: *p<0.05; **p<0.01; ***p<0.001; ****p<0.0001. *Imax = maximum moment of inertia; Imin = minimum moment of inertia; TMD = tissue mineral density*

Toughness was significantly lower in all groups vs CTRL. Fracture toughness testing performed on left femora revealed a downward trend in all toughness parameters in the disease groups. No differences in crack initiation or maximum load were found between groups (**Fig. 4.8A-B**) while fracture instability was significantly lower in AD and STZ+AD vs CTRL (**Fig. 4.8C**).

Table 4.2: Structural Mechanical Properties of the Tibia. Data are shown as mean ± SD and analyzed by one-way ANOVA with posthoc Tukey's test: [a]$p<0.05$ vs CTRL; [b]$p<0.05$ vs STZ; [c]$p<0.05$ vs AD

	Yield force (N)	Ultimate force (N)	Total displacement (μm)	Displacement to yield (μm)	Postyield displacement (μm)	Stiffness (N/mm)	Total work (mJ)	Work to Yield (mJ)	Postyield Work (mJ)
CTRL	17.4 ± 3.9	18.4 ± 3.4	571 ± 245	267 ± 68.4	304 ± 254	74.4 ± 19	7.50 ± 4.2	2.68 ± 0.9	4.82 ± 4.2
STZ	9.73 ± 4.3[a]	11.5 ± 4.3[a]	451 ± 239	216 ± 36.9	235 ± 216	53.9 ± 26	3.54 ± 2.1[a]	1.17 ± 0.5[a]	2.37 ± 2.0
AD	11.0 ± 2.7[a]	13.6 ± 1.9[a]	435 ± 83.8	256 ± 40.9	178 ± 118	48.2 ± 8.7[a]	3.73 ± 1.1[a]	1.57 ± 0.5[a]	2.15 ± 1.3
STZ+AD	8.59 ± 3.6[a]	8.96 ± 3.8[a,c]	298 ± 14.8[a]	219 ± 26.0	78.8 ± 20.8	44.4 ± 15[a]	1.74 ± 0.8[a]	1.07 ± 0.5[a]	0.66 ± 0.3[a]

Table 4.3: Tissue-level Mechanical Properties of the Tibia. Data are shown as mean ± SD and analyzed by one-way ANOVA with posthoc Tukey's test: [a]$p<0.05$ vs CTRL; [b]$p<0.05$ vs STZ; [c]$p<0.05$ vs AD

	Yield stress (MPa)	Ultimate stress (MPa)	Total strain (mε)	Strain to yield (mε)	Modulus (GPa)	Resilience (MPa)	Toughness (MPa)
CTRL	121.± 23	208 ± 48	44.2 ± 18.8	20.7 ± 5.16	11.5 ± 3.00	2.48 ± 0.85	6.86 ± 3.60
STZ	119 ± 22[a]	145 ± 42[a]	32.9 ± 16.2	15.9 ± 2.38[a]	10.6 ± 3.07	1.30 ± 0.41[a]	3.81 ± 2.01[a]
AD	134 ± 26	163 ± 37	33.6 ± 7.33	19.7 ± 3.49	9.35 ± 1.68	1.78 ± 0.56	4.16 ± 0.96[a]
STZ+AD	135 ± 19[a]	146 ± 39[a,c]	21.5 ± 1.13[a]	15.8 ± 1.77[a]	10.5 ± 2.04	1.31 ± 0.47[a]	2.12 ± 0.59[a]

4.5 Discussion

In this study, we found that mice with STZ-induced T1D combined with AD-induced CKD develop a set of biochemical and skeletal alterations that are distinct from either disease individually while retaining many features of the individual disease states. STZ primarily drove decreased trabecular BV/TV, TMD in all locations, and ultimate stress while AD led to higher cortical porosity in the proximal tibia, trabecular number, bone turnover, and lower stiffness. While these changes were present in STZ+AD animals, combination animals displayed unique

mechanical detriments vs CTRL including lower total displacement/strain and postyield work and had lower ultimate force and stress vs AD alone (**Table 4.1,4.2**). Intriguingly, STZ+AD animals did not have higher serum phosphorus or PTH despite having lower kidney function vs CTRL (**Fig. 4.4**). Taken together, these data support the idea that combined T1D and CKD results in a different global phenotype vs the individual disease states and may provide an opportunity to study the complex interactions between diabetes and kidney disease.

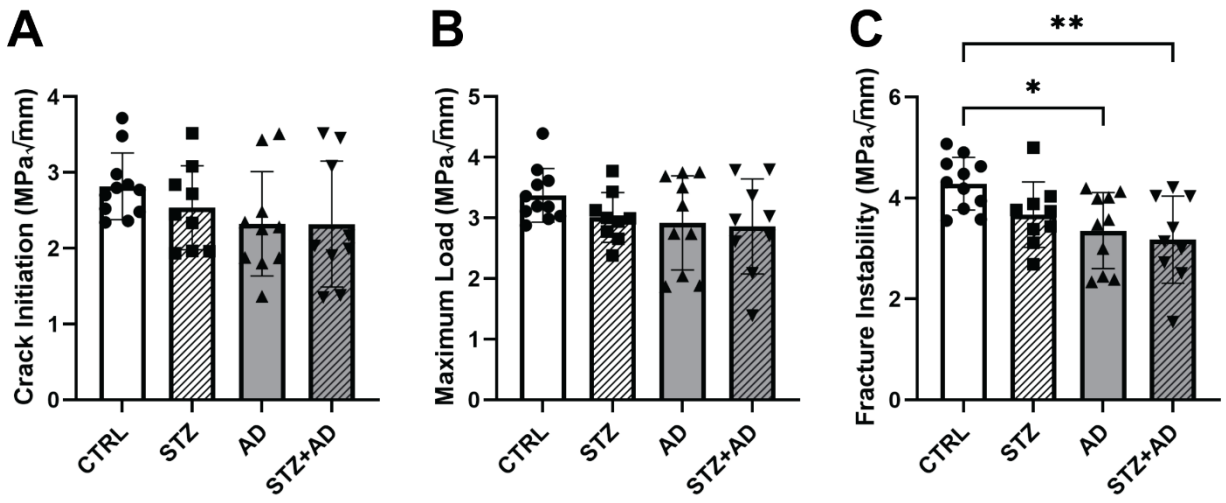

Fig. 4.8: Fracture Toughness is Lower in AD and Combination Mice. Crack initiation and maximum load trended down in all disease groups but were not significantly different from CTRL (A-B). Fracture Instability was significantly lower in AD and STZ+AD vs CTRL (C). **p*<0.05; ***p*<0.01.

Our data confirmed that most STZ and STZ+AD animals experienced long-term hyperglycemia and glucose intolerance as measured by serial glucose measurements, GTTs, and HbA1c (**Fig. 4.2**). However, two animals in the STZ group and four animals in the STZ+AD group did not display elevated blood glucose, HbA1c, or glucose intolerance at any point throughout the study. While C57BL/6 mice are reported to be highly susceptible to the β cell-toxic effects of STZ, persistent hyperglycemia can be challenging to maintain, especially in female mice [(182)]. STZ dose titration studies from our group have demonstrated that at least 80 mg/kg of STZ daily for five days is necessary to reliably induce T1D in female mice, likely due to the protective effects of estrogen signaling on β cell viability [(183)]. We also observed that non-fasting blood glucose levels continued to increase throughout the study, indicating that disease duration impacts glucose

handling in STZ mice (**Fig. 4.2**). This finding is unlikely due to persistent effects of STZ, as the chemical half-life is generally reported as 15 minutes before rapid metabolism by the liver and excretion by the kidney [179]. Future studies performing serial insulin measures and/or β cell mass at various intervals may help reveal the long-term fate of β cells following STZ administration, particularly in female C57BL/6 mice.

The adenine-containing diet led to higher BUN levels in AD and STZ+AD animals, indicating lower kidney function (**Fig. 4.4A**). While AD mice demonstrated disturbed mineral homeostasis indicated by elevated serum phosphorus and PTH, we found no differences between phosphorus or PTH in STZ+AD animals vs CTRL, indicating an interaction between the two conditions (**Fig. 4.4**). Hyperparathyroidism is inherently related to the skeletal alterations seen in CKD – namely altered bone turnover and the development of cortical porosity [184]. While little research has specifically examined the bone in patients with T1D and CKD, PTH levels are frequently low in patients with T1D, especially when their blood glucose levels are poorly controlled [185-187]. The mechanism behind diabetes-induced hypoparathyroidism remains unclear but is thought to involve an impaired PTH secretion in response to low serum calcium and possibly diabetes-induced fibrosis of the parathyroid glands [188,189]. While the lack of high PTH was surprising, the STZ+AD model may be useful to investigate the interaction between T1D and PTH secretion.

Curiously, we found lower β cell mass in AD mice vs CTRL despite having intact glucose handling (**Fig. 4.3**). On histology, we found that the islets in AD mice had a dark insulin stain and were frequently torn during sectioning. PTH has been shown to facilitate insulin release from pancreatic β cells, and we hypothesize that CKD-induced dysregulations in mineral handling caused aberrant mineralization of the pancreas [190]. AD also lowered raw pancreas weight vs CTRL, but this difference was not significant when normalized by endpoint body weight (**Appendix B.2**). Therefore, it is possible that AD-induced CKD causes β cell stress without altering β cell function.

Bone turnover status is related to PTH levels and has implications for treatment in CKD. Patients with CKD can be categorized into high, normal, or low turnover bone disease, as determined by bone biopsy, and patients with diabetes and CKD have high turnover bone disease less frequently than patients with CKD and no diabetes [191,192]. Turnover, indicated by bone formation rate, was high in AD mice vs STZ and combination mice, possibly due to the loss of

insulin from STZ administration, reducing osteoblast differentiation and subsequent bone formation (**Fig. 4.5C**) [193]. The percent mineralizing surface (MS/BS) was lower in combined mice vs all groups. The trends in the data suggest an additive effect of STZ and AD on this property, indicating that fewer mineralizing surfaces may contribute to the low turnover seen in combined diabetes and CKD. Overall, the differences in turnover between disease groups matched what was expected based on PTH levels – however, these trends were not strong enough to see differences vs CTRL. Importantly, several samples from the disease groups were excluded from the analysis due to the absence of a second calcein label. We did observe some double labels in the primary spongiosa of these animals, indicating the animals received both injections, but that bone formation was low in animals receiving STZ and/or that resorption was occurring rapidly. While we expected to see ample label in all AD mice given the typical high turnover phenotype in this model, we observed three animals with a broad, diffuse region of calcein-labeled bone, indicating a defect at the mineralization front. Given the generally high MAR in AD mice, we hypothesize that missing labels in this group are due to a high rate of osteoclastic resorption. Previous studies confirm low turnover in mice given STZ, and we hypothesize that the long duration of T1D in our model further suppresses this effect.

Cortical porosity is a hallmark of renal osteodystrophy, the skeletal component of CKD in humans. Rodent studies have shown that high PTH is correlated with the formation of intracortical pores, whether caused by CKD or continuous infusion of PTH(1-34) [194]. Despite this finding, we observed that while cortical porosity was not higher at the mid-diaphysis or distal tibia, porosity was higher in the proximal tibia in STZ, AD, and STZ+AD mice despite the lack of high PTH in STZ and STZ+AD mice (**Fig. 4.7**). While increased PTH and porosity are linked, studies in female C57BL/6 mice fed a 0.2% adenine diet showed that cortical porosity increases prior to a measurable increase in PTH [195]. Cortical porosity is also increased in mice administered STZ and is accompanied by increased osteocyte RANKL expression [141]. Taken together, these data suggest that additional mechanisms may contribute to proximal tibia cortical porosity that are independent of high PTH in STZ+AD animals. We hypothesize that cortical porosity may contribute to skeletal fragility in the combined disease state even if PTH levels are normal.

T1D is known to lower bone mineral density in some patients while CKD preferentially deteriorates the cortical bone compartment. We therefore hypothesized that the combined disease state would display unique or worsened microarchitecture and material properties compared to the

single disease states. We found that STZ, AD, and STZ+AD mice had decreased cortical thickness and increased proximal cortical porosity at the 30% region vs CTRL, but these properties were not worsened in STZ+AD mice (**Fig. 4.7**). This finding points to an overlapping mechanism between STZ- and AD-induced cortical bone loss in this model, possibly caused by higher osteocyte RANKL and inflammatory cytokines, which have been shown to increase osteoclast activity in both models individually [196-198]. We hypothesize that the saturation of the pro-osteoclastic signals and activity that drive endocortical resorption and pore formation limited further cortical deterioration in the combined model.

Trabecular bone loss has been reported in patients with T1D but is not frequently characterized in CKD. We found that all groups exhibited lower trabecular thickness vs CTRL in tibiae and vertebrae, but this reduction was not as severe in AD vs STZ (**Fig. 4.6B,G**). Trabecular number was increased in AD, likely due to the anabolic effects of PTH, and drove an increase in BV/TV in AD vs all groups in the tibia and vs STZ in the vertebrae (**Fig. 4.6**). Interestingly, these effects counteracted each other in STZ+AD mice, indicating that elevated PTH may be responsible for the increased trabecular bone mass in AD mice. Indeed, trabecular bone mass is typically lower in male C57BL/6 mice fed an AD [199]. This sex-specific effect may point to an interactive effect between PTH and estrogens in female mice fed an adenine diet.

STZ and STZ+AD mice displayed slightly but significantly lowered TMD in the tibia while all groups had significantly lowered TMD in the vertebrae (**Fig. 4.6J**). This finding indicates that AD may preferentially reduce mineralization in the axial skeleton, and that lower material quality may contribute to vertebral fractures in CKD. Taken together, the data indicate that STZ and AD have additive effects on trabecular properties that results in a phenotype that does not fully resemble either of the single disease states.

All disease groups displayed reduced structural mechanical properties (summarized in **Table 4.1**) including yield force and ultimate force vs CTRL, which we hypothesize is due to lower cortical thickness and moment of inertia (**Fig. 4.7**). At the material level, STZ primarily drove lower ultimate stress in STZ and STZ+AD mice. We hypothesize that this change is due to the decreased cortical TMD seen in STZ and STZ+AD mice, as ultimate stress is highly dependent on bone mineral content and quality. Interestingly, we found that stiffness, the structural resistance to elastic/reversible deformation, was decreased in AD and STZ+AD vs CTRL while elastic modulus was not different between groups. This may indicate that lower cortical thickness and

moment of inertia drove lower stiffness while TMD maintained resistance to deformation on the matrix level.

Tissue-level properties (summarized in **Table 4.2**) including toughness were significantly lower in all groups vs CTRL. Bone toughness determines its ability to dissipate the energy induced by bending and is critical for preventing accumulated damage from progressing to catastrophic failure [163]. Bone mineral alone is poorly designed to dissipate energy effectively, and therefore, this finding indicates that STZ and AD may impact collagen matrix quality and/or bone water content [156]. Driving reduced toughness, total displacement and strain trended lower in all disease groups but were only significantly lower in STZ+AD vs CTRL. Importantly, all three fracture toughness parameters trended lower in the disease groups vs CTRL, and fracture instability was significantly lower in AD and STZ+AD mice vs CTRL (**Fig. 4.8**). Fracture toughness reflects the true material quality of the bone and its ability to resist crack growth, the dominant fracture mechanism in brittle materials.We hypothesize that these alterations are driven by lower collagen quality, possibly due to the non-enzymatic crosslinks caused by AGEs. While we did not find increased fluorescent AGEs in any group vs CTRL (**Appendix B.3**), the majority of non-enzymatic crosslinks, such as carboxymethyllysine, do not fluoresce and are not detected by this method. Therefore, future studies that distinguish between AGEs are warranted to understand the mechanism by which matrix quality is disrupted by STZ and AD. Altogether, the mechanical data portrays a combined disease model with more structural and tissue-level defects than either disease alone, culminating in a material that poorly resists bending and damage propagation.

One limitation of this study is the general lack of differences between the STZ and STZ+AD groups. The animals in this study were diabetic for six weeks prior to the onset of kidney disease. While this models the human disease timeline more accurately than initiating the diseases at the same time, the bone loss caused by STZ may have limited the ability for CKD to develop additional porosity. While recent trials have improved our understanding of skeletal alterations in CKD, the number of patients with diabetes as their primary cause of CKD is typically restricted in these studies due to potential differences in the skeletal phenotype. Furthermore, patients with diabetes and/or CKD are routinely excluded from trials for osteoporosis drugs. Therefore, we must consider that the skeletal phenotype of patients with diabetes and CKD (nearly half of all CKD patients) is incompletely understood. While we are still in the early stages of examining the

complexities or co-morbid disease states, our data may support that T1D has significant impacts on bone health prior to the onset of CKD.

We did not include male mice in this study, as several studies report that male mice have a more severe response to the AD [200]. Body weights were significantly lower in STZ+AD vs CTRL at all timepoints, and some STZ+AD mice approached dangerously low weights at the end of the study. Thus, the study timeline may need to be amended to promote survival in male mice. Finally, we chose to model T1D+CKD instead of type 2 diabetes (T2D), the most common form of diabetes. T2D is frequently induced by high fat and/or high sucrose-containing diets or by genetic alterations in leptin signaling. While these models recapitulate the dysregulations in sugars, lipids, and inflammation seen in T2D, leptin deletion has complex effects on cortical and trabecular bone while the diet models do not achieve late-stage T2D where insulin levels fall [201,202]. Therefore, we began by modeling T1D with STZ treatment which consistently produces high glucose and low insulin, important determinants or morbidity in all types of diabetes [203]. Therefore, developing a robust model of T2D+CKD is of critical importance, and in conjunction with treatment studies, is a major focus of our future directions.

In conclusion, this study describes a model of combined STZ and AD to mimic human T1D+CKD. STZ+AD animals experienced long-term persistent hyperglycemia and reduced kidney function without overt signs of disrupted mineral homeostasis. We found significant cortical deficits in all groups, but additional sites of porosity in the proximal tibia of AD mice. The trabecular bone displayed an additive phenotype in STZ+AD animals. Bone turnover was increased by AD but not in STZ+AD, likely due to the lack of high PTH. Finally, bending tests demonstrated that each disease impacted structural- and material-level mechanical properties while STZ+AD mice demonstrated a unique reduction in ductility, indicating that these conditions impact more than just bone mineral. Taken together, our findings indicate that combined T1D and CKD has a unique global phenotype that may warrant different therapeutic approaches compared to patients with either disease alone.

5. CONTRIBUTIONS TO SCIENTIFIC KNOWLEDGE

5.1 Summary and Impact of Research Findings

In this dissertation, we have described how bone matrix composition and material properties are altered in a spatially dependent manner in early chronic kidney disease (CKD) with and without calcimimetic treatment. These differences were found despite the lack of detectable changes in bone microarchitecture, indicating that bone deterioration may occur in localized regions prior to the formation of cortical porosity in CKD. The colocalized Raman spectroscopy and nanoindentation method in particular allows for unambiguous characterization these properties on hydrated bone specimens of known tissue age and likely contributed to our ability to detect differences in new periosteal bone and the spatial variation in matrix composition and mechanics in the osteocyte perilacunar region.

Furthermore, we expanded upon our current animal disease models and incorporated the leading cause of CKD: diabetes. We found that a novel combined model of type 1 diabetes (T1D) and CKD had a combination of biochemical and skeletal alterations that did not fully match either single disease state. Streptozotocin-induced diabetes resulted in chronic hyperglycemia and glucose intolerance while the adenine-containing diet lowered kidney function but did not cause hyperparathyroidism in combined disease mice. The trabecular bone exhibited a phenotype resembling a combination of the two disease states while cortical bone geometry was deteriorated by both conditions. Trabecular mineralizing surface was uniquely lower in combination mice but turnover was not altered. Mechanical properties showed that both disease lowered ultimate force and toughness while the adenine diet lowered stiffness and fracture toughness. Total displacement and strain were uniquely lower in STZ+AD animals, indicating tissue-level detriments become more prominent in combined disease mice.

Taken together, the findings of this dissertation indicate that common chronic diseases can severely impact the bone, a tissue long thought to be a passive player in systemic health. Furthermore, chronic diseases may begin by altering bone properties on the tissue level prior to clinically visible signs of disease. The idea that changes to the individual constituents of bone can have widespread detrimental effects is not new, but robust methods to characterize bone quality on the nano- and micro-scale are not commonly used in the literature, a shortcoming we have

worked to address here. Additionally, the combined model of T1D and CKD described herein attempts to encourage the use of preclinical models that model the additional complexities in the human disease state. While T1D is less common than type 2 diabetes (T2D), the model described allows for tight control over the onset of hyperglycemia and the loss of kidney function while using commonly available reagents in the scientific community. Therefore, this model is suitable to be implemented in a wide array of scientific fields and has the potential to impact medical fields beyond the bone.

5.2 Directions for Future Research

Future work is planned to expand upon the technologies presented herein and to apply our animal models to broader scientific questions. Further development of the colocalized Raman spectroscopy and nanoindentation system has opened the possibility for dynamic mechanical analysis, which can be used to analyze the viscoelastic properties of the bone. These metrics are well suited for our setup, as preserving the native hydration state of the tissue is essential to accurately capture the innate viscoelasticity brought by bound water and collagen in the bone. As for the combined T1D and CKD model, the tunability opens the opportunity to determine the effects of age of onset and disease duration on skeletal properties. Intervention studies using agents to improve bone quantity and quality can also be performed to determine whether the skeletal detriments can be corrected in the combined disease state. Finally, this model can be applied to the aging population by using an aged cohort of mice.

APPENDIX A. SUPPLEMENTAL DATA TO CHAPTER 3

Table A.1: Trabecular and Cortical Microarchitecture of the Tibia. Data are shown as mean ± SD and analyzed as one-way ANOVA. Dunnett's multiple comparison test was performed for each group versus CKD: ****$p<0.0001$. *BV/TV = bone volume/total volume; Tb.N = trabecular number; Tb.Th = trabecular thickness; Tb.Sp = trabecular separation; Ct.Porosity = cortical porosity; Ct.Th = cortical thickness.*

	BV/TV (%)	Tb.N (#/mm)	Tb.Th (mm)	Tb.Sp (mm)	Ct.Porosity (%)	Ct.Th (mm)	Bone Area (mm^2)
NL	6.68 ± 2.7****	0.84 ± 0.3****	0.08 ± 0.01	0.77 ± 0.09****	0.95.± 0.42	0.51 ± 0.02	7.01 ± 0.46
CKD	2.56 ± 1.0	0.30 ± 0.1	0.09 ± 0.01	0.54 ± 0.10	0.80 ± 0.25	0.50 ± 0.02	6.67 ± 0.24
CKD/KP	3.65 ± 2.0	0.40 ± 0.2	0.09 ± 0.01	0.74 ± 0.08	0.74 ± 0.32	0.52 ± 0.03	6.83 ± 0.38

APPENDIX B. SUPPLEMENTAL DATA TO CHAPTER 4

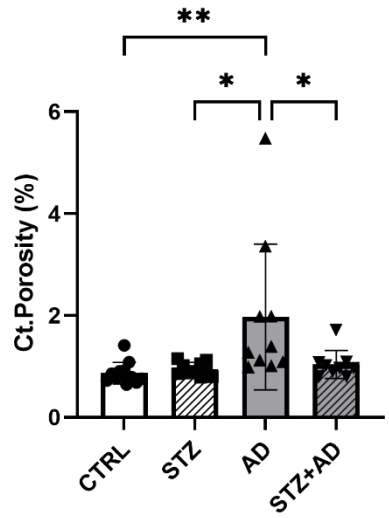

Fig. B.1: AD Increases Cortical Porosity in the Femur Mid-diaphysis. Cortical porosity was calculated using a 1 mm region of interest centered at 50% of the left femur length. Porosity was significantly higher in AD vs all groups. *p<0.05; **p<0.01.

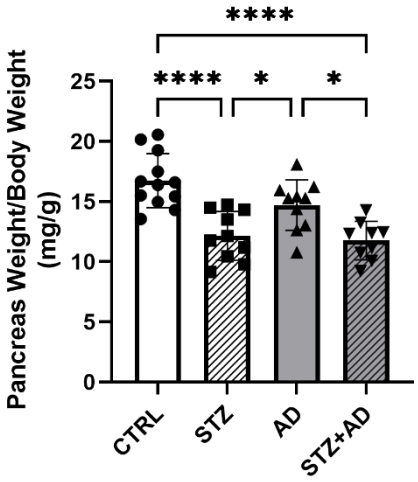

Fig. B.2: STZ Administration Lowered Pancreas Weight. Pancreas weight was significantly lower in STZ and STZ+AD vs CTRL and AD. *p<0.05; ****p<0.0001.

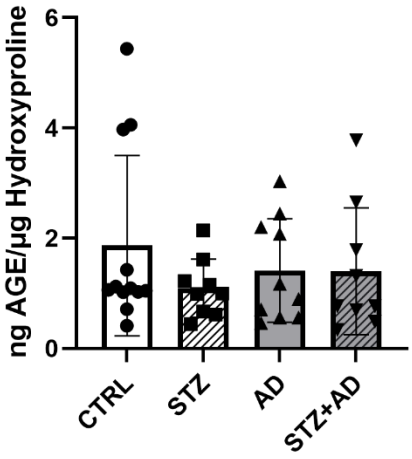

Fig. B.3: STZ and AD do not alter Fluorescent AGE content in Bone. AGE content was normalized by hydroxyproline content to calculate the amount of AGE per unit collagen. No differences were seen between groups. *AGE = advanced glycation end product*.

REFERENCES

1. Besarab A, Levin A. Defining a renal anemia management period. American journal of kidney diseases : the official journal of the National Kidney Foundation. Dec 2000;36(6 Suppl 3):S13-23. Epub 2000/01/11.
2. Muntner P, He J, Astor BC, Folsom AR, Coresh J. Traditional and nontraditional risk factors predict coronary heart disease in chronic kidney disease: results from the atherosclerosis risk in communities study. Journal of the American Society of Nephrology : JASN. Feb 2005;16(2):529-38. Epub 2004/12/31.
3. Moe S, Drüeke T, Cunningham J, Goodman W, Martin K, Olgaard K, et al. Definition, evaluation, and classification of renal osteodystrophy: a position statement from Kidney Disease: Improving Global Outcomes (KDIGO). Kidney Int. Jun 2006;69(11):1945-53. Epub 2006/04/28.
4. Hill NR, Fatoba ST, Oke JL, Hirst JA, O'Callaghan CA, Lasserson DS, et al. Global Prevalence of Chronic Kidney Disease - A Systematic Review and Meta-Analysis. PLoS One. 2016;11(7):e0158765-e.
5. Go AS, Chertow GM, Fan D, McCulloch CE, Hsu CY. Chronic kidney disease and the risks of death, cardiovascular events, and hospitalization. The New England journal of medicine. Sep 23 2004;351(13):1296-305. Epub 2004/09/24.
6. Moe SM, Drueke T, Lameire N, Eknoyan G. Chronic kidney disease-mineral-bone disorder: a new paradigm. Advances in chronic kidney disease. Jan 2007;14(1):3-12. Epub 2007/01/04.
7. Moe SM, Nickolas TL. Fractures in Patients with CKD: Time for Action. Clinical journal of the American Society of Nephrology : CJASN. Nov 7 2016;11(11):1929-31. Epub 2016/11/01.
8. Coco M, Rush H. Increased incidence of hip fractures in dialysis patients with low serum parathyroid hormone. American journal of kidney diseases : the official journal of the National Kidney Foundation. Dec 2000;36(6):1115-21. Epub 2000/11/30.
9. Moe SM, Chen NX, Newman CL, Gattone VH, 2nd, Organ JM, Chen X, et al. A comparison of calcium to zoledronic acid for improvement of cortical bone in an animal model of CKD. Journal of bone and mineral research : the official journal of the American Society for Bone and Mineral Research. Apr 2014;29(4):902-10. Epub 2013/09/17.
10. Sharma AK, Toussaint ND, Masterson R, Holt SG, Rajapakse CS, Ebeling PR, et al. Deterioration of Cortical Bone Microarchitecture: Critical Component of Renal Osteodystrophy Evaluation. American journal of nephrology. 2018;47(6):376-84. Epub 2018/05/24.
11. Newman CL, Moe SM, Chen NX, Hammond MA, Wallace JM, Nyman JS, et al. Cortical bone mechanical properties are altered in an animal model of progressive chronic kidney disease. PLoS One. 2014;9(6):e99262. Epub 2014/06/10.
12. Krege JH, Wan X, Lentle BC, Berger C, Langsetmo L, Adachi JD, et al. Fracture risk prediction: importance of age, BMD and spine fracture status. BoneKEy reports. 2013;2:404. Epub 2013/11/15.

13. Jorgensen HS, Winther S, Bottcher M, Hauge EM, Rejnmark L, Svensson M, et al. Bone turnover markers are associated with bone density, but not with fracture in end stage kidney disease: a cross-sectional study. BMC nephrology. Sep 6 2017;18(1):284. Epub 2017/09/07.
14. Shantouf R, Ahmadi N, Flores F, Tiano J, Gopal A, Kalantar-Zadeh K, et al. Impact of phosphate binder type on coronary artery calcification in hemodialysis patients. Clin Nephrol. Jul 2010;74(1):12-8. Epub 2010/06/19.
15. Pimentel A, Ureña-Torres P, Zillikens MC, Bover J, Cohen-Solal M. Fractures in patients with CKD-diagnosis, treatment, and prevention: a review by members of the European Calcified Tissue Society and the European Renal Association of Nephrology Dialysis and Transplantation. Kidney Int. Dec 2017;92(6):1343-55. Epub 2017/10/02.
16. Moe SM, Abdalla S, Chertow GM, Parfrey PS, Block GA, Correa-Rotter R, et al. Effects of Cinacalcet on Fracture Events in Patients Receiving Hemodialysis: The EVOLVE Trial. Journal of the American Society of Nephrology : JASN. Jun 2015;26(6):1466-75. Epub 2014/12/17.
17. Wuthrich RP, Martin D, Bilezikian JP. The role of calcimimetics in the treatment of hyperparathyroidism. European journal of clinical investigation. Dec 2007;37(12):915-22. Epub 2007/11/27.
18. J. L. Fowlkes JSN, R. C. Bunn, E. C. Wahl, L. Lichu, G. E. Cockrell, L M. Morris, C. K. Lumpkin, K. M. Thrailkill. Osteo-promoting effects of insulin-like growth factor 1 (IGF-1) in a mouse model of type 1 diabetes. Bone. 2013;57:36-40.
19. Li X, Yu L, Asuncion F, Grisanti M, Alexander S, Hensley K, et al. Etelcalcetide (AMG 416), a peptide agonist of the calcium-sensing receptor, preserved cortical bone structure and bone strength in subtotal nephrectomized rats with established secondary hyperparathyroidism. Bone. Dec 2017;105:163-72. Epub 2017/09/05.
20. Block GA, Bushinsky DA, Cunningham J, Drueke TB, Ketteler M, Kewalramani R, et al. Effect of Etelcalcetide vs Placebo on Serum Parathyroid Hormone in Patients Receiving Hemodialysis With Secondary Hyperparathyroidism: Two Randomized Clinical Trials. Jama. Jan 10 2017;317(2):146-55. Epub 2017/01/18.
21. Block GA, Bushinsky DA, Cheng S, Cunningham J, Dehmel B, Drueke TB, et al. Effect of Etelcalcetide vs Cinacalcet on Serum Parathyroid Hormone in Patients Receiving Hemodialysis With Secondary Hyperparathyroidism: A Randomized Clinical Trial. Jama. Jan 10 2017;317(2):156-64. Epub 2017/01/18.
22. Shigematsu T, Fukagawa M, Yokoyama K, Akiba T, Fujii A, Odani M, et al. Long-term effects of etelcalcetide as intravenous calcimimetic therapy in hemodialysis patients with secondary hyperparathyroidism. Clinical and experimental nephrology. Apr 2018;22(2):426-36. Epub 2017/08/25.
23. National Diabetes Statistics Report, 2017. In: Serv. UDHH, editor. Atlanta, GA: Center for Disease Control and Prevention; 2017.
24. Seliger SL, Siscovick DS, Stehman-Breen CO, Gillen DL, Fitzpatrick A, Bleyer A, et al. Moderate renal impairment and risk of dementia among older adults: the Cardiovascular Health Cognition Study. Journal of the American Society of Nephrology : JASN. Jul 2004;15(7):1904-11. Epub 2004/06/24.
25. Bianchi L, Volpato S. Muscle dysfunction in type 2 diabetes: a major threat to patient's mobility and independence. Acta diabetologica. Dec 2016;53(6):879-89. Epub 2016/07/10.

26. Pereira RA, Cordeiro AC, Avesani CM, Carrero JJ, Lindholm B, Amparo FC, et al. Sarcopenia in chronic kidney disease on conservative therapy: prevalence and association with mortality. Nephrology, dialysis, transplantation : official publication of the European Dialysis and Transplant Association - European Renal Association. Oct 2015;30(10):1718-25. Epub 2015/05/23.
27. T. L. Nickolas EMS, E. Dworakowski, K. K. Nishiyama, M. Komandah-Kosseh, C. A. Zhang, D. J. McMahon, X. S. Liu, S. Boutroy, S. Cremers, E. Shane. Rapid cortical bone loss in patients with chronic kidney disease. Journal of Bone and Mineral Research. 2013;28(8):1811-20.
28. L. C. Plantinga DCC, J. Coresh, E. R. Miller, R. Saran, J. Yee, E. Hedgeman, M. Pavkov, M. S. Eberhardt, D. E. Williams, N. R. Powe. Prevalence of Chronic Kidney Disease in US Adults with Undiagnosed Diabetes or Prediabetes. Clinical Journal of the American Society of Nephrology. 2010;5(4):673-82.
29. The Staggering Costs of Diabetes. American Diabetes Association; 2018.
30. Valderrábano RJ, Linares MI. Diabetes mellitus and bone health: epidemiology, etiology and implications for fracture risk stratification. Clin Diabetes Endocrinol. 2018;4:9. Epub 2018/05/04.
31. Schwartz AV. Diabetes Mellitus: Does it Affect Bone? Calcified Tissue International. 2003;73(6):515-9.
32. V. N. Shah KKH, C. S. Shah, T. L. Gall, P. Joshee, J. K. Snell-Bergeon, W. M. Kohrt. Bone mineral density at femoral neck and lumbar spine in adults with type 1 diabetes: a meta-analysis and review of the literature. Osteoporosis International. 2017;28(9):2601-10.
33. J. N. Farr MTD, S. Amin, L. J. M. Iii, K. Louise. In Vivo Assessment of Bone Quality in Postmenopausal Women with Type 2 Diabetes. Journal of Bone and Mineral Research. 2014;29(4):787-95.
34. D. R. Weber KH, M. B. Leonard, S. M. Willi, M. R. Denburg. Type 1 Diabetes is Associated with an Increased Risk of Fracture Across the Life Span: A Population-Based Cohort Using the Health Improvement Network (THIN). Diabetes Care. 2015;38(10):1913-20.
35. Yamamoto M, Sugimoto T. Advanced Glycation End Products, Diabetes, and Bone Strength. Curr Osteoporos Rep. Dec 2016;14(6):320-6. Epub 2016/10/06.
36. Bosch A, Scheppach JB, Harazny JM, Raff U, Eckardt KU, Schmieder RE, et al. Retinal capillary and arteriolar changes in patients with chronic kidney disease. Microvascular research. Jul 2018;118:121-7. Epub 2018/03/22.
37. Ranger TA, Wong AM, Cook JL, Gaida JE. Is there an association between tendinopathy and diabetes mellitus? A systematic review with meta-analysis. British journal of sports medicine. Aug 2016;50(16):982-9. Epub 2015/11/26.
38. Jones N, Kjellstrand CM. Spontaneous tendon ruptures in patients on chronic dialysis. American journal of kidney diseases : the official journal of the National Kidney Foundation. Dec 1996;28(6):861-6. Epub 1996/12/01.
39. Iwasaki Y, Kazama JJ, Yamato H, Fukagawa M. Changes in chemical composition of cortical bone associated with bone fragility in rat model with chronic kidney disease. Bone. Jun 1 2011;48(6):1260-7. Epub 2011/03/15.
40. Ciubuc JD, Manciu M, Maran A, Yaszemski MJ, Sundin EM, Bennet KE, et al. Raman Spectroscopic and Microscopic Analysis for Monitoring Renal Osteodystrophy Signatures. Biosensors. Apr 8 2018;8(2). Epub 2018/04/13.

41. Webster AC, Nagler EV, Morton RL, Masson P. Chronic Kidney Disease. Lancet (London, England). Mar 25 2017;389(10075):1238-52. Epub 2016/11/27.
42. Papadakis MA, Arieff AI. Unpredictability of clinical evaluation of renal function in cirrhosis. Prospective study. The American journal of medicine. May 1987;82(5):945-52. Epub 1987/05/01.
43. Levey AS, Coresh J. Chronic kidney disease. Lancet (London, England). Jan 14 2012;379(9811):165-80. Epub 2011/08/16.
44. Levey AS, de Jong PE, Coresh J, El Nahas M, Astor BC, Matsushita K, et al. The definition, classification, and prognosis of chronic kidney disease: a KDIGO Controversies Conference report. Kidney Int. Jul 2011;80(1):17-28. Epub 2010/12/15.
45. Shimada T, Hasegawa H, Yamazaki Y, Muto T, Hino R, Takeuchi Y, et al. FGF-23 is a potent regulator of vitamin D metabolism and phosphate homeostasis. Journal of bone and mineral research : the official journal of the American Society for Bone and Mineral Research. Mar 2004;19(3):429-35. Epub 2004/03/26.
46. Shimada T, Kakitani M, Yamazaki Y, Hasegawa H, Takeuchi Y, Fujita T, et al. Targeted ablation of Fgf23 demonstrates an essential physiological role of FGF23 in phosphate and vitamin D metabolism. The Journal of clinical investigation. Feb 2004;113(4):561-8. Epub 2004/02/18.
47. Stocklin E, Eggersdorfer M. Vitamin D, an essential nutrient with versatile functions in nearly all organs. International journal for vitamin and nutrition research Internationale Zeitschrift fur Vitamin- und Ernahrungsforschung Journal international de vitaminologie et de nutrition. 2013;83(2):92-100. Epub 2014/02/05.
48. Brown EM, Gamba G, Riccardi D, Lombardi M, Butters R, Kifor O, et al. Cloning and characterization of an extracellular Ca(2+)-sensing receptor from bovine parathyroid. Nature. Dec 9 1993;366(6455):575-80. Epub 1993/12/09.
49. Brown EM. Calcium receptor and regulation of parathyroid hormone secretion. Reviews in endocrine & metabolic disorders. Nov 2000;1(4):307-15. Epub 2001/11/15.
50. Spichtig D, Zhang H, Mohebbi N, Pavik I, Petzold K, Stange G, et al. Renal expression of FGF23 and peripheral resistance to elevated FGF23 in rodent models of polycystic kidney disease. Kidney Int. Jun 2014;85(6):1340-50. Epub 2014/01/10.
51. Lavi-Moshayoff V, Wasserman G, Meir T, Silver J, Naveh-Many T. PTH increases FGF23 gene expression and mediates the high-FGF23 levels of experimental kidney failure: a bone parathyroid feedback loop. American journal of physiology Renal physiology. Oct 2010;299(4):F882-9. Epub 2010/08/06.
52. Silver J, Naveh-Many T. FGF23 and the parathyroid glands. Pediatric nephrology (Berlin, Germany). Nov 2010;25(11):2241-5. Epub 2010/06/08.
53. Malluche HH, Porter DS, Monier-Faugere M-C, Mawad H, Pienkowski D. Differences in bone quality in low- and high-turnover renal osteodystrophy. Journal of the American Society of Nephrology : JASN. 2012;23(3):525-32. Epub 2011/12/22.
54. Ketteler M, Block GA, Evenepoel P, Fukagawa M, Herzog CA, McCann L, et al. Executive summary of the 2017 KDIGO Chronic Kidney Disease-Mineral and Bone Disorder (CKD-MBD) Guideline Update: what's changed and why it matters. Kidney Int. Jul 2017;92(1):26-36. Epub 2017/06/26.

55. Sprague SM, Bellorin-Font E, Jorgetti V, Carvalho AB, Malluche HH, Ferreira A, et al. Diagnostic Accuracy of Bone Turnover Markers and Bone Histology in Patients With CKD Treated by Dialysis. American journal of kidney diseases : the official journal of the National Kidney Foundation. Apr 2016;67(4):559-66. Epub 2015/09/01.
56. Gava AL, Freitas FP, Balarini CM, Vasquez EC, Meyrelles SS. Effects of 5/6 nephrectomy on renal function and blood pressure in mice. International journal of physiology, pathophysiology and pharmacology. 2012;4(3):167-73. Epub 2012/10/17.
57. Wang X, Chaudhry MA, Nie Y, Xie Z, Shapiro JI, Liu J. A Mouse 5/6th Nephrectomy Model That Induces Experimental Uremic Cardiomyopathy. Journal of visualized experiments : JoVE. Nov 7 2017(129). Epub 2017/11/21.
58. Pulskens WP, Verkaik M, Sheedfar F, van Loon EP, van de Sluis B, Vervloet MG, et al. Deregulated Renal Calcium and Phosphate Transport during Experimental Kidney Failure. PLoS One. 2015;10(11):e0142510. Epub 2015/11/14.
59. Ferrari GO, Ferreira JC, Cavallari RT, Neves KR, dos Reis LM, Dominguez WV, et al. Mineral bone disorder in chronic kidney disease: head-to-head comparison of the 5/6 nephrectomy and adenine models. BMC nephrology. May 3 2014;15:69. Epub 2014/06/03.
60. Heveran CM, Ortega AM, Cureton A, Clark R, Livingston EW, Bateman TA, et al. Moderate chronic kidney disease impairs bone quality in C57Bl/6J mice. Bone. May 2016;86:1-9. Epub 2016/02/11.
61. Askari H, Seifi B, Kadkhodaee M. Evaluation of Renal-Hepatic Functional Indices and Blood Pressure Based on the Progress of Time in a Rat Model of Chronic Kidney Disease. Nephro-urology monthly. May 2016;8(3):e37840. Epub 2016/08/30.
62. Diwan V, Brown L, Gobe GC. Adenine-induced chronic kidney disease in rats. Nephrology (Carlton, Vic). Jan 2018;23(1):5-11. Epub 2017/10/17.
63. Yokozawa T, Zheng PD, Oura H, Koizumi F. Animal model of adenine-induced chronic renal failure in rats. Nephron. 1986;44(3):230-4. Epub 1986/01/01.
64. Yokozawa T, Oura H, Koizumi F. 2,8-Dihydroxyadenine urolithiasis induced by dietary adenine in rats. Nihon Jinzo Gakkai shi. Mar 1985;27(3):371-8. Epub 1985/03/01.
65. Yokozawa T, Zheng PD, Oura H. Biochemical features induced by adenine feeding in rats. Polyuria, electrolyte disorders, and 2,8-dihydroxyadenine deposits. Journal of nutritional science and vitaminology. Jun 1984;30(3):245-54. Epub 1984/06/01.
66. Munoz Abellan C, Mangold-Gehring S, Micus S, Beddies G, Moritz A, Hartmann E, et al. A Novel Model of Chronic Kidney Disease in Rats: Dietary Adenine in Combination with Unilateral Nephrectomy. Kidney diseases (Basel, Switzerland). Jun 2019;5(3):135-43. Epub 2019/07/02.
67. Tani T, Orimo H, Shimizu A, Tsuruoka S. Development of a novel chronic kidney disease mouse model to evaluate the progression of hyperphosphatemia and associated mineral bone disease. Scientific reports. May 22 2017;7(1):2233. Epub 2017/05/24.
68. Niemczyk M, Niemczyk S, Paczek L. Autosomal dominant polycystic kidney disease and transplantation. Ann Transplant. Oct-Dec 2009;14(4):86-90.
69. Halvorson CR, Bremmer MS, Jacobs SC. Polycystic kidney disease: inheritance, pathophysiology, prognosis, and treatment. Int J Nephrol Renovasc Dis. 2010;3:69-83. Epub 2010/06/24.
70. Cowley BD, Jr., Gudapaty S, Kraybill AL, Barash BD, Harding MA, Calvet JP, et al. Autosomal-dominant polycystic kidney disease in the rat. Kidney Int. Mar 1993;43(3):522-34. Epub 1993/03/01.

71. Nagao S, Kugita M, Yoshihara D, Yamaguchi T. Animal models for human polycystic kidney disease. Experimental animals. 2012;61(5):477-88. Epub 2012/10/26.
72. Kaspareit-Rittinghausen J, Deerberg F, Wcislo A. Hereditary polycystic kidney disease. Adult polycystic kidney disease associated with renal hypertension, renal osteodystrophy, and uremic enteritis in SPRD rats. Am J Pathol. 1991;139(3):693-6.
73. Moe SM, Chen NX, Seifert MF, Sinders RM, Duan D, Chen X, et al. A rat model of chronic kidney disease-mineral bone disorder. Kidney Int. Jan 2009;75(2):176-84. Epub 2008/09/19.
74. Kaspareit-Rittinghausen J, Deerberg F, Rapp KG, Wcislo A. A new rat model for polycystic kidney disease of humans. Transplantation proceedings. Dec 1990;22(6):2582-3. Epub 1990/12/01.
75. Vorland CJ, Lachcik PJ, Swallow EA, Metzger CE, Allen MR, Chen NX, et al. Effect of ovariectomy on the progression of chronic kidney disease-mineral bone disorder (CKD-MBD) in female Cy/+ rats. Scientific reports. May 28 2019;9(1):7936. Epub 2019/05/30.
76. van der Meulen MC, Jepsen KJ, Mikic B. Understanding bone strength: size isn't everything. Bone. Aug 2001;29(2):101-4. Epub 2001/08/15.
77. Keaveny TM, Kopperdahl DL, Melton LJ, 3rd, Hoffmann PF, Amin S, Riggs BL, et al. Age-dependence of femoral strength in white women and men. Journal of bone and mineral research : the official journal of the American Society for Bone and Mineral Research. 2010;25(5):994-1001.
78. Nordin M, Frankel VH. Basic biomechanics of the musculoskeletal system: Lippincott Williams & Wilkins; 2001.
79. Galante J, Rostoker W, Ray RD. Physical properties of trabecular bone. Calcified tissue research. 1970;5(3):236-46. Epub 1970/01/01.
80. Eastell R, Mosekilde L, Hodgson SF, Riggs BL. Proportion of human vertebral body bone that is cancellous. Journal of bone and mineral research : the official journal of the American Society for Bone and Mineral Research. Dec 1990;5(12):1237-41. Epub 1990/12/01.
81. Zysset PK, Goulet RW, Hollister SJ. A global relationship between trabecular bone morphology and homogenized elastic properties. Journal of biomechanical engineering. Oct 1998;120(5):640-6. Epub 1999/07/21.
82. Odgaard A, Kabel J, van Rietbergen B, Dalstra M, Huiskes R. Fabric and elastic principal directions of cancellous bone are closely related. Journal of biomechanics. May 1997;30(5):487-95. Epub 1997/05/01.
83. Feldkamp LA, Goldstein SA, Parfitt AM, Jesion G, Kleerekoper M. The direct examination of three-dimensional bone architecture in vitro by computed tomography. Journal of bone and mineral research : the official journal of the American Society for Bone and Mineral Research. Feb 1989;4(1):3-11. Epub 1989/02/01.
84. Turner CH, Burr DB. Basic biomechanical measurements of bone: a tutorial. Bone. Jul-Aug 1993;14(4):595-608. Epub 1993/07/01.
85. Barbier A, Martel C, de Vernejoul MC, Tirode F, Nys M, Mocaer G, et al. The visualization and evaluation of bone architecture in the rat using three-dimensional X-ray microcomputed tomography. Journal of bone and mineral metabolism. 1999;17(1):37-44. Epub 1999/03/20.

86. Cejka D, Patsch JM, Weber M, Diarra D, Riegersperger M, Kikic Z, et al. Bone microarchitecture in hemodialysis patients assessed by HR-pQCT. Clinical journal of the American Society of Nephrology : CJASN. Sep 2011;6(9):2264-71. Epub 2011/07/09.
87. Nickolas TL, Stein E, Cohen A, Thomas V, Staron RB, McMahon DJ, et al. Bone mass and microarchitecture in CKD patients with fracture. Journal of the American Society of Nephrology : JASN. Aug 2010;21(8):1371-80. Epub 2010/04/17.
88. Bouxsein ML, Boyd SK, Christiansen BA, Guldberg RE, Jepsen KJ, Muller R. Guidelines for assessment of bone microstructure in rodents using micro-computed tomography. Journal of bone and mineral research : the official journal of the American Society for Bone and Mineral Research. Jul 2010;25(7):1468-86. Epub 2010/06/10.
89. McNerny EMB, Buening DT, Aref MW, Chen NX, Moe SM, Allen MR. Time course of rapid bone loss and cortical porosity formation observed by longitudinal muCT in a rat model of CKD. Bone. Aug 2019;125:16-24. Epub 2019/05/07.
90. Nishiyama KK, Shane E. Clinical imaging of bone microarchitecture with HR-pQCT. Current osteoporosis reports. 2013;11(2):147-55.
91. Reznikov N, Shahar R, Weiner S. Three-dimensional structure of human lamellar bone: the presence of two different materials and new insights into the hierarchical organization. Bone. Feb 2014;59:93-104. Epub 2013/11/12.
92. Wang Y, Von Euw S, Fernandes FM, Cassaignon S, Selmane M, Laurent G, et al. Water-mediated structuring of bone apatite. Nature materials. Dec 2013;12(12):1144-53. Epub 2013/11/07.
93. Hansson T, Roos B, Nachemson A. The bone mineral content and ultimate compressive strength of lumbar vertebrae. Spine. Jan-Feb 1980;5(1):46-55. Epub 1980/01/01.
94. Wang X, Shen X, Li X, Agrawal CM. Age-related changes in the collagen network and toughness of bone. Bone. Jul 2002;31(1):1-7. Epub 2002/07/12.
95. Hammond MA, Laine TJ, Berman AG, Wallace JM. Treadmill Exercise Improves Fracture Toughness and Indentation Modulus without Altering the Nanoscale Morphology of Collagen in Mice. PLoS One. 2016;11(9):e0163273. Epub 2016/09/23.
96. Berman AG, Clauser CA, Wunderlin C, Hammond MA, Wallace JM. Structural and Mechanical Improvements to Bone Are Strain Dependent with Axial Compression of the Tibia in Female C57BL/6 Mice. PLoS One. 2015;10(6):e0130504. Epub 2015/06/27.
97. Nagler J. Failure Mechanics of Multi Materials Laminated Systems Review Analysis-Based Project2019.
98. Wallace JM, Golcuk K, Morris MD, Kohn DH. Inbred strain-specific response to biglycan deficiency in the cortical bone of C57BL6/129 and C3H/He mice. Journal of bone and mineral research : the official journal of the American Society for Bone and Mineral Research. Jun 2009;24(6):1002-12. Epub 2008/12/31.
99. Bart ZR, Hammond MA, Wallace JM. Multi-scale analysis of bone chemistry, morphology and mechanics in the oim model of osteogenesis imperfecta. Connective tissue research. Aug 2014;55 Suppl 1:4-8. Epub 2014/08/27.
100. Baratta FI. Requirements for Flexure Testing of Brittle Materials. In: Freiman SW, Michael CH, editors. West Conshohocken, PA: ASTM International; 1984. p. 194-222.
101. Zysset PK, Guo XE, Hoffler CE, Moore KE, Goldstein SA. Elastic modulus and hardness of cortical and trabecular bone lamellae measured by nanoindentation in the human femur. Journal of biomechanics. Oct 1999;32(10):1005-12. Epub 1999/09/07.

102. Yassine RA, Elham MK, Mustapha S, Hamade RF. Heterogeneous Versus Homogeneous Material Considerations in Determining the Modal Frequencies of Long Tibia Bones. Journal of Engineering and Science in Medical Diagnostics and Therapy. 2018;1(2):021001--5.
103. Allen MR, Chen NX, Gattone VH, 2nd, Chen X, Carr AJ, LeBlanc P, et al. Skeletal effects of zoledronic acid in an animal model of chronic kidney disease. Osteoporos Int. 2013;24(4):1471-81. Epub 2012/08/21.
104. Newman CL, Creecy A, Granke M, Nyman JS, Tian N, Hammond MA, et al. Raloxifene improves skeletal properties in an animal model of cystic chronic kidney disease. Kidney Int. Jan 2016;89(1):95-104. Epub 2015/10/22.
105. Oliver W, M. Pharr G. Measurement of hardness and elastic modulus by instrumented indentation: Advances in understanding and refinements to methodology. Journal of Materials Research - J MATER RES. 01/01 2004;19:3-20.
106. Guillonneau G, Kermouche G, Bec S, Loubet J-L. Determination of mechanical properties by nanoindentation independently of indentation depth measurement. Journal of Materials Research. 10/14 2012;27.
107. van Gaalen SM, Kruyt MC, Geuze RE, de Bruijn JD, Alblas J, Dhert WJ. Use of fluorochrome labels in in vivo bone tissue engineering research. Tissue engineering Part B, Reviews. Apr 2010;16(2):209-17. Epub 2009/10/28.
108. Newman CL, Tian N, Hammond MA, Wallace JM, Brown DM, Chen NX, et al. Calcitriol Suppression of Parathyroid Hormone Fails to Improve Skeletal Properties in an Animal Model of Chronic Kidney Disease. American journal of nephrology. 2016;43(1):20-31. Epub 2016/02/17.
109. Nielsen HE, Mosekilde L, Mosekilde L, Melsen B, Christensen P, Olsen KJ, et al. Relations of bone mineral content, ash weight and bone mass: implication for correction of bone mineral content for bone size. Clinical orthopaedics and related research. Nov-Dec 1980(153):241-7. Epub 1980/11/01.
110. Paschalis EP, Tatakis DN, Robins S, Fratzl P, Manjubala I, Zoehrer R, et al. Lathyrism-induced alterations in collagen cross-links influence the mechanical properties of bone material without affecting the mineral. Bone. 2011;49(6):1232-41. Epub 2011/09/02.
111. Gamsjaeger S, Mendelsohn R, Boskey AL, Gourion-Arsiquaud S, Klaushofer K, Paschalis EP. Vibrational spectroscopic imaging for the evaluation of matrix and mineral chemistry. Curr Osteoporos Rep. Dec 2014;12(4):454-64. Epub 2014/09/23.
112. Aparicio S, Doty SB, Camacho NP, Paschalis EP, Spevak L, Mendelsohn R, et al. Optimal methods for processing mineralized tissues for Fourier transform infrared microspectroscopy. Calcif Tissue Int. May 2002;70(5):422-9. Epub 2002/06/11.
113. Kazanci M, Fratzl P, Klaushofer K, Paschalis EP. Complementary information on in vitro conversion of amorphous (precursor) calcium phosphate to hydroxyapatite from Raman microspectroscopy and wide-angle X-ray scattering. Calcif Tissue Int. Nov 2006;79(5):354-9. Epub 2006/11/23.
114. Akkus O, Adar F, Schaffler MB. Age-related changes in physicochemical properties of mineral crystals are related to impaired mechanical function of cortical bone. Bone. Mar 2004;34(3):443-53. Epub 2004/03/09.
115. Rieppo L, Rieppo J, Jurvelin JS, Saarakkala S. Fourier transform infrared spectroscopic imaging and multivariate regression for prediction of proteoglycan content of articular cartilage. PLoS One. 2012;7(2):e32344. Epub 2012/02/24.

116. Gazi E, Gardner P, Lockyer NP, Hart CA, Brown MD, Clarke NW. Direct evidence of lipid translocation between adipocytes and prostate cancer cells with imaging FTIR microspectroscopy. Journal of lipid research. Aug 2007;48(8):1846-56. Epub 2007/05/15.
117. Zhang Y, McNerny EG, Terajima M, Raghavan M, Romanowicz G, Zhang Z, et al. Loss of BMP signaling through BMPR1A in osteoblasts leads to greater collagen cross-link maturation and material-level mechanical properties in mouse femoral trabecular compartments. Bone. 2016;88:74-84. Epub 2016/04/23.
118. Paschalis EP, Verdelis K, Doty SB, Boskey AL, Mendelsohn R, Yamauchi M. Spectroscopic characterization of collagen cross-links in bone. Journal of bone and mineral research : the official journal of the American Society for Bone and Mineral Research. Oct 2001;16(10):1821-8. Epub 2001/10/05.
119. Farlay D, Duclos ME, Gineyts E, Bertholon C, Viguet-Carrin S, Nallala J, et al. The ratio 1660/1690 cm(-1) measured by infrared microspectroscopy is not specific of enzymatic collagen cross-links in bone tissue. PLoS One. 2011;6(12):e28736. Epub 2011/12/24.
120. Oxlund H, Barckman M, Ortoft G, Andreassen TT. Reduced concentrations of collagen cross-links are associated with reduced strength of bone. Bone. Oct 1995;17(4 Suppl):365s-71s. Epub 1995/10/01.
121. Ross RD, Mashiatulla M, Robling AG, Miller LM, Sumner DR. Bone Matrix Composition Following PTH Treatment is Not Dependent on Sclerostin Status. Calcif Tissue Int. Feb 2016;98(2):149-57. Epub 2015/10/31.
122. Paschalis EP, Glass EV, Donley DW, Eriksen EF. Bone mineral and collagen quality in iliac crest biopsies of patients given teriparatide: new results from the fracture prevention trial. The Journal of clinical endocrinology and metabolism. Aug 2005;90(8):4644-9. Epub 2005/05/26.
123. Salem MM. Hyperparathyroidism in the hemodialysis population: a survey of 612 patients. American journal of kidney diseases : the official journal of the National Kidney Foundation. Jun 1997;29(6):862-5. Epub 1997/06/01.
124. Slatopolsky E, Delmez JA. Pathogenesis of secondary hyperparathyroidism. American journal of kidney diseases : the official journal of the National Kidney Foundation. Feb 1994;23(2):229-36. Epub 1994/02/01.
125. Apetrii M, Goldsmith D, Nistor I, Siriopol D, Voroneanu L, Scripcariu D, et al. Impact of surgical parathyroidectomy on chronic kidney disease-mineral and bone disorder (CKD-MBD) - A systematic review and meta-analysis. PLoS One. 2017;12(11):e0187025. Epub 2017/11/07.
126. Rudser KD, de Boer IH, Dooley A, Young B, Kestenbaum B. Fracture risk after parathyroidectomy among chronic hemodialysis patients. Journal of the American Society of Nephrology : JASN. Aug 2007;18(8):2401-7. Epub 2007/07/20.
127. Toromanoff A, Ammann P, Mosekilde L, Thomsen JS, Riond JL. Parathyroid hormone increases bone formation and improves mineral balance in vitamin D-deficient female rats. Endocrinology. Jun 1997;138(6):2449-57. Epub 1997/06/01.
128. Kandula P, Dobre M, Schold JD, Schreiber MJ, Jr., Mehrotra R, Navaneethan SD. Vitamin D supplementation in chronic kidney disease: a systematic review and meta-analysis of observational studies and randomized controlled trials. Clinical journal of the American Society of Nephrology : CJASN. 2011;6(1):50-62. Epub 2010/09/28.

129. Alexander ST, Hunter T, Walter S, Dong J, Maclean D, Baruch A, et al. Critical Cysteine Residues in Both the Calcium-Sensing Receptor and the Allosteric Activator AMG 416 Underlie the Mechanism of Action. Molecular pharmacology. Nov 2015;88(5):853-65. Epub 2015/08/21.
130. Block GA, Martin KJ, de Francisco AL, Turner SA, Avram MM, Suranyi MG, et al. Cinacalcet for secondary hyperparathyroidism in patients receiving hemodialysis. The New England journal of medicine. Apr 8 2004;350(15):1516-25. Epub 2004/04/09.
131. Moe SM, Cunningham J, Bommer J, Adler S, Rosansky SJ, Urena-Torres P, et al. Long-term treatment of secondary hyperparathyroidism with the calcimimetic cinacalcet HCl. Nephrology, dialysis, transplantation : official publication of the European Dialysis and Transplant Association - European Renal Association. Oct 2005;20(10):2186-93. Epub 2005/07/21.
132. Prevention CfDCa. Chronic Kidney Disease in the United States, 2021. In: Atlanta GUDoHaHS, Centers for Disease Control and Prevention, editor. 2021.
133. Nickolas TL, Stein EM, Dworakowski E, Nishiyama KK, Komandah-Kosseh M, Zhang CA, et al. Rapid cortical bone loss in patients with chronic kidney disease. Journal of bone and mineral research : the official journal of the American Society for Bone and Mineral Research. Aug 2013;28(8):1811-20. Epub 2013/03/05.
134. Metzger CE, Swallow EA, Stacy AJ, Tippen SP, Hammond MA, Chen NX, et al. Reversing cortical porosity: Cortical pore infilling in preclinical models of chronic kidney disease. Bone. Feb 2021;143:115632. Epub 2020/09/15.
135. Hernandez CJ, van der Meulen MC. Understanding Bone Strength Is Not Enough. Journal of bone and mineral research : the official journal of the American Society for Bone and Mineral Research. Jun 2017;32(6):1157-62. Epub 2017/01/10.
136. Morris MD, Mandair GS. Raman assessment of bone quality. Clinical orthopaedics and related research. Aug 2011;469(8):2160-9. Epub 2010/12/01.
137. Paschalis EP, Mendelsohn R, Boskey AL. Infrared assessment of bone quality: a review. Clinical orthopaedics and related research. Aug 2011;469(8):2170-8. Epub 2011/01/07.
138. Hoffler CE, Guo XE, Zysset PK, Goldstein SA. An application of nanoindentation technique to measure bone tissue Lamellae properties. Journal of biomechanical engineering. Dec 2005;127(7):1046-53. Epub 2006/03/01.
139. Donnelly E, Boskey AL, Baker SP, van der Meulen MC. Effects of tissue age on bone tissue material composition and nanomechanical properties in the rat cortex. J Biomed Mater Res A. Mar 1 2010;92(3):1048-56. Epub 2009/03/21.
140. Bellido T, Ali AA, Gubrij I, Plotkin LI, Fu Q, O'Brien CA, et al. Chronic elevation of parathyroid hormone in mice reduces expression of sclerostin by osteocytes: a novel mechanism for hormonal control of osteoblastogenesis. Endocrinology. Nov 2005;146(11):4577-83. Epub 2005/08/06.
141. Xiong J, Piemontese M, Thostenson JD, Weinstein RS, Manolagas SC, O'Brien CA. Osteocyte-derived RANKL is a critical mediator of the increased bone resorption caused by dietary calcium deficiency. Bone. Sep 2014;66:146-54. Epub 2014/06/17.
142. Gardinier JD, Al-Omaishi S, Morris MD, Kohn DH. PTH signaling mediates perilacunar remodeling during exercise. Matrix Biol. May-Jul 2016;52-54:162-75. Epub 2016/03/01.

143. Qing H, Ardeshirpour L, Pajevic PD, Dusevich V, Jähn K, Kato S, et al. Demonstration of osteocytic perilacunar/canalicular remodeling in mice during lactation. Journal of bone and mineral research : the official journal of the American Society for Bone and Mineral Research. May 2012;27(5):1018-29. Epub 2012/02/07.
144. Dole NS, Mazur CM, Acevedo C, Lopez JP, Monteiro DA, Fowler TW, et al. Osteocyte-Intrinsic TGF-β Signaling Regulates Bone Quality through Perilacunar/Canalicular Remodeling. Cell Rep. Nov 28 2017;21(9):2585-96. Epub 2017/12/01.
145. Creecy A, Damrath JG, Wallace JM. Control of Bone Matrix Properties by Osteocytes. Front Endocrinol (Lausanne). 2020;11:578477. Epub 2021/02/05.
146. Tanaka T, Hoshijima M, Sunaga J, Nishida T, Hashimoto M, Odagaki N, et al. Analysis of Ca(2+) response of osteocyte network by three-dimensional time-lapse imaging in living bone. Journal of bone and mineral metabolism. Sep 2018;36(5):519-28. Epub 2017/10/14.
147. Jähn K, Kelkar S, Zhao H, Xie Y, Tiede-Lewis LM, Dusevich V, et al. Osteocytes Acidify Their Microenvironment in Response to PTHrP In Vitro and in Lactating Mice In Vivo. Journal of bone and mineral research : the official journal of the American Society for Bone and Mineral Research. Aug 2017;32(8):1761-72. Epub 2017/05/05.
148. Damrath JG, Chen NX, Metzger CE, Srinivasan S, O'Neill K, Biruete A, et al. Non-additive effects of combined NOX1/4 inhibition and calcimimetic treatment on a rat model of chronic kidney disease-mineral and bone disorder (CKD-MBD). J Bone Miner Res Plus. 2022. Epub 2022/01/12.
149. Moe SM, Chen NX, Newman CL, Organ JM, Kneissel M, Kramer I, et al. Anti-sclerostin antibody treatment in a rat model of progressive renal osteodystrophy. Journal of bone and mineral research : the official journal of the American Society for Bone and Mineral Research. Mar 2015;30(3):499-509. Epub 2014/11/20.
150. Guo J, Liu M, Yang D, Bouxsein ML, Saito H, Galvin RJ, et al. Suppression of Wnt signaling by Dkk1 attenuates PTH-mediated stromal cell response and new bone formation. Cell metabolism. Feb 3 2010;11(2):161-71.
151. Hirano T, Turner CH, Forwood MR, Johnston CC, Burr DB. Does suppression of bone turnover impair mechanical properties by allowing microdamage accumulation? Bone. Jul 2000;27(1):13-20.
152. Berman AG, Damrath JG, Hatch J, Pulliam AN, Powell KM, Hinton M, et al. Effects of Raloxifene and tibial loading on bone mass and mechanics in male and female mice. Connective tissue research. Jan 2022;63(1):3-15. Epub 2021/01/12.
153. Roschger P, Fratzl P, Eschberger J, Klaushofer K. Validation of quantitative backscattered electron imaging for the measurement of mineral density distribution in human bone biopsies. Bone. Oct 1998;23(4):319-26. Epub 1998/10/08.
154. Heveran CM, Schurman CA, Acevedo C, Livingston EW, Howe D, Schaible EG, et al. Chronic kidney disease and aging differentially diminish bone material and microarchitecture in C57Bl/6 mice. Bone. Oct 2019;127:91-103. Epub 2019/05/06.
155. Gardinier JD, Al-Omaishi S, Rostami N, Morris MD, Kohn DH. Examining the influence of PTH(1-34) on tissue strength and composition. Bone. Dec 2018;117:130-7. Epub 2018/09/28.
156. Nyman JS, Roy A, Shen X, Acuna RL, Tyler JH, Wang X. The influence of water removal on the strength and toughness of cortical bone. Journal of biomechanics. 2006;39(5):931-8. Epub 2006/02/21.

157. Vesper EO, Hammond MA, Allen MR, Wallace JM. Even with rehydration, preservation in ethanol influences the mechanical properties of bone and how bone responds to experimental manipulation. Bone. Apr 2017;97:49-53. Epub 2017/01/07.
158. Ibrahim A, Magliulo N, Groben J, Padilla A, Akbik F, Abdel Hamid Z. Hardness, an Important Indicator of Bone Quality, and the Role of Collagen in Bone Hardness. J Funct Biomater. Dec 1 2020;11(4). Epub 2020/12/05.
159. Yeni YN, Yerramshetty J, Akkus O, Pechey C, Les CM. Effect of fixation and embedding on Raman spectroscopic analysis of bone tissue. Calcif Tissue Int. Jun 2006;78(6):363-71. Epub 2006/07/11.
160. Fleet ME, Liu X, King PL. Accommodation of the carbonate ion in apatite: An FTIR and X-ray structure study of crystals synthesized at 2–4 GPa. American Mineralogist. 2004;89(10):1422-32.
161. Yerramshetty JS, Akkus O. The associations between mineral crystallinity and the mechanical properties of human cortical bone. Bone. Mar 2008;42(3):476-82. Epub 2008/01/12.
162. Rapa SF, Di Iorio BR, Campiglia P, Heidland A, Marzocco S. Inflammation and Oxidative Stress in Chronic Kidney Disease-Potential Therapeutic Role of Minerals, Vitamins and Plant-Derived Metabolites. Int J Mol Sci. Dec 30 2019;21(1). Epub 2020/01/08.
163. Damrath JG, Creecy A, Wallace JM, Moe SM. The impact of advanced glycation end products on bone properties in chronic kidney disease. Curr Opin Nephrol Hypertens. Jul 1 2021;30(4):411-7. Epub 2021/05/01.
164. DiMeglio LA, Evans-Molina C, Oram RA. Type 1 diabetes. Lancet (London, England). Jun 16 2018;391(10138):2449-62. Epub 2018/06/20.
165. Prevention CfDCa. National Diabetes Statistics Report, 2020. Atlanta, GA: Centers for Disease Control and Prevention, US Dept of Health and Human Services2020.
166. Costacou T, Orchard TJ. Cumulative Kidney Complication Risk by 50 Years of Type 1 Diabetes: The Effects of Sex, Age, and Calendar Year at Onset. Diabetes Care. Mar 2018;41(3):426-33. Epub 2017/09/22.
167. Popolo A, Autore G, Pinto A, Marzocco S. Oxidative stress in patients with cardiovascular disease and chronic renal failure. Free Radic Res. May 2013;47(5):346-56. Epub 2013/02/27.
168. Adesso S, Popolo A, Bianco G, Sorrentino R, Pinto A, Autore G, et al. The uremic toxin indoxyl sulphate enhances macrophage response to LPS. PLoS One. 2013;8(9):e76778. Epub 2013/10/08.
169. Weber DR, Haynes K, Leonard MB, Willi SM, Denburg MR. Type 1 diabetes is associated with an increased risk of fracture across the life span: a population-based cohort study using The Health Improvement Network (THIN). Diabetes Care. Oct 2015;38(10):1913-20. Epub 2015/07/29.
170. Hu F, Jiang C, Shen J, Tang P, Wang Y. Preoperative predictors for mortality following hip fracture surgery: a systematic review and meta-analysis. Injury. Jun 2012;43(6):676-85. Epub 2011/06/21.
171. Loureiro MB, Ururahy MA, Freire-Neto FP, Oliveira GH, Duarte VM, Luchessi AD, et al. Low bone mineral density is associated to poor glycemic control and increased OPG expression in children and adolescents with type 1 diabetes. Diabetes Res Clin Pract. Mar 2014;103(3):452-7. Epub 2014/02/18.

172. Hygum K, Starup-Linde J, Harsløf T, Vestergaard P, Langdahl BL. MECHANISMS IN ENDOCRINOLOGY: Diabetes mellitus, a state of low bone turnover - a systematic review and meta-analysis. Eur J Endocrinol. Mar 2017;176(3):R137-r57. Epub 2017/01/05.
173. Willett TL, Pasquale J, Grynpas MD. Collagen modifications in postmenopausal osteoporosis: advanced glycation endproducts may affect bone volume, structure and quality. Curr Osteoporos Rep. Sep 2014;12(3):329-37. Epub 2014/06/02.
174. Poundarik AA, Wu PC, Evis Z, Sroga GE, Ural A, Rubin M, et al. A direct role of collagen glycation in bone fracture. J Mech Behav Biomed Mater. Dec 2015;52:120-30. Epub 2015/11/05.
175. Van Belle TL, Taylor P, von Herrath MG. Mouse Models for Type 1 Diabetes. Drug Discov Today Dis Models. Summer 2009;6(2):41-5. Epub 2010/04/22.
176. Kitada M, Ogura Y, Koya D. Rodent models of diabetic nephropathy: their utility and limitations. Int J Nephrol Renovasc Dis. 2016;9:279-90. Epub 2016/11/25.
177. Breyer MD, Böttinger E, Brosius FC, 3rd, Coffman TM, Harris RC, Heilig CW, et al. Mouse models of diabetic nephropathy. Journal of the American Society of Nephrology : JASN. Jan 2005;16(1):27-45. Epub 2004/11/26.
178. Yang HC, Zuo Y, Fogo AB. Models of chronic kidney disease. Drug Discov Today Dis Models. 2010;7(1-2):13-9. Epub 2011/02/03.
179. Eleazu CO, Eleazu KC, Chukwuma S, Essien UN. Review of the mechanism of cell death resulting from streptozotocin challenge in experimental animals, its practical use and potential risk to humans. J Diabetes Metab Disord. Dec 23 2013;12(1):60. Epub 2013/12/25.
180. Virtue S, Vidal-Puig A. GTTs and ITTs in mice: simple tests, complex answers. Nat Metab. Jul 2021;3(7):883-6. Epub 2021/06/13.
181. Dempster DW, Compston JE, Drezner MK, Glorieux FH, Kanis JA, Malluche H, et al. Standardized nomenclature, symbols, and units for bone histomorphometry: a 2012 update of the report of the ASBMR Histomorphometry Nomenclature Committee. Journal of bone and mineral research : the official journal of the American Society for Bone and Mineral Research. Jan 2013;28(1):2-17. Epub 2012/12/01.
182. Saadane A, Lessieur EM, Du Y, Liu H, Kern TS. Successful induction of diabetes in mice demonstrates no gender difference in development of early diabetic retinopathy. PLoS One. 2020;15(9):e0238727. Epub 2020/09/18.
183. Le May C, Chu K, Hu M, Ortega CS, Simpson ER, Korach KS, et al. Estrogens protect pancreatic beta-cells from apoptosis and prevent insulin-deficient diabetes mellitus in mice. Proc Natl Acad Sci U S A. Jun 13 2006;103(24):9232-7. Epub 2006/06/07.
184. Nickolas TL, Cremers S, Zhang A, Thomas V, Stein E, Cohen A, et al. Discriminants of prevalent fractures in chronic kidney disease. Journal of the American Society of Nephrology : JASN. Aug 2011;22(8):1560-72. Epub 2011/07/26.
185. Vincenti F, Hattner R, Amend WJ, Jr., Feduska NJ, Duca RM, Salvatierra O, Jr. Decreased secondary hyperparathyroidism in diabetic patients receiving hemodialysis. Jama. Mar 6 1981;245(9):930-3. Epub 1981/03/06.
186. Inaba M, Okuno S, Nagasue K, Otoshi T, Kurioka Y, Maekawa K, et al. Impaired secretion of parathyroid hormone is coherent to diabetic hemodialyzed patients. American journal of kidney diseases : the official journal of the National Kidney Foundation. Oct 2001;38(4 Suppl 1):S139-42. Epub 2001/09/29.

187. Paula FJ, Lanna CM, Shuhama T, Foss MC. Effect of metabolic control on parathyroid hormone secretion in diabetic patients. Braz J Med Biol Res. Sep 2001;34(9):1139-45. Epub 2001/08/22.
188. Pabico RC, Rivero AJ, McKenna BA, Freeman RB. Parathyroid hormone in patients with diabetes mellitus and end-stage renal disease on chronic haemodialysis. Proc Eur Dial Transplant Assoc. 1983;19:221-6. Epub 1983/01/01.
189. Heidbreder E, Götz R, Schafferhans K, Heidland A. Diminished parathyroid gland responsiveness to hypocalcemia in diabetic patients with uremia. Nephron. 1986;42(4):285-9. Epub 1986/01/01.
190. Chiu KC, Chuang LM, Lee NP, Ryu JM, McGullam JL, Tsai GP, et al. Insulin sensitivity is inversely correlated with plasma intact parathyroid hormone level. Metabolism. Nov 2000;49(11):1501-5. Epub 2000/11/25.
191. Ray S, Beatrice AM, Ghosh A, Pramanik S, Bhattacharjee R, Ghosh S, et al. Profile of chronic kidney disease related-mineral bone disorders in newly diagnosed advanced predialysis diabetic kidney disease patients: A hospital based cross-sectional study. Diabetes Metab Syndr. Dec 2017;11 Suppl 2:S931-s7. Epub 2017/07/22.
192. Carvalho C, Magalhães J, Neto R, Pereira L, Branco P, Adragão T, et al. Cortical bone analysis in a predialysis population: a comparison with a dialysis population. Journal of bone and mineral metabolism. Sep 2017;35(5):513-21. Epub 2016/11/11.
193. Hie M, Iitsuka N, Otsuka T, Tsukamoto I. Insulin-dependent diabetes mellitus decreases osteoblastogenesis associated with the inhibition of Wnt signaling through increased expression of Sost and Dkk1 and inhibition of Akt activation. Int J Mol Med. Sep 2011;28(3):455-62. Epub 2011/05/14.
194. Uzawa T, Hori M, Ejiri S, Ozawa H. Comparison of the effects of intermittent and continuous administration of human parathyroid hormone(1-34) on rat bone. Bone. Apr 1995;16(4):477-84. Epub 1995/04/01.
195. Metzger CE, Swallow EA, Allen MR. Elevations in Cortical Porosity Occur Prior to Significant Rise in Serum Parathyroid Hormone in Young Female Mice with Adenine-Induced CKD. Calcif Tissue Int. Apr 2020;106(4):392-400. Epub 2019/12/14.
196. Li JY, D'Amelio P, Robinson J, Walker LD, Vaccaro C, Luo T, et al. IL-17A Is Increased in Humans with Primary Hyperparathyroidism and Mediates PTH-Induced Bone Loss in Mice. Cell metabolism. Nov 3 2015;22(5):799-810. Epub 2015/10/13.
197. Motyl KJ, Botolin S, Irwin R, Appledorn DM, Kadakia T, Amalfitano A, et al. Bone inflammation and altered gene expression with type I diabetes early onset. J Cell Physiol. Mar 2009;218(3):575-83. Epub 2008/11/14.
198. Metzger CE, Swallow EA, Stacy AJ, Allen MR. Strain-specific alterations in the skeletal response to adenine-induced chronic kidney disease are associated with differences in parathyroid hormone levels. Bone. Jul 2021;148:115963. Epub 2021/04/21.
199. Metzger CE, Swallow EA, Stacy AJ, Allen MR. Adenine-induced chronic kidney disease induces a similar skeletal phenotype in male and female C57BL/6 mice with more severe deficits in cortical bone properties of male mice. PLoS One. 2021;16(4):e0250438. Epub 2021/04/24.
200. Ogirima T, Tano K, Kanehara M, Gao M, Wang X, Guo Y, et al. Sex difference of adenine effects in rats: renal function, bone mineral density and sex steroidogenesis. Endocr J. Jun 2006;53(3):407-13. Epub 2006/05/26.

201. Cirmanová V, Bayer M, Stárka L, Zajíčková K. The effect of leptin on bone: an evolving concept of action. Physiol Res. 2008;57 Suppl 1:S143-s51. Epub 2008/02/15.
202. King AJ. The use of animal models in diabetes research. Br J Pharmacol. Jun 2012;166(3):877-94. Epub 2012/02/23.
203. Twito O, Frankel M, Nabriski D. Impact of glucose level on morbidity and mortality in elderly with diabetes and pre-diabetes. World J Diabetes. Mar 15 2015;6(2):345-51. Epub 2015/03/20.

PUBLICATIONS

The following list provides a comprehensive view of all published manuscripts and manuscripts in preparation with their scientific impact, quantified by number of citations.

1. Creecy A*, **Damrath JG***, Wallace JM. Control of Bone Matrix Properties by Osteocytes. Front Endocrinol (Lausanne). 2020;11:578477. Epub 2021/02/05. Citations: 9
2. Yajima A, Tsuchiya K, Burr DB, Wallace JM, **Damrath JG**, Inaba M, et al. The Importance of Biologically Active Vitamin D for Mineralization by Osteocytes After Parathyroidectomy for Renal Hyperparathyroidism. JBMR Plus. Nov 2019;3(11):e10234. Epub 2019/11/27. Citations: 2
3. **Damrath JG***, Creecy A*, Wallace JM, Moe SM. The impact of advanced glycation end products on bone properties in chronic kidney disease. Curr Opin Nephrol Hypertens. Jul 1 2021;30(4):411-7. Epub 2021/05/01. Citations: 1
4. Berman AG*, **Damrath JG***, Hatch J, Pulliam AN, Powell KM, Hinton M, et al. Effects of Raloxifene and tibial loading on bone mass and mechanics in male and female mice. Connect Tissue Res. Jan 2022;63(1):3-15. Epub 2021/01/12. Citations: 0
5. **Damrath JG**, Chen NX, Metzger CE, Srinivasan S, O'Neill K, Biruete A, et al. Non-additive effects of combined NOX1/4 inhibition and calcimimetic treatment on a rat model of chronic kidney disease-mineral and bone disorder (CKD-MBD). J Bone Miner Res Plus. 2022. Epub 2022/01/12. Citations: 0
6. **Damrath JG**, Moe SM, Wallace JM. Calcimimetics Alter Periosteal and Perilacunar Bone Matrix Properties in Early Chronic Kidney Disease. J Bone Miner Res. (submitted).
7. **Damrath JG**, Metzger CE, Allen MR, Wallace JM. A Novel Murine Model of Combined Type 1 Diabetes and Chronic Kidney Disease Exhibits a Unique Skeletal Phenotype Versus the Single Disease States. J Bone Miner Res. (submitted).

*Co-first authors